Technical Report of the sPHENIX Hadronic Calorimeter Prototype Simulation Study and the Beam Test Data Analysis

L. Xue[c], C. Aidala[e], S. Beckman[b], C. Biggs[a], S. Boose[a], M. Chiu[a], A. Franz[a], Y. Goto[g], J. Haggerty[a], X. He[c], K. Jones[a], E. Kistenev[a], B. Lenz[a], M. Lenz[a], D. Lynch[a], E. Mannel[a], M. McCumber[d], D. Morrison[a], J. Nagle[b], E. Obrien[a], C. Pinkenburg[a], S. Polizzo[a], B. Ramson[e], J. Rubin[e], R. Ruggeiro[a], A. Sickles[a], P. Stankus[a], S. Stoll[a], A. Sukhanov[a], F. Toldo[a], C. Woody[a]

[a] Brookhaven National Laboratory
[b] Colorado University
[c] Georgia State University
[d] Los Alamos National Lab
[e] University of Michigan
[f] Oak Ridge National Lab
[g] RIKEN

April 23, 2015

Abstract

This technical note documents the details of the GEANT4 simulations and test beam data analysis of the sPHENIX hadronic calorimeter prototype. The test beam experiment was performed at the test beam facility at Fermlib in February of 2014. The results of this study shed lights on the fundamental understanding of the performance of an accordion-like hadronic calorimeter which includes the energy resolution, signal linearity and the e/h ratio. It is important to note that a Geant4-based simulation shows very consistent results in comparison with the test beam measurement.

Contents

1 Introduction **2**

2 Experimental Setup **3**
2.1 HCal Prototype . . . 3
2.2 Fermilab Test Beam Line . . . 3

3 Geant4 Simulation **8**
3.1 Analysis Code . . . 8
3.2 Detector Setup . . . 8
3.3 Procedure . . . 13
3.4 Results . . . 14
3.4.1 Tower Energy Distribution . . . 14
3.4.2 Single Particle Response . . . 23
3.4.3 Sampling Fraction Factor . . . 25
3.4.4 Energy Reconstruction . . . 27
3.4.5 Energy Resolution and Linearity . . . 32
3.4.6 Energy Leakage . . . 35
3.4.7 e/π Ratio . . . 38
3.4.8 Cosmic Muon Simulation . . . 38

4 Test Beam Data Analysis **42**
4.1 Analysis Code . . . 42
4.2 ADC Readout . . . 42
4.3 Optimizing Signal ADC Ingration . . . 42
4.4 Energy Calibration and Correction with Cosmic Ray Muons . . . 43

5 Beam Test Results **50**
5.1 Beam Spot Distribution . . . 50
5.2 Beam Particle Identification . . . 50
5.3 Energy Leveling and Scaling . . . 54
5.4 Reconstructed Energy Spectra . . . 57
5.5 Calorimeter Energy Resolution and Linearity . . . 63
5.6 Reconstructed e/π Ratio . . . 63
5.7 Comparison with Geant4 Simulation . . . 65

6 Summary **69**

A HCal Design Drawings **71**

1 Introduction

An accordion-like hadronic calorimeter (HCAL) prototype based on scintillator plates and steel absorber plates has been constructed and tested at the test beam facility at Fermilab for the sPHENIX project. The design of the sPHENIX detector system when the prototype was constructed is shown in Fig. 1. The sPHENIX detector design is constrained by the

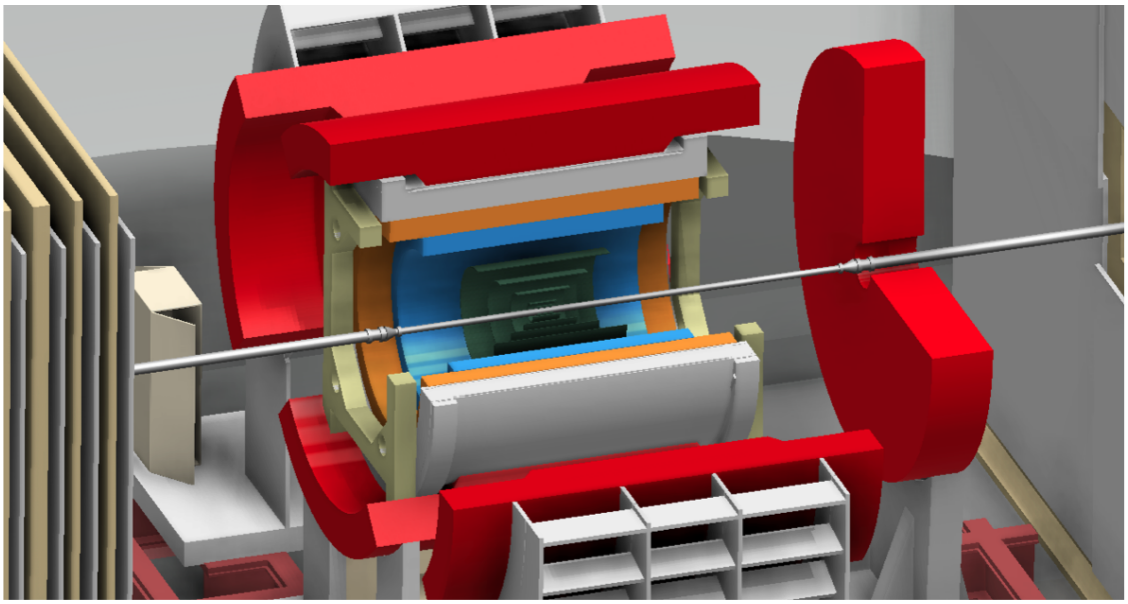

Figure 1: Engineering rendering of the sPHENIX detector design, which consists of a set of inner silicon tracking layers, an electromagnetic calorimeter (in blue), a superconducting solenoid (BaBar magnet), and a hadronic calorimeter (in red).

BaBar solenoid magnet, which starts at 140 cm and ends at 173 cm in radial direction. The magnet is 385 cm long and provides a central field of 1.5 T.

The design specifications of the sPHENIX calorimeters are given in Table 1, which are driven by the sPHENIX physics goals [1].

The prototype consists of two sections with a total depth of about 5 interaction lengths. It was built and assembled at Brookhaven National Lab by the PHENIX Tech Team. In this technical note, we document the HCAL prototype detector design, the test beam data analysis as well as the Geant4 simulation results. This note is organized into six sections. Following the introduction section, we briefly describe the experimental setup in Section 2. Geant4 simulation of the prototype is given in Section 3 which is followed with the detailed description of test beam data analysis in Section 4. The main results of this study is given in Section 5 and the overall summary is given in Section 6.

We acknowledge the contributions to this project from Aria Soha, Todd Nebel, J.J. Schmidt, Ewa Skup, and Erik Ramberg. We also acknowledge the superb support we received at the Fermilab Beam Test Facility.

Table 1: Summary of detector requirements, showing the capabilities needed for various physics observables.

Physics	Detectors	Requirements
Full jet reconstruction	EMCal	$\sigma/E < 20\%/\sqrt{E}$
	HCal	$\sigma/E < 100\%/\sqrt{E}$
		$\Delta\eta \times \Delta\phi \sim 0.1$ x 0.1
		uniform within $\lvert\eta\rvert < 1$
Direct γ, p_T >10GeV/c	EMCal	$\sigma/E < 15\%/\sqrt{E}$
		$\Delta\eta \times \Delta\phi \sim 0.03$ x 0.03
Heavy quarkonia	EMCal	$\sigma/E < 15\%/\sqrt{E}$
		$\Delta\eta \times \Delta\phi \sim 0.03$ x 0.03
π^0 *to* $p_T = 40$ GeV/c	EMCal	$\sigma/E < 15\%/\sqrt{E}$
		$\Delta\eta \times \Delta\phi \sim 0.03$ x 0.03

2 Experimental Setup

2.1 HCal Prototype

The HCal prototype consists two segments: inner HCal (H1) and outer HCal (H2). Both H1 and H2 have 16 layers of steel plates and scintillator tiles as shown in Fig. 2. Figure 2 also shows photos of making groves on scintillator sheets. The steel plates and scintillator titles in H1 and H2 are tilted in opposite directions to avoid particle channeling. The dimensions of H1 and H2 steel plates are given in Appendix A (Fig. 2 and Fig. 3 in n Appendix A). Each scintillator tile is divided into 4 sheets, each of which has a U-shaped fiber embedded for light collection (see Fig. 4 in Appendix A for the drawing of the H2 1U scintillator sheet as an example). The fibers from four scintillator tiles are bundled together to form four towers for readout. Both H1 and H2 have sixteen towers (4x4) as shown in Fig. 3. The whole HCal prototype measures 1.2 m x 1.7 m x 1.3 m and weights about 8,000 lbs mounted on a support structure (Fig. 5 in Appendix A).

2.2 Fermilab Test Beam Line

Figure 4 shows the layout of the Fermilab MT6 test beam line. The HCal prototype is located at the end of the beam line. Figure 5 shows the HCal prototype mounted on a moveable lift table which can be moved horizontally along the z-axis (perpendicular to the beam) and vertically along the y-axis. One can also rotate the HCAL prototype about the z and y axis. Four scintillator paddles are used (two at the top and two on bottom) as the cosmic ray trigger.

Test beam data were recorded with beam energies ranging from 4 GeV to 60 GeV for normal detector configuration (i.e. 28.5 inches in height and no rotation about x and y

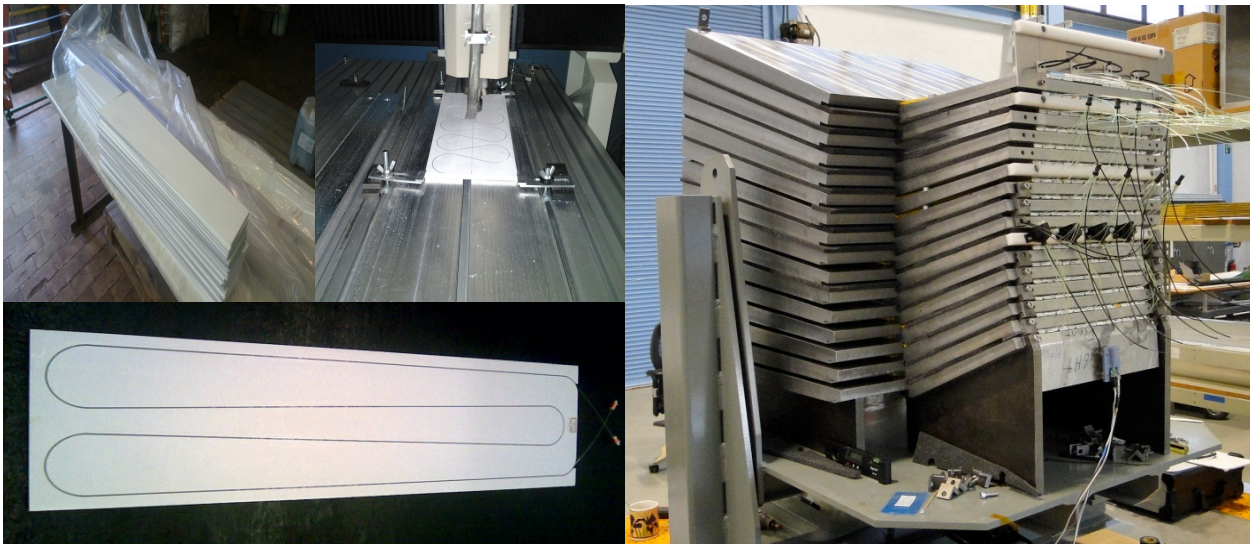

Figure 2: Scintillating tiles with embedded wavelength shifting fibers (left panel) and the HCal prototype calorimeter (right panel).

axis). We also took HCal data by moving it vertically to different heights together with a few selected rotational angles at 30 GeV beam energy. The data-taking run list is given in Table 2 and 3. In total, 142 k events were recorded in nominal detector configuration with beam energies between 4 and 60 GeV, and 254 k events were recorded in various detector height and rotation with 30 GeV beam.

Table 2: HCal prototype detector beam energy scan runs at the FNAL test beam.

Run #	**Beam energy**	**Total events**	**Detector configuration**
459	4 GeV	7.6 k	nominal setup
460	8 GeV	11.6 k	nominal setup
463	16 GeV	14 k	nominal setup
465	25 GeV	15 k	nominal setup
466	32 GeV	23 k	nominal setup
467	40 GeV	23 k	nominal setup
468	50 GeV	23 k	nominal setup
469	60 GeV	23 k	nominal setup
479	16 GeV	10 k	EMCal+HCal, nominal setup
480	32 GeV	10 k	EMCal+HCal, nominal setup
483	40 GeV	-	EMCal+HCal, nominal setup

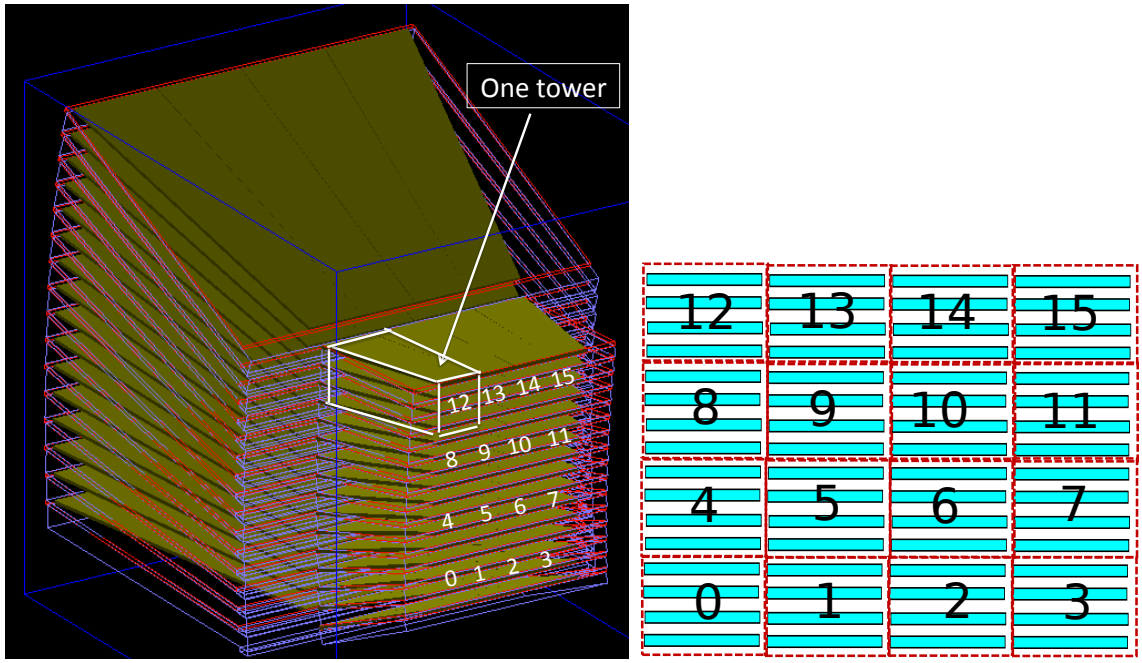

Figure 3: HCal tower layout viewed from the front both for H1 and H2.

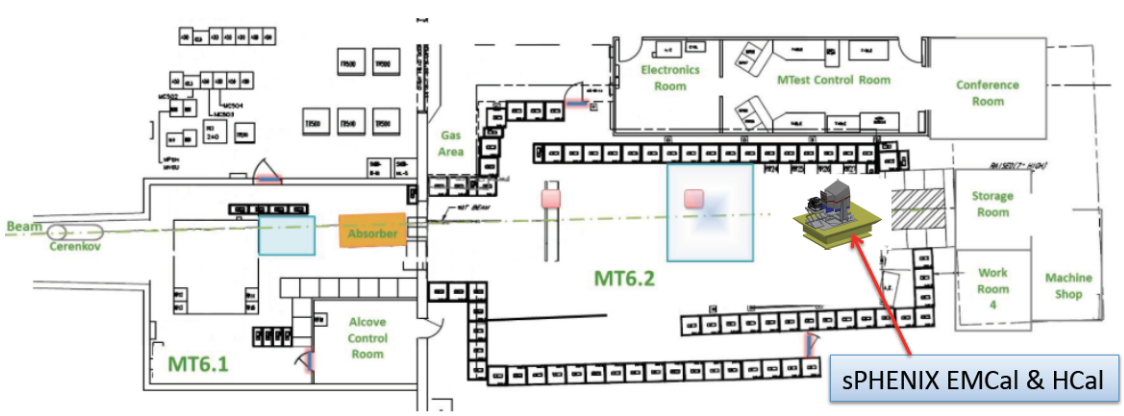

Figure 4: Layout of the Fermilab MT6 test beam line. HCal is located at the end of the beam line.

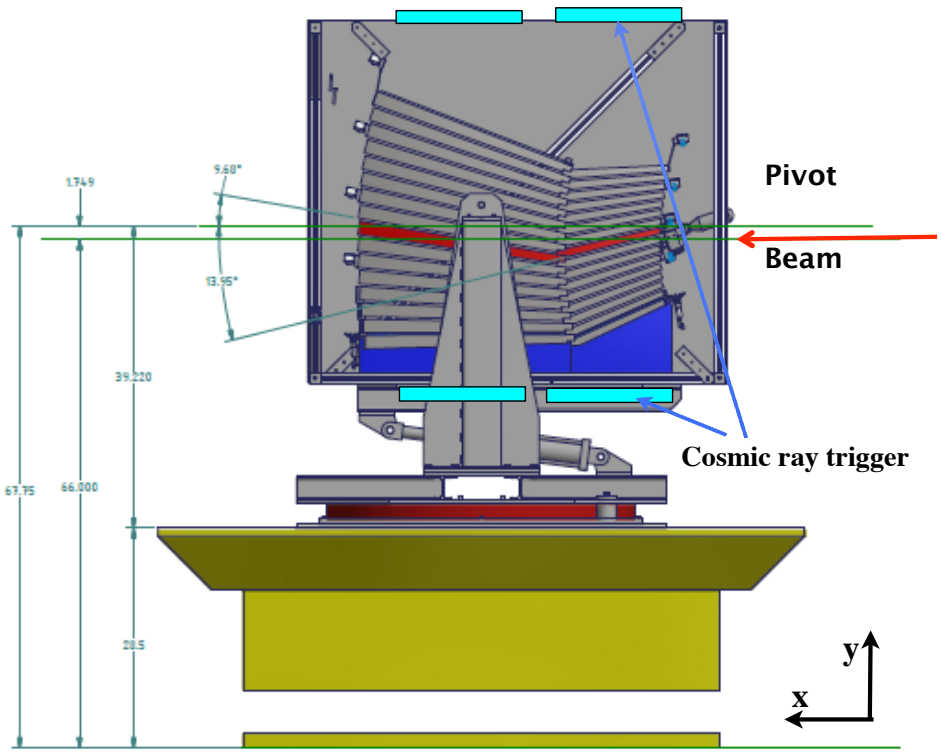

Figure 5: Sideview of the layout of the HCal prototype detector at the Fermilab test beam facility. Beam comes from right as indicated by the red arrow.

Table 3: HCal prototype detector survey runs at the FNAL test beam.

Run #	**Beam energy**	**Total events**	**Detector configuration (in inches)**
262	30 GeV	10 k	height: 25.25, rotation: 0°
263	30 GeV	10 k	height: 29, rotation: 0°
264	30 GeV	10 k	height: 31, rotation: 0°
265	30 GeV	10 k	height: 31, rotation: 0°
266	30 GeV	10 k	height: 33, rotation: 0°
267	30 GeV	10 k	height: 33, rotation: -5° Y
269	30 GeV	1.7 k	height: 33, rotation: -10° Y
270	30 GeV	10 k	height: 33, rotation: -10° Y
271	30 GeV	10 k	height: 33, rotation: -14° Y
272	30 GeV	14 k	height: 30, rotation: -7° Y
273	30 GeV	10 k	height: 27.5, rotation: -6° Y
274	30 GeV	10 k	height: 24, rotation: -6° Y
275	30 GeV	10 k	height: 24, rotation: +6.5° Y
276	30 GeV	10 k	height: 24, rotation: 0° Y
277	30 GeV	10 k	height: 24, rotation: +6° Y
278	30 GeV	10 k	height: 24, rotation: +12° Y
279	30 GeV	10 k	height: 26.5, rotation: +12° Y
280	30 GeV	10 k	height: 29, rotation: +12° Y
281	30 GeV	10 k	height: 28.5, rotation: +12° Z, +9° Y
282	30 GeV	20 k	height: 28.5, rotation: +12° Z, -8.2° Y
283	30 GeV	10 k	height: 28.5, rotation: 0° Z, -8.2° Y
284	30 GeV	10 k	height: 28.5, rotation: 0° Z, 0° Y
285	30 GeV	10 k	height: 28.5, rotation: 0° Z, +9° Y
286	30 GeV	5 k	height: 28.5, rotation: -12° Z, +9° Y
287	30 GeV	5 k	height: 28.5, rotation: -12° Z, 0° Y
288	30 GeV	8.7 k	height: 28.5, rotation: -12° Z, -8.2° Y

3 Geant4 Simulation

The simulation of the HCal prototype detector is implemented within the sPHENIX simulation framework, which is based on the Geant4 (version 10.0.2) simulation toolkits [2, 3]. The physics list is QGSP_BERT which is recommended for high energy physics processes. The QGSP_BERT physics list contains the standard electromagnetic process, uses Bertini cascade for hadrons of energy below 10 GeV, employs Quark gluon string model for high energies (> 20 GeV).

We obtain the calorimeter sampling fraction factor and the energy calibration constant from the simulation study and use them for reconstructing the energy measured by the calorimeter.

3.1 Analysis Code

The analysis macros and code have been committed into the PHENIX CVS repository.

- HCal prototype detector construction
  `simulation/g4simulation/g4detectors/PHG4HcalPrototype*`
- Single particle event generator macro
  `offline/analysis/sphnx_hcalprotosim/Fun4All_G4_HcalPrototype.C`
- Analysis code for determining material thickness and detector sampling fraction factors
  `offline/analysis/sphnx_hcalprotosim/g4hits_analysis/geantino/`
  `offline/analysis/sphnx_hcalprotosim/g4hits_analysis/mu-/`
- Code for building towers
  `offline/analysis/sphnx_hcalprotosim/towerbuild/`
- Tower level analysis code
  `offline/analysis/sphnx_hcalprotosim/towerbuild/analysis/`
- Macros for making plots of the technique note
  `offline/analysis/sphnx_hcalprotosim/towerbuild/analysis/technote/`

3.2 Detector Setup

The dimensions of the HCal prototype detector are based the mechanical drawings obtained from Don Lynch. These drawings are included in Appendix A. A large effort was put into the matching of the detector geometry in simulation against the dimensions of the real prototype. As described in the previous section, the simulated detector consists of 16 layers of alternately arranged steel and scintillator tiles for each segment. Each scintillator tile is divided into 4 sheets and is grouped together with other tiles to form the same tower configuration as the readout towers. A function is implemented in the simulation for rotating the detector along the Y, and Z axises in order to match the running configurations at the test beam.

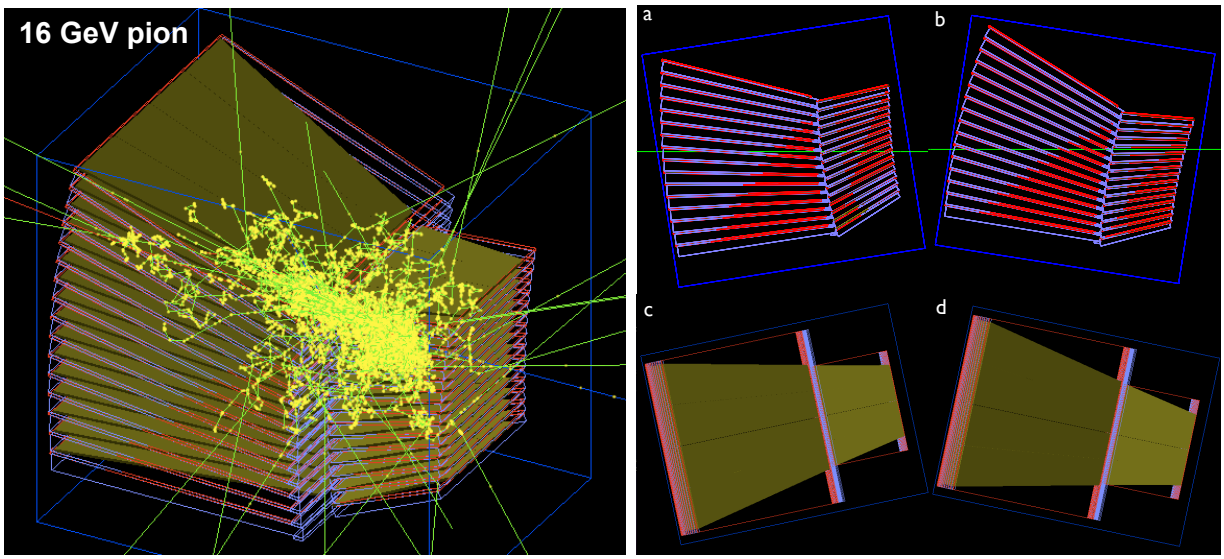

Figure 6: (Left panel) The HCal prototype calorimeter event display with hadronic shower from 16 GeV single pion. (Right panel) Rotation of HCal prototype in along Z (a, and b), and Y (c, and d) axises.

The HCal prototype material thickness is surveyed at a given pseudo-rapidity and azimuthal angle using geantinos. Geantino is a virtual particle implemented in Geant4 simulation which does not interact with materials and undertake transport processes only. The survey results are shown in Fig. 7 in units of cm and in Fig. 8 in units of interaction length (λ_I). Figure 9 shows the total material thickness of the HCal prototype in units of interaction length. On average, particles striking the HCAL prototype will traverse 5.8 cm of scintillator material and 21.4 cm of steel in H1, and 9.8 cm of scintillator, 55 cm of steel in H2.

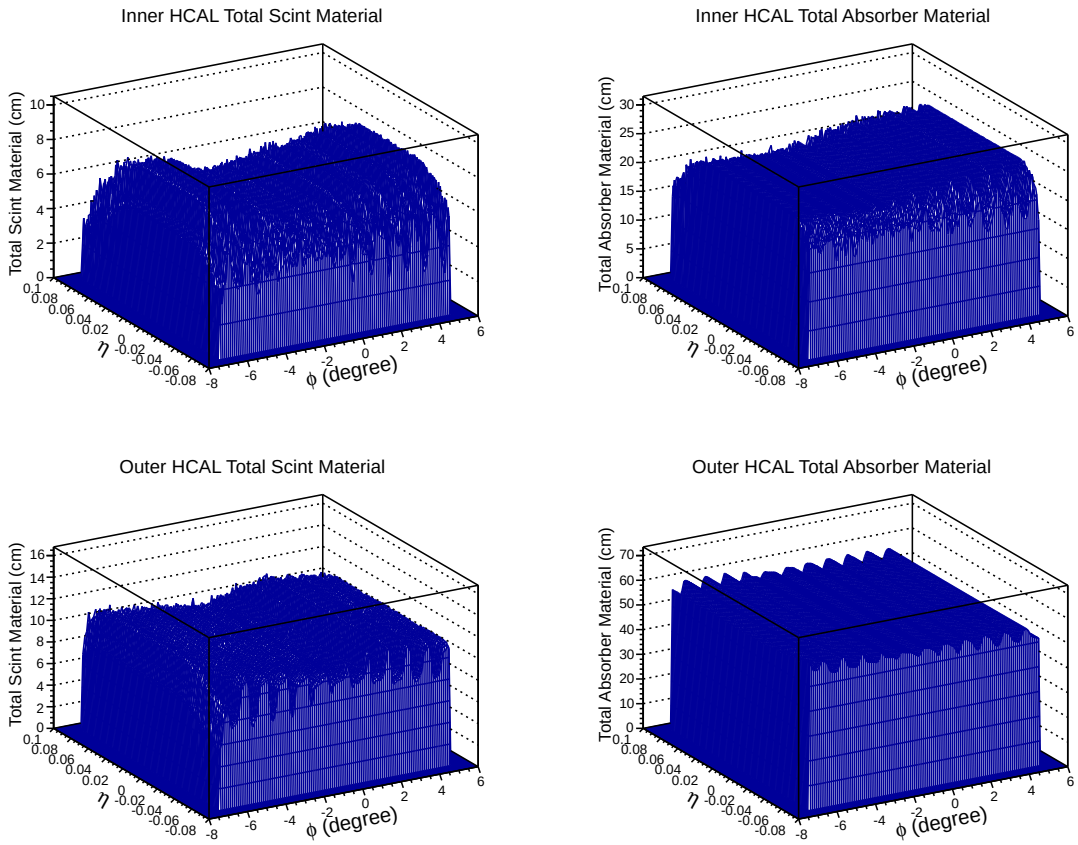

Figure 7: Total scintillator and absorber material thickness in units of cm for the Inner and the Outer HCal prototype, obtained from simulation with geantinos.

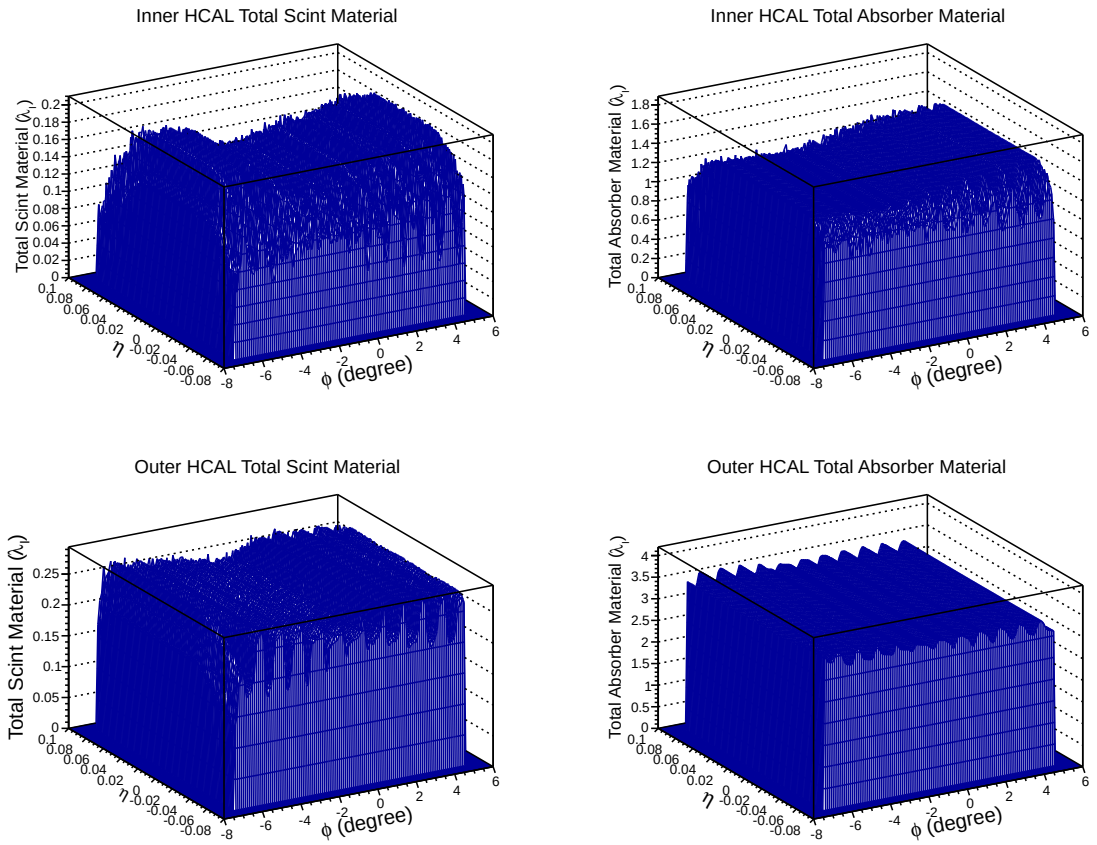

Figure 8: Total scintillator and absorber material thickness in units of interaction length (λ_I) for the Inner and the Outer HCal prototype, obtained from simulation with geantinos.

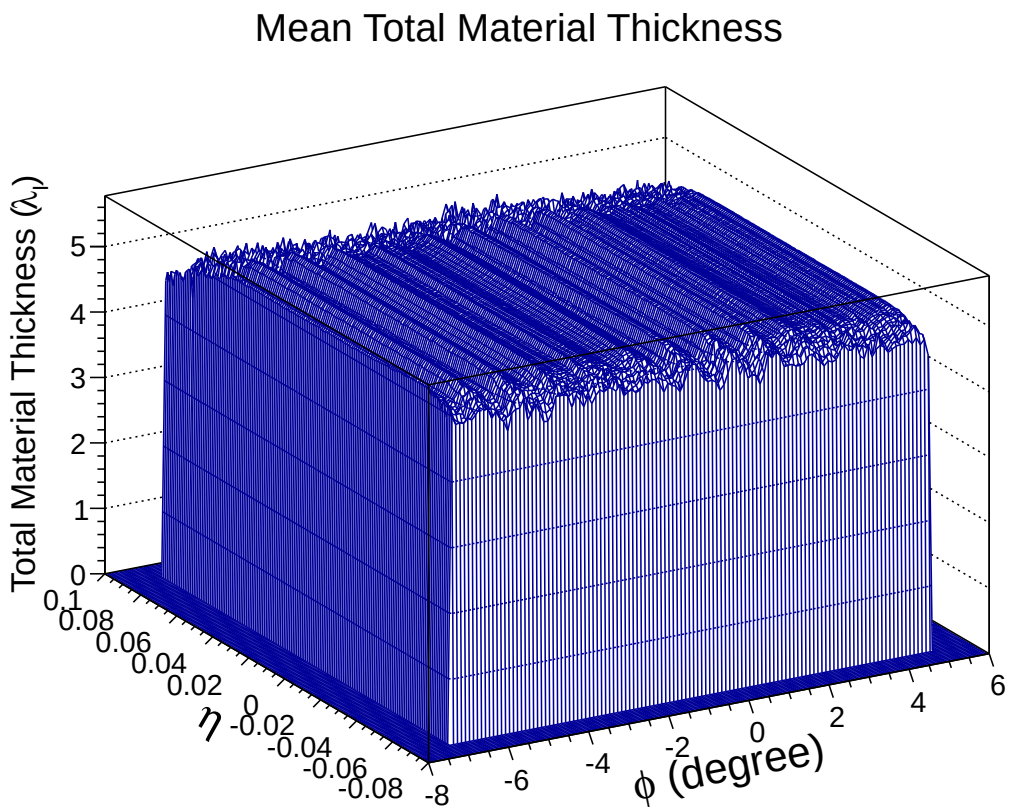

Figure 9: Total material thickness in units of interaction length (λ_I) for the HCal prototype, obtained from simulation with geantinos.

3.3 Procedure

Here we briefly describe the simulation procedure and start by listing the variables used in this simulation:

$\mathbf{E_{vis}}$ is the visible energy deposited in the scintillators.

$\mathbf{E_{invis}}$ is the energy deposited in the absorbers, which can not be seen experimentally.

$\mathbf{E_{leak}}$ includes the energy leakage at the back of the calorimeters, lateral or sideway energy leakage, and the energy with the escaped particles.

Sampling fraction factor (SF) is the ratio between the visible energy and total deposited energy

$$SF = \frac{E_{vis}}{E_{vis} + E_{invis}},$$

which is usually determined by the minimum ionization muons.

Shower center of gravity (CG) is calculated as

$$CG = \frac{\sum_{i=1}^{n} E_i^{dep} \times r_i}{\sum_{i=1}^{n} E_i^{dep}},$$

where r_i and E_i^{dep} are the position and energy loss of track hit i.

Longitudinal shower center of gravity (LCG) is defined as an energy-weighted CG from the two calorimeter segments (HCal inner and outer layer), i.e.,

$$LCG = \frac{E_{H1} \times CG_{H1} + E_{H2} \times CG_{H2}}{E_{H1} + E_{H2}},$$

where CG and E are the real center of gravity and reconstructed energy in each segment.

Energy asymmetry (E_{Asy}) is calculated as

$$E_{Asy} = \frac{E_{H1} - E_{H2}}{E_{H1} + E_{H2}},$$

where E_{H1}, and E_{H2} are the visible energy collected by the inner and the outer HCal prototype, respectively.

The simulation procedure for calorimeter study is generally divided into a sequence of steps, which is described as follows:

Step-1 Generate single particle G4 hits for $\mu^{\pm}$, $e^{\pm}$, and $\pi^{\pm}$, with energies ranging from 4 to 60 GeV.

Step-2 Calculate sampling fraction factors (SF) based on hits from single muon samples.

Step-3 Reconstruct electron, and pion energy using the SF from the previous step for studying energy resolution, linearity, e/π ratio, and compared with the FNAL test beam raw energy reconstructions.

Step-4 Normalize the reconstructed energy to the incident beam energy and evaluate energy resolution, compare with test beam results.

3.4 Results

We summarize the Geant4 simulation results in the following subsections.

3.4.1 Tower Energy Distribution

We launched 1,000 single $\mu^{\pm}$, $e^{\pm}$, and $\pi^{\pm}$ at 4, 8,16, 25, 32, 40, 50, and 60 GeV toward the nominal beam center of H1 with a varying pseudorapidity range from -0.01 and 0.01 and a varying ϕ range of $\pm 0.5°$. The nominal beam center is determined based on the calculated center of gravity (weighted by the tower energy) as shown in Figs. 10 and 11, which is very consistent with the beam spot distribution seen in data (see Figs. 39 and 40).

Figures from 12 to 17 show the raw energy distributions in towers from muons, electrons and pions, respectively. The patterns of the energy distribution in towers are very consistent with the expectation (i.e., test beam mostly hit on tower 9 and 10 in H1, see Fig. 3 for tower numbering scheme). It is also clear to see a broadening of the distributions in towers in H2. Energies in H2 are mostly distributed in the 5th, 6th, 9th and 10th towers because of the hadronic shower spread.

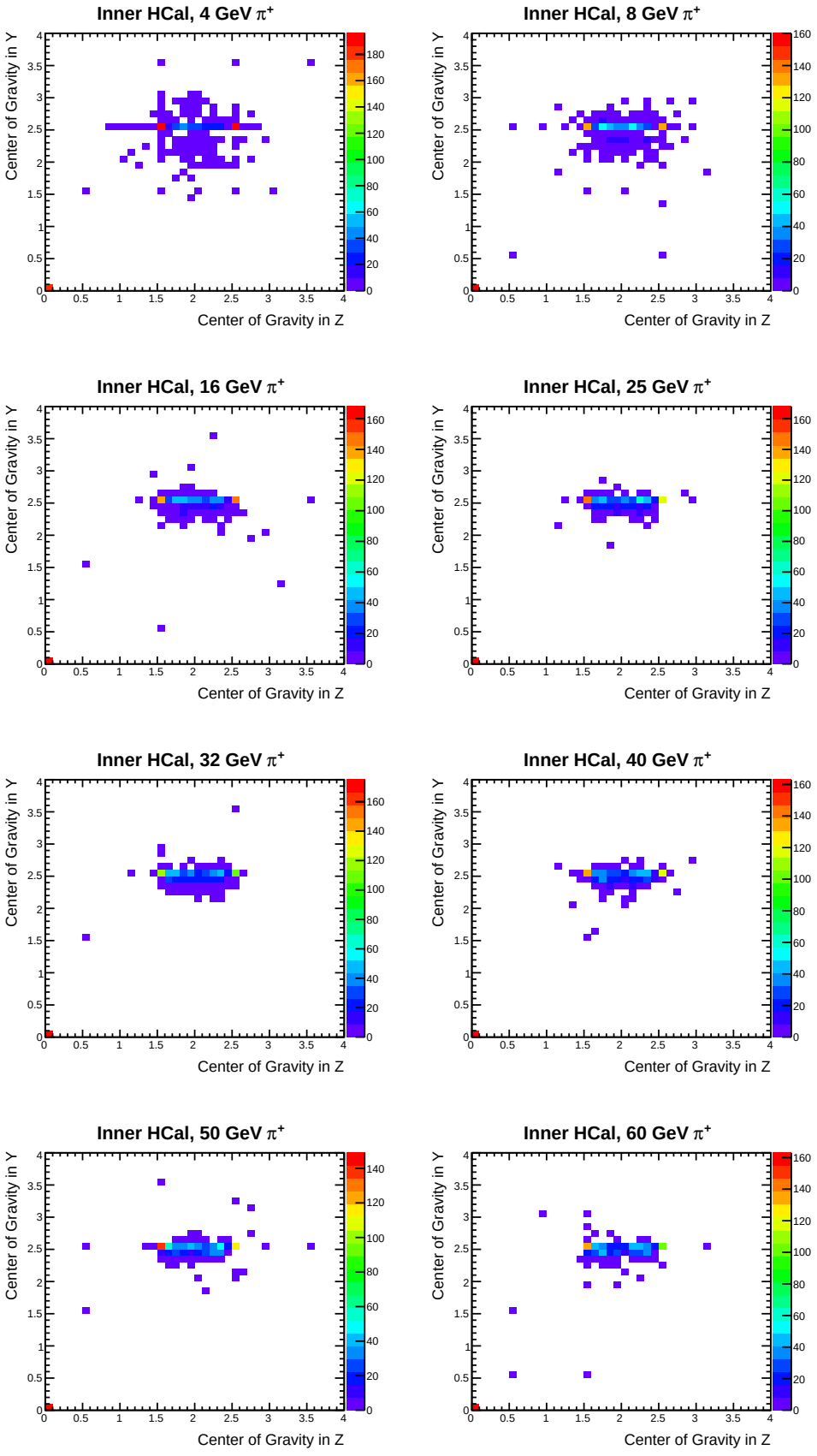

Figure 10: Beam spot distribution in simulation in H1.

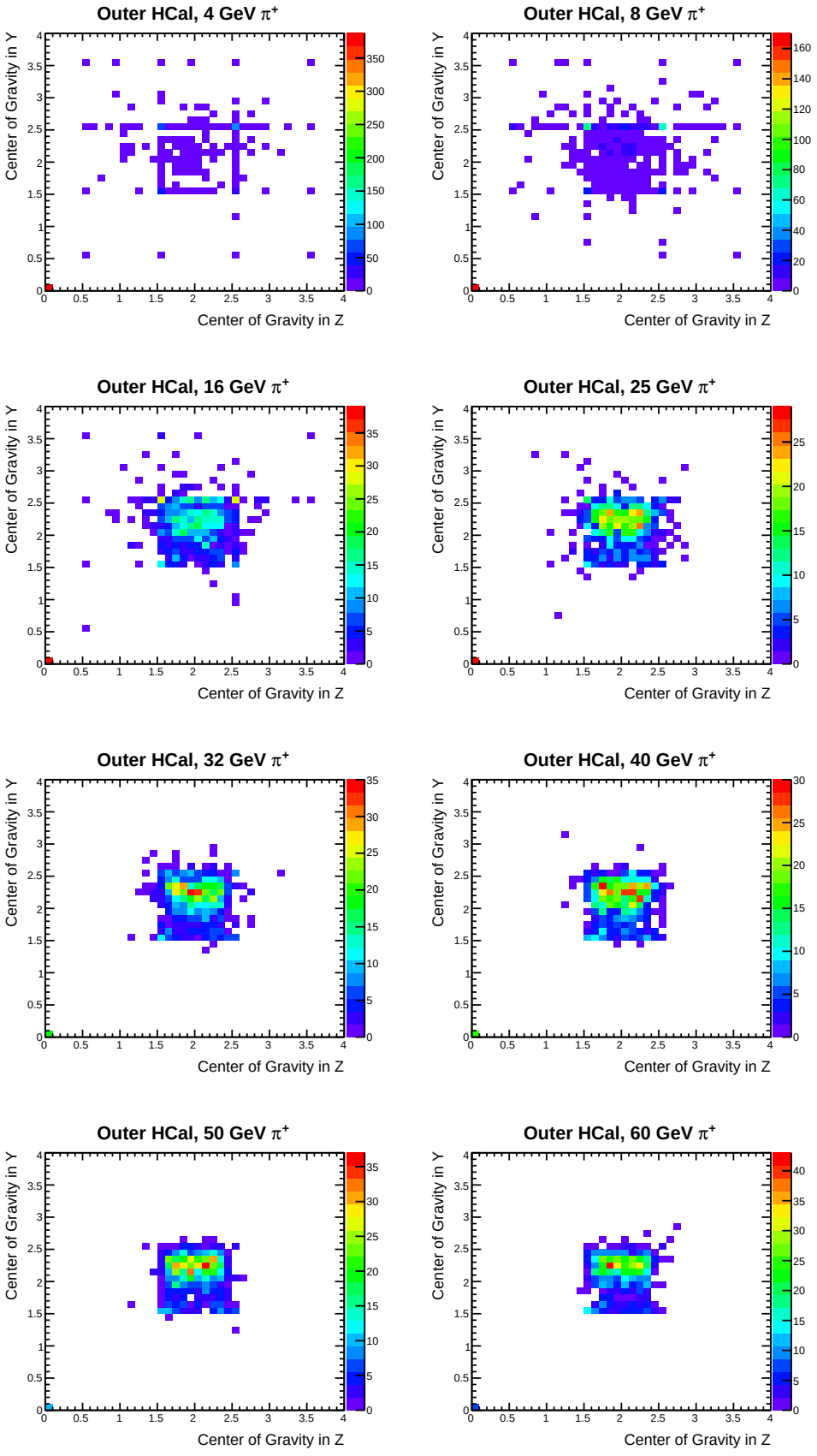

Figure 11: Beam spot distribution in simulation in H2.

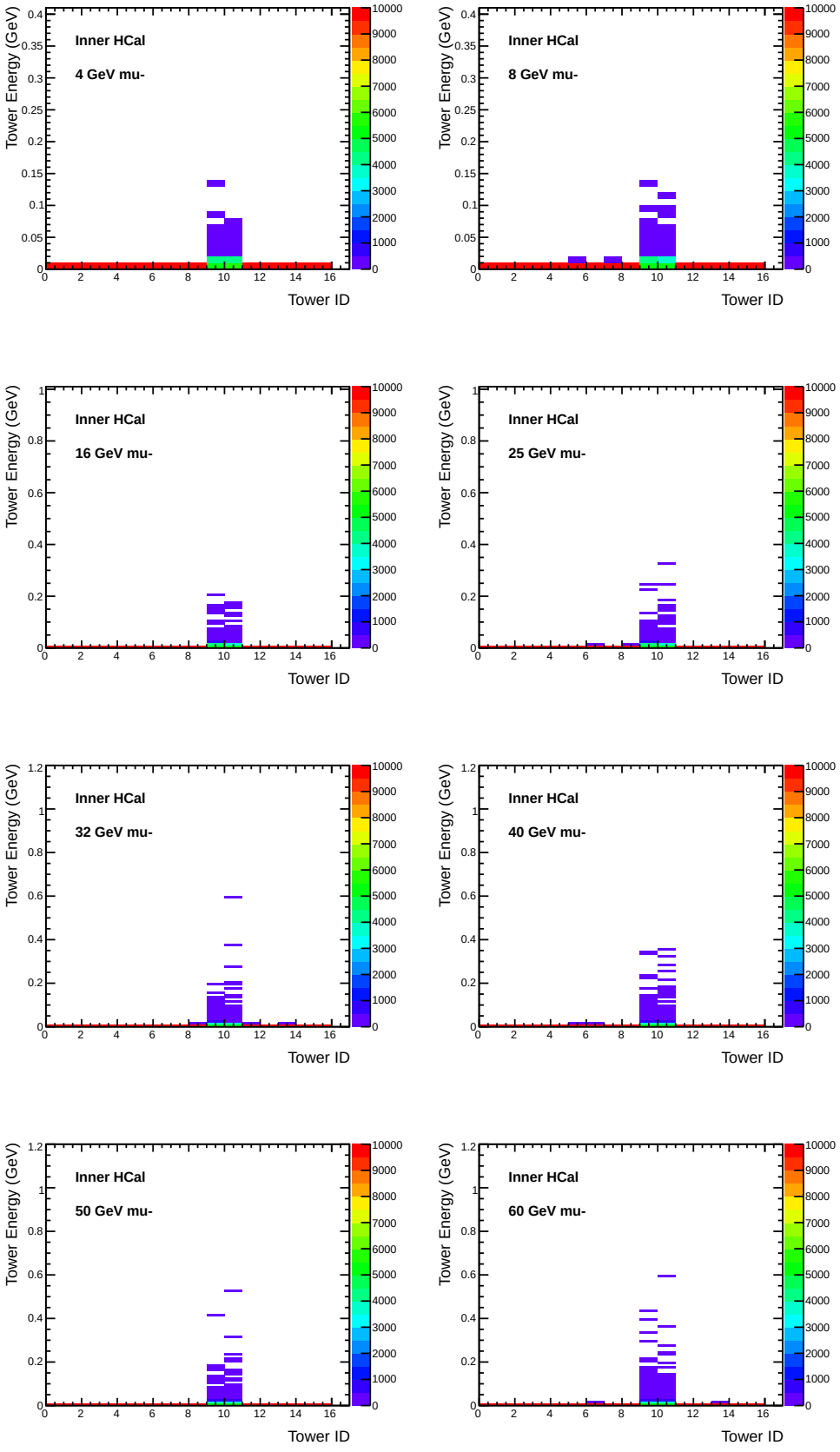

Figure 12: Simulated tower energy distributions in H1 for muons at 4, 8, 16, 25, 32, 40, 50 and 60 GeV.

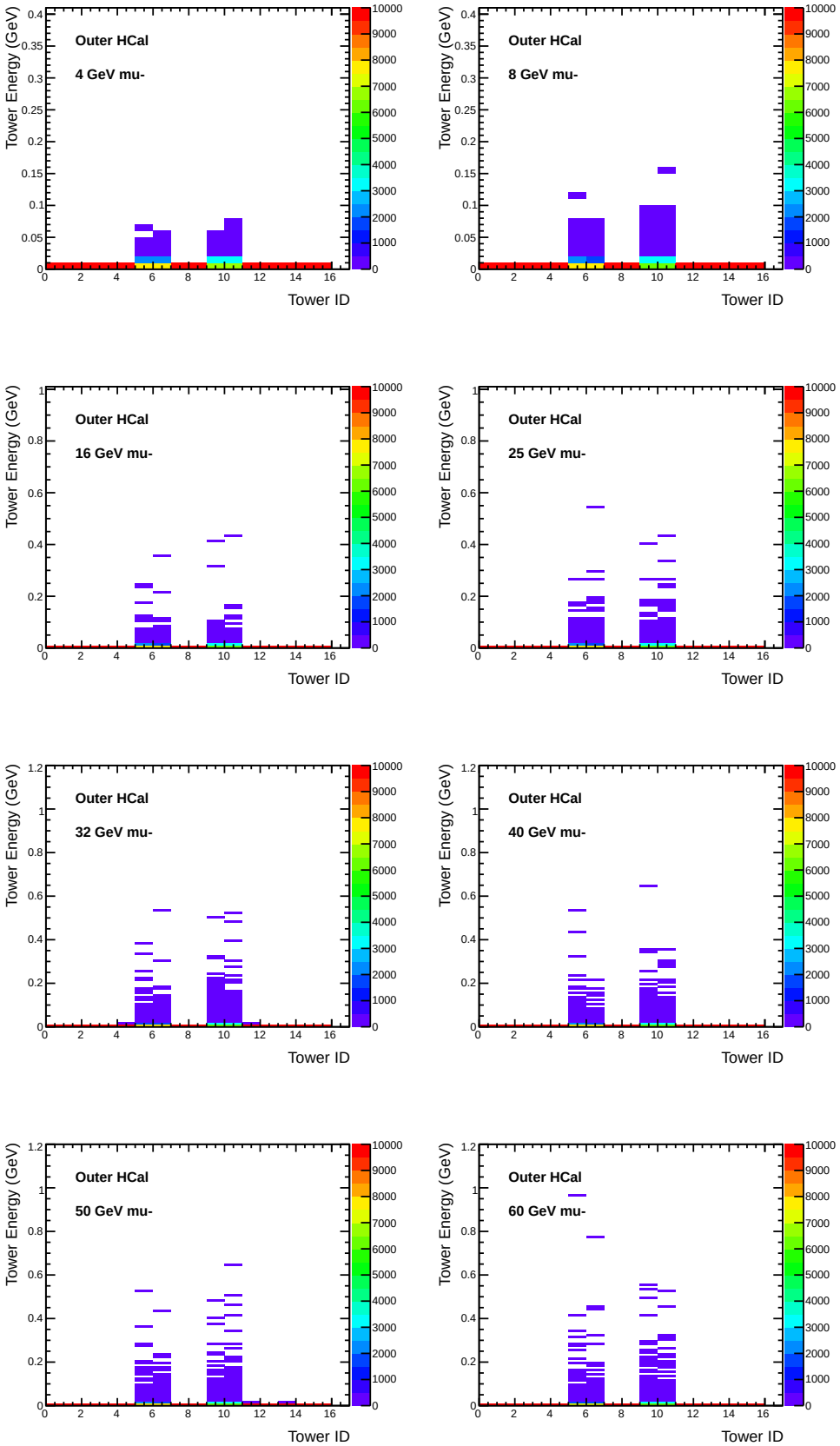

Figure 13: Simulated ower energy distributions in H2 for muons at 4, 8, 16, 25, 32, 40, 50 and 60 GeV.

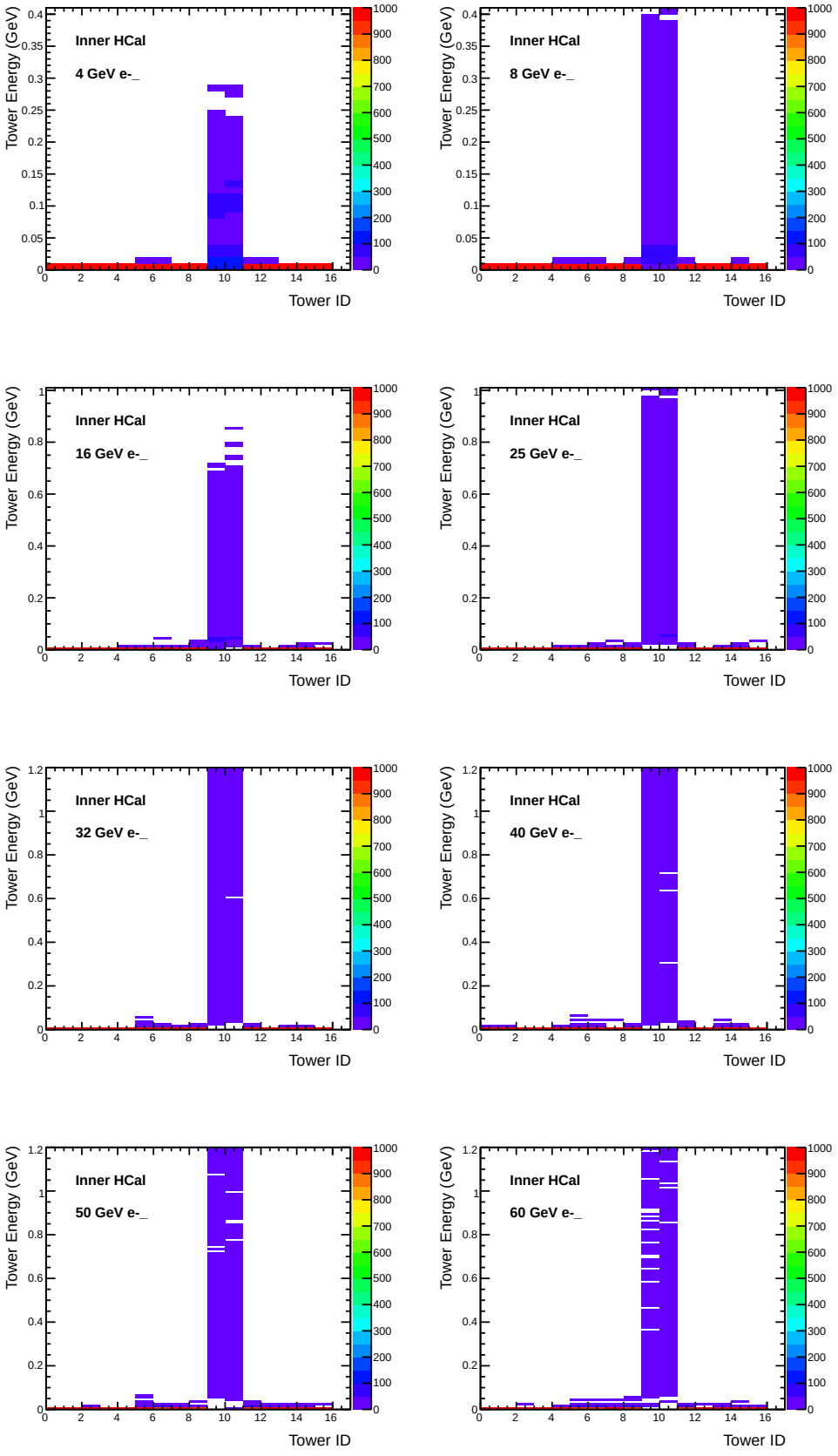

Figure 14: Simulated tower energy distributions in H1 for electrons at 4, 8, 16, 25, 32, 40, 50 and 60 GeV.

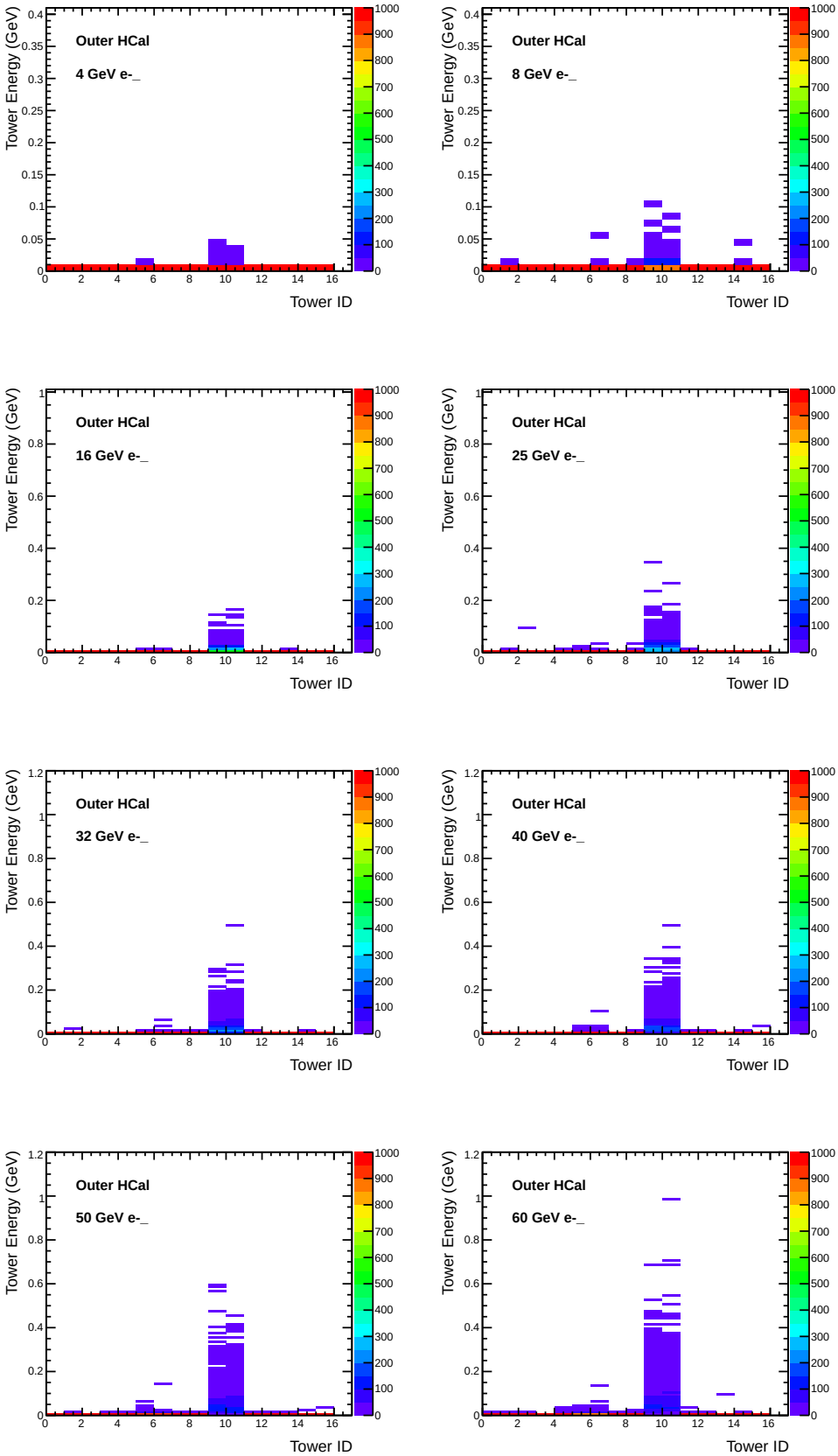

Figure 15: Simulated tower energy distributions in H2 for electrons at 4, 8, 16, 25, 32, 40, 50 and 60 GeV.

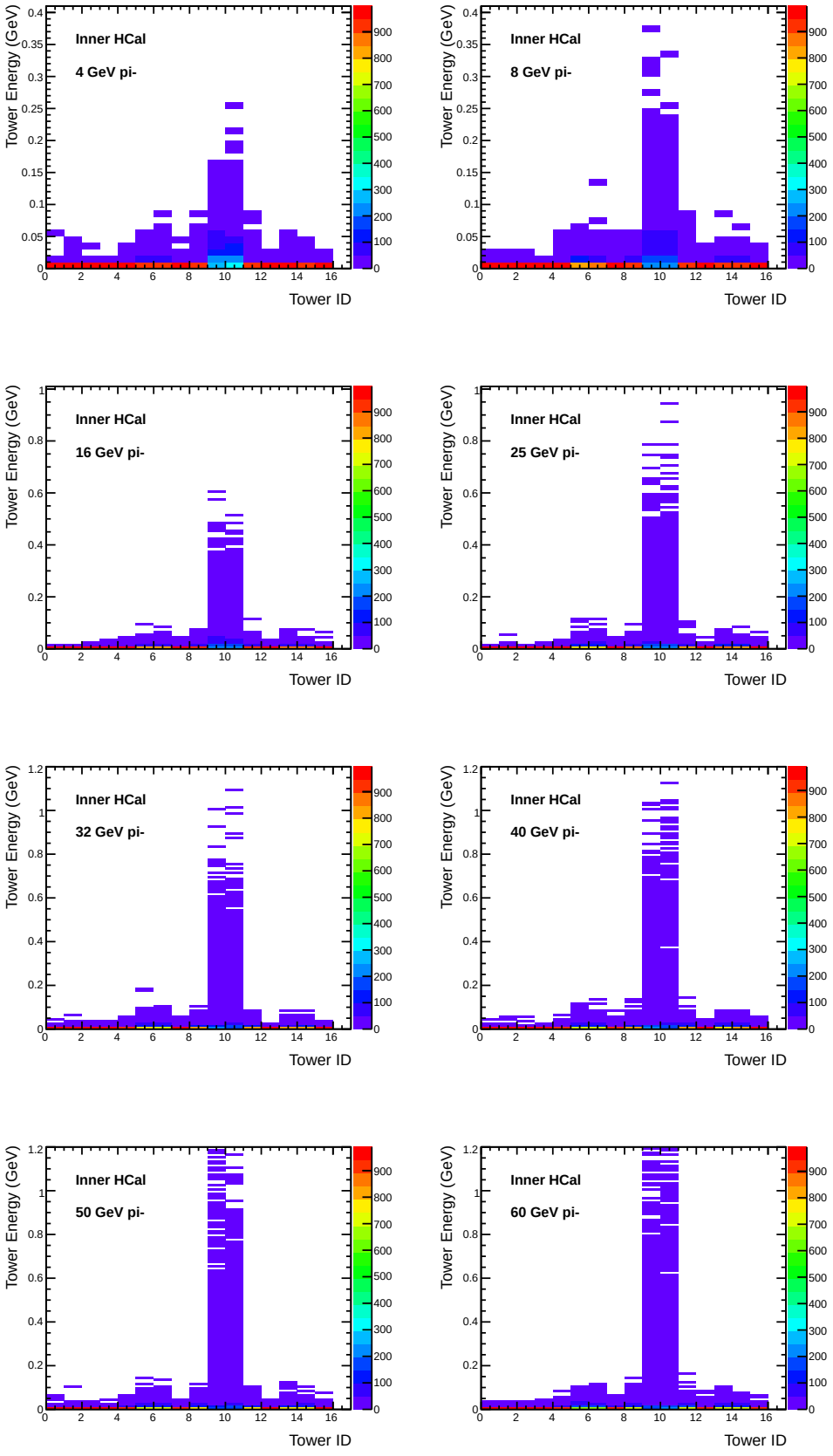

Figure 16: Simulated tower energy distributions in H1 for pions at 4, 8, 16, 25, 32, 40, 50 and 60 GeV.

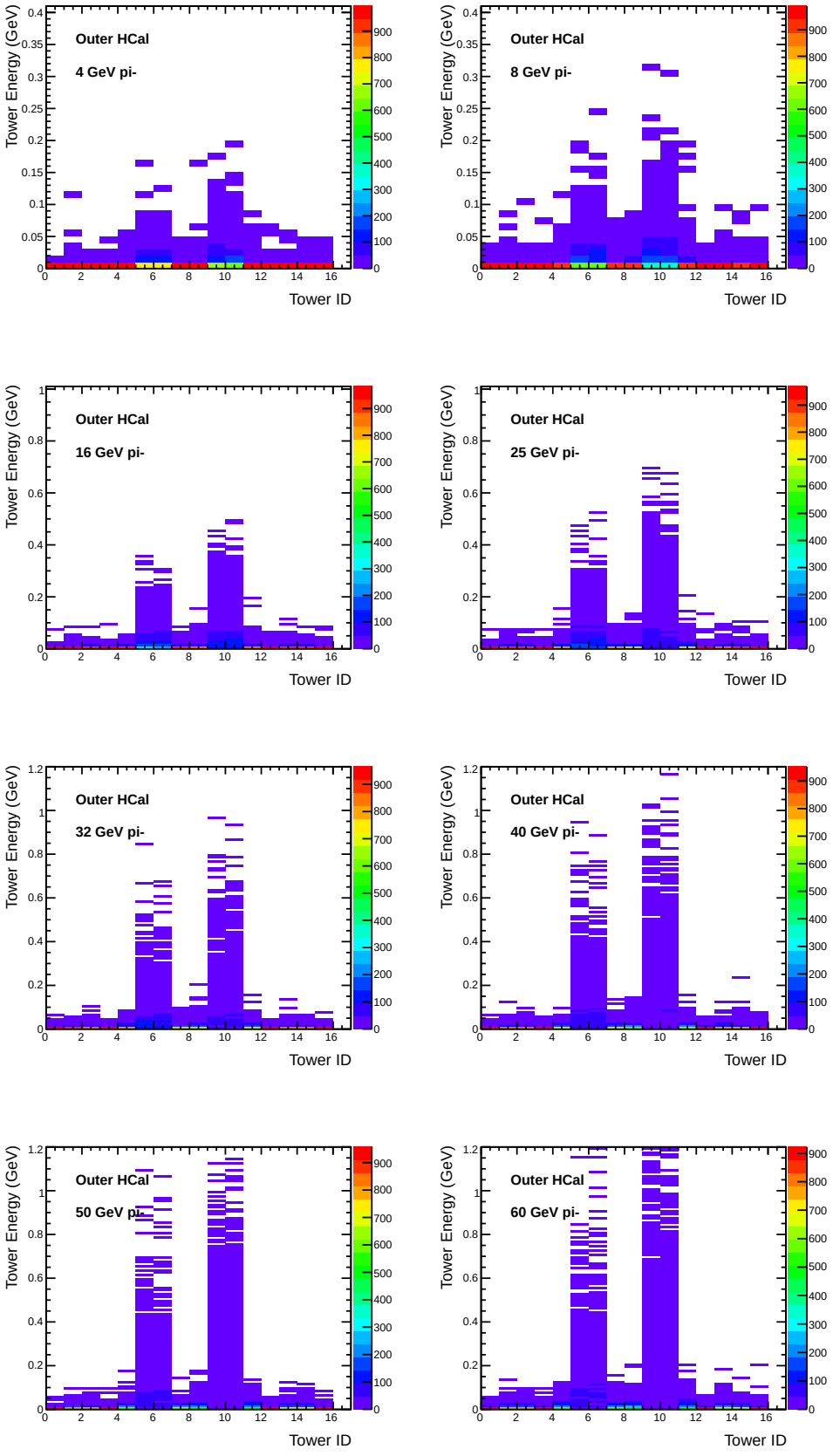

Figure 17: Simulated tower energy distributions in H1 for pions at 4, 8, 16, 25, 32, 40, 50 and 60 GeV.

3.4.2 Single Particle Response

The total raw energy in the scintillator (i.e., energy response) is calculated by summing up the deposited energy in each tower both in H1 and H2. We also studied the energy response with different energy thresholds in towers at 5, 10, 15 and 20 MeV (see Figs. from 12 to 17 for the tower energy distributions). The results are shown in Fig. 18. A given tower energy is excluded in the energy summation if the tower energy is below the chosen energy threshold. As it is discussed in the later Section 3.4.5, the energy resolution gets worse for higher tower energy threshold cuts.

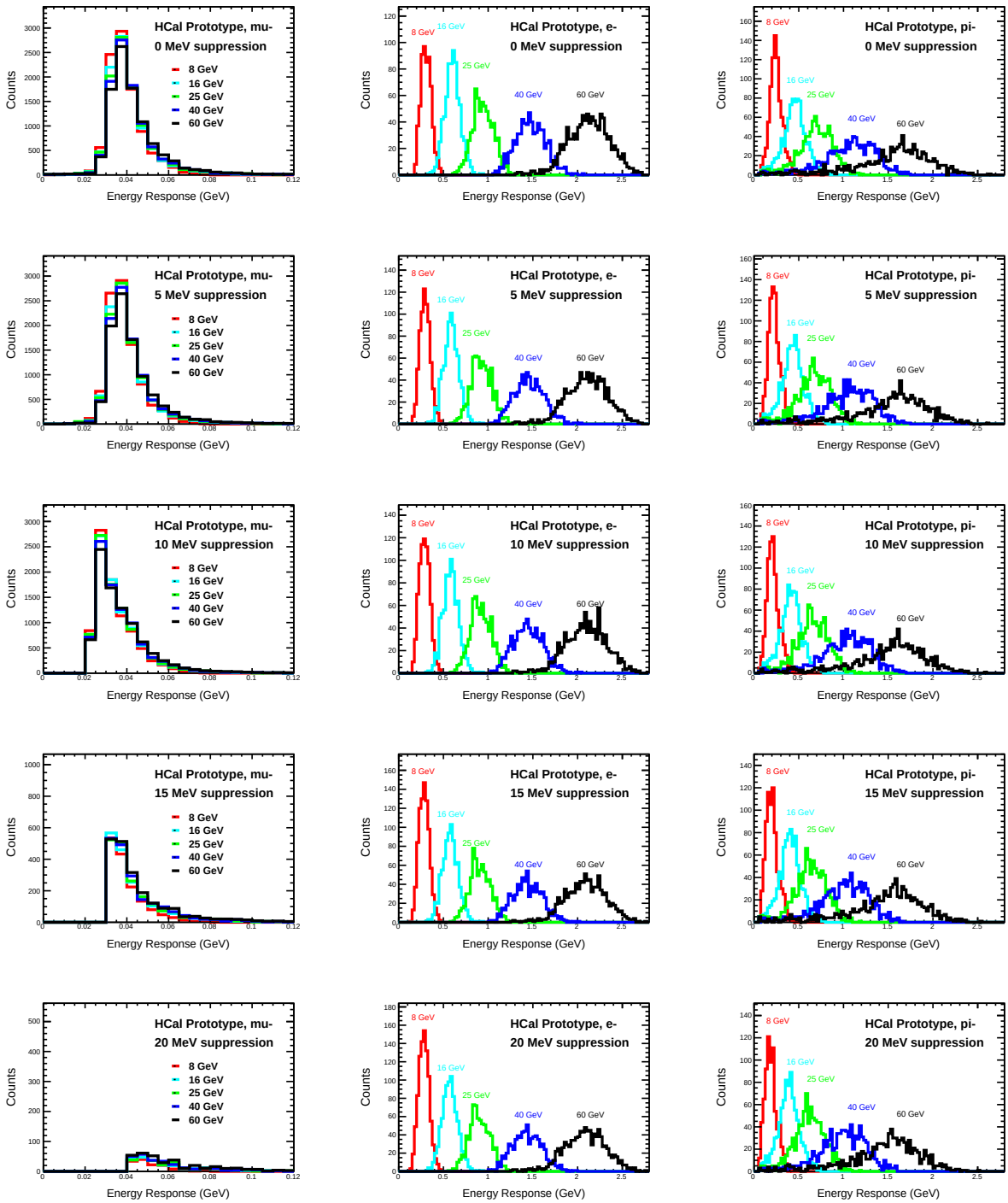

Figure 18: Simulated energy responses for negatively charged muons (left panels), electrons (middle panels), and pions (right panels) with different tower energy thresholds at 5, 10, 15 and 20 MeV from the top row to the bottom row.

3.4.3 Sampling Fraction Factor

The sampling fraction factor represents the sampling power of a calorimeter which is determined by running single muon simulation. The sampling fraction factor can be calculated in two ways. One is evaluated by directly dividing the visible energy by the total deposited energy (visible plus invisible energy in absorbers) from the muons in the whole detector. Figure 19 shows the sampling fraction factor distributions for muons at energies of 2, 4, 6 and 100 GeV using this method.

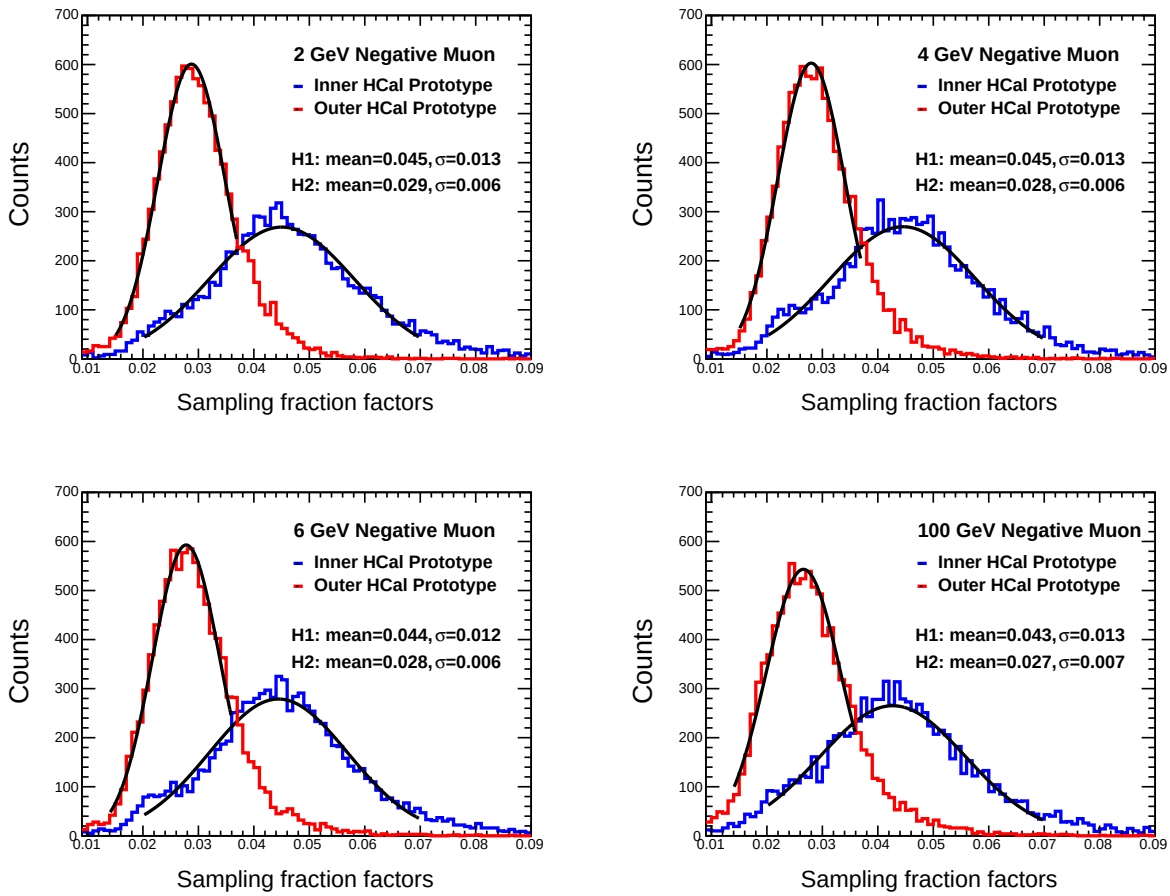

Figure 19: Sampling fraction factors calculated using muons at different energy from simulation.

The second method of determining the sample fraction factor is given as follows:

$$SF = \frac{dE/dx(\mu) \times L(scint)}{dE/dx(\mu) \times L(scint) + dE/dx(\mu) \times L(abs)},$$

where dE/dx is obtained from [4] and is equal to 2.051 for muons for the scintillator we are using (C_8H_8) and 1.587 for Fe. The scintillator and the absorber lengths are obtained

from Geantino simulation as seen in Fig. 7. Figure 20 shows the sampling fraction factor determined with this method by Geantino simulations. The average sampling fraction factors for H1 and H2 calculated with this method is 0.044 and 0.030, respectively. These numbers are very consistent with the results from the first method.

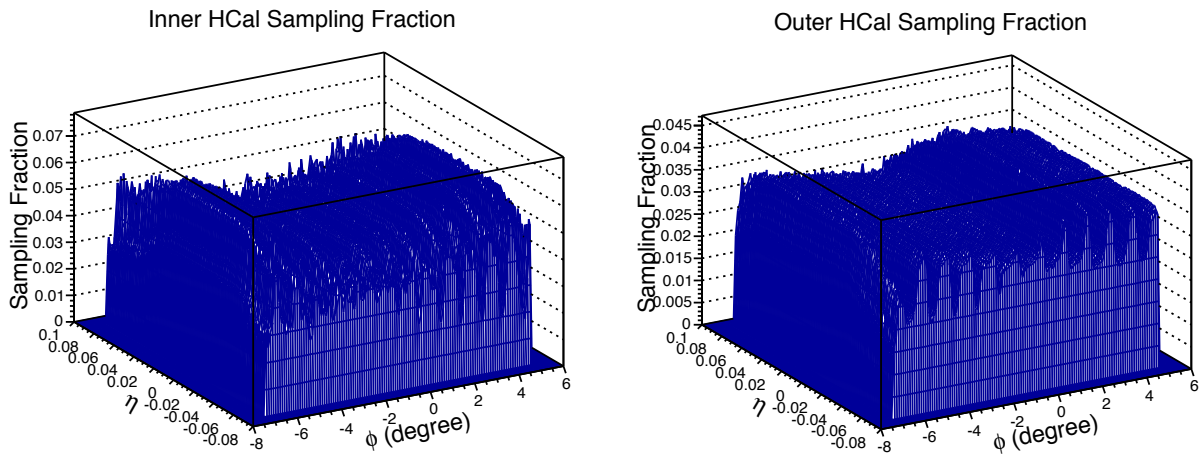

Figure 20: Left panel: sampling fractions for inner HCal prototype calculated with Geantinos. Right panel: sampling fractions for outer HCal prototype calculated with Geantinos.

3.4.4 Energy Reconstruction

Once the sampling fraction factor is obtained, it is relatively easy to reconstruct the total energy from the calorimeter response. We use the sampling fraction factors of 4.5% and 2.9% for the H1 and H2, respectively. The total reconstructed energy for muons, electrons and pions are shown in Fig. 21 at each tower energy threshold chosen. It is NOT surprising to see that the reconstructed total energy for muons is far less than the incident energy as expected since muons are simply traversing the whole detector.

It is also straightforward to calculate the energy asymmetry in H1 and H2. It is found that this is an important quantity one could use to differentiate the hadronic and electromagnetic showers. Figure 22 shows a compilation of the 2-D scatter plots between the reconstructed total energy and the energy asymmetry for particle energies at 4, 8, 16, 25, 32, 40, 50 and 60 GeV. The red points are from electrons, blue for muons and black for pions. It is clear to see that one could apply a proper cut in combination with the energy asymmetry and the total energy for identifying the particle type by the two-segment calorimeter. A set of particle identification cuts extracted based on the energy asymmetry distribution (Fig 23) and the total energy distribution (Fig 24) is shown in Table 4. It turns out that we could use this cut in the test beam data analysis to quantity the particle composition in the test beam at each beam energy. See Section 5.2 for details.

Table 4: Cuts extracted from GEANT4 simulation for particle identification in the test beam.

Beam Energy	Pions	Electrons	Muons
4 GeV	$E_{total} > 1$ GeV $-1.0 \leq E_{asy} < 0.7$	$E_{total} > 1$ GeV $0.9 < E_{asy} \leq 1.0$	$E_{total} < 2$ GeV $-0.8 < E_{asy} < 0.5$
8 GeV	$E_{total} > 2$ GeV $-1.0 \leq E_{asy} < 0.7$	$E_{total} > 2$ GeV $0.9 < E_{asy} \leq 1.0$	$E_{total} < 2$ GeV $-0.8 < E_{asy} < 0.5$
16 GeV, 25 GeV	$E_{total} > 2$ GeV $-1.0 \leq E_{asy} < 0.6$	$E_{total} > 2$ GeV $0.8 < E_{asy} \leq 1.0$	$E_{total} < 5$ GeV $-0.8 < E_{asy} < 0.5$
32 GeV, 40 GeV	$E_{total} > 2$ GeV $-1.0 \leq E_{asy} < 0.55$	$E_{total} > 2$ GeV $0.75 < E_{asy} \leq 1.0$	$E_{total} < 5$ GeV $-0.8 < E_{asy} < 0.5$
50 GeV, 60 GeV	$E_{total} > 2$ GeV $-1.0 \leq E_{asy} < 0.4$	- -	$E_{total} < 5$ GeV $-0.8 < E_{asy} < 0.5$

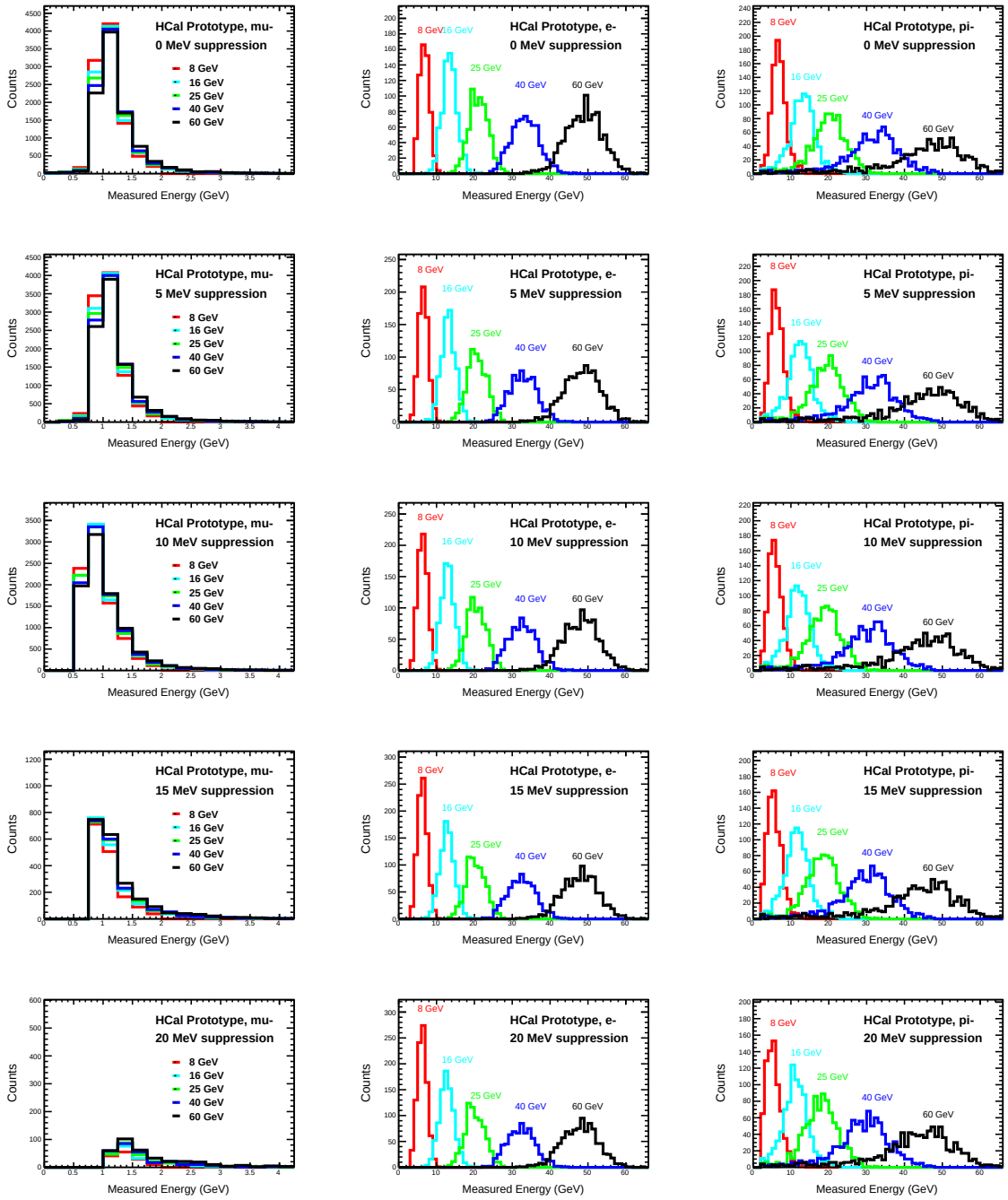

Figure 21: Total reconstructed energy spectrums from simulations for muon (left), electron (middle) and pion (right) as a function of beam energy with different tower energy thresholds.

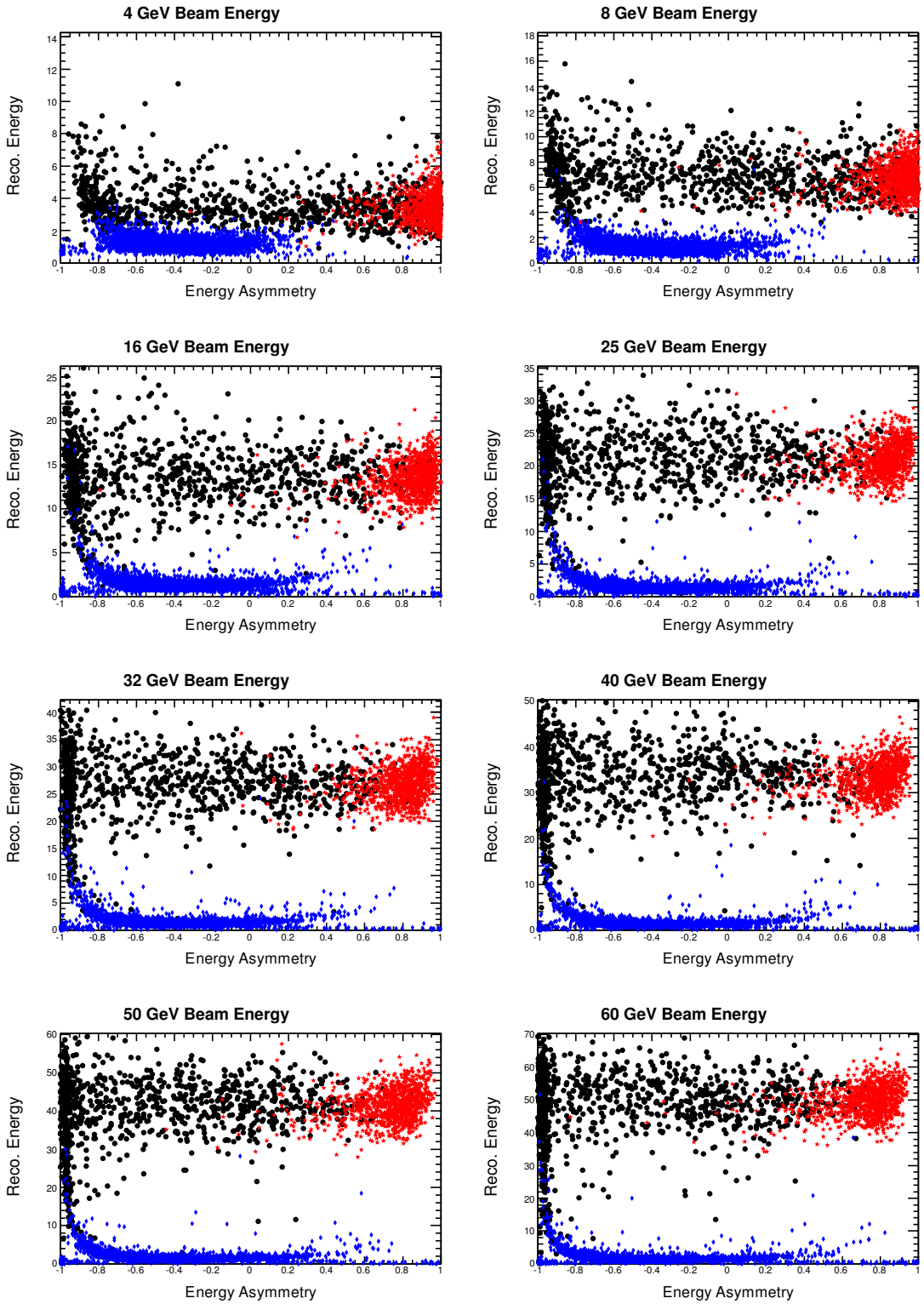

Figure 22: Total reconstructed energy from simulations for muons (blue), electrons (red), and pions (black) as a function of the energy asymmetry for beam energy from 4 to 60 GeV.

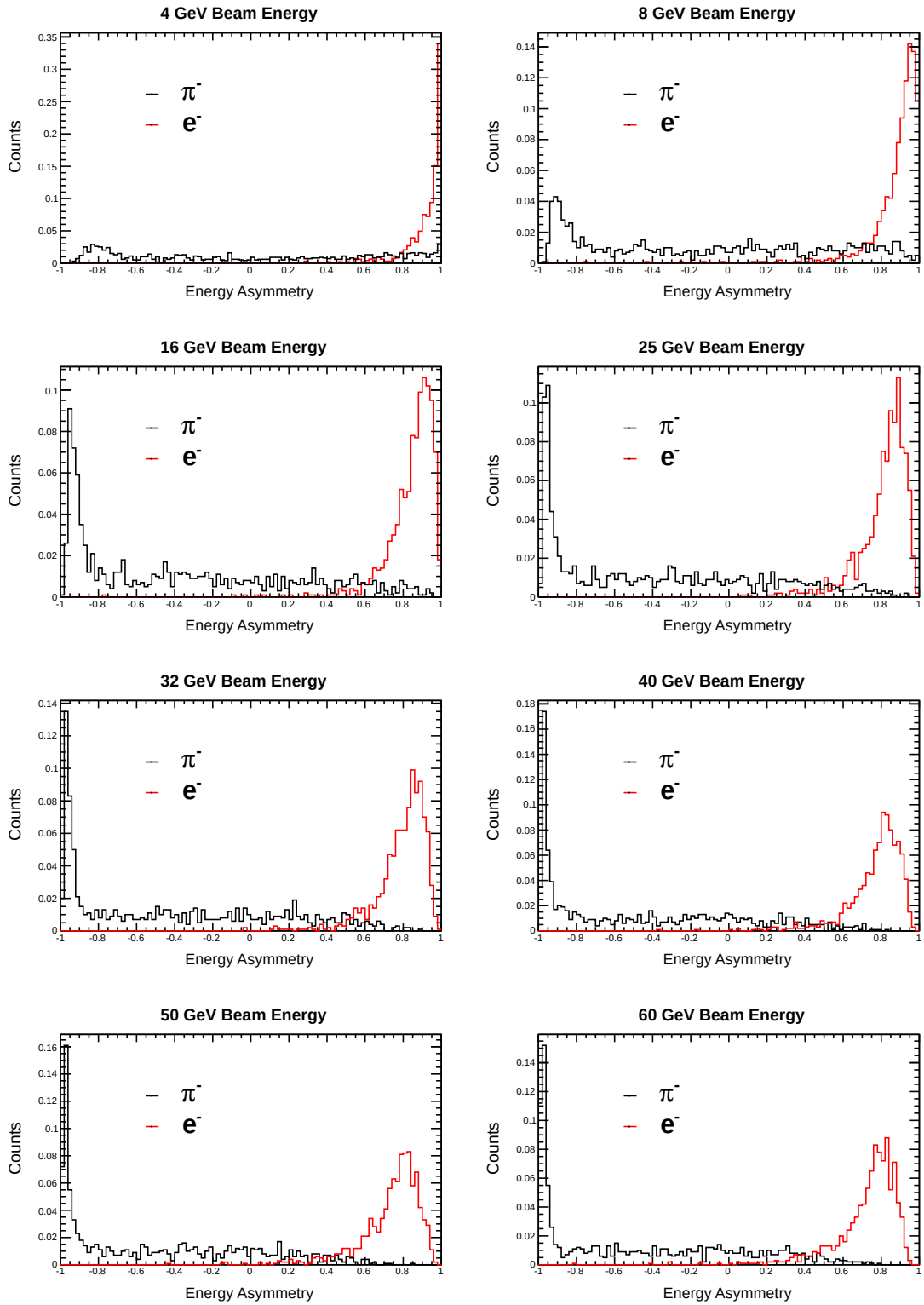

Figure 23: Energy asymmetry distributions for electrons (red), and pions (black) for beam energy from 4 to 60 GeV.

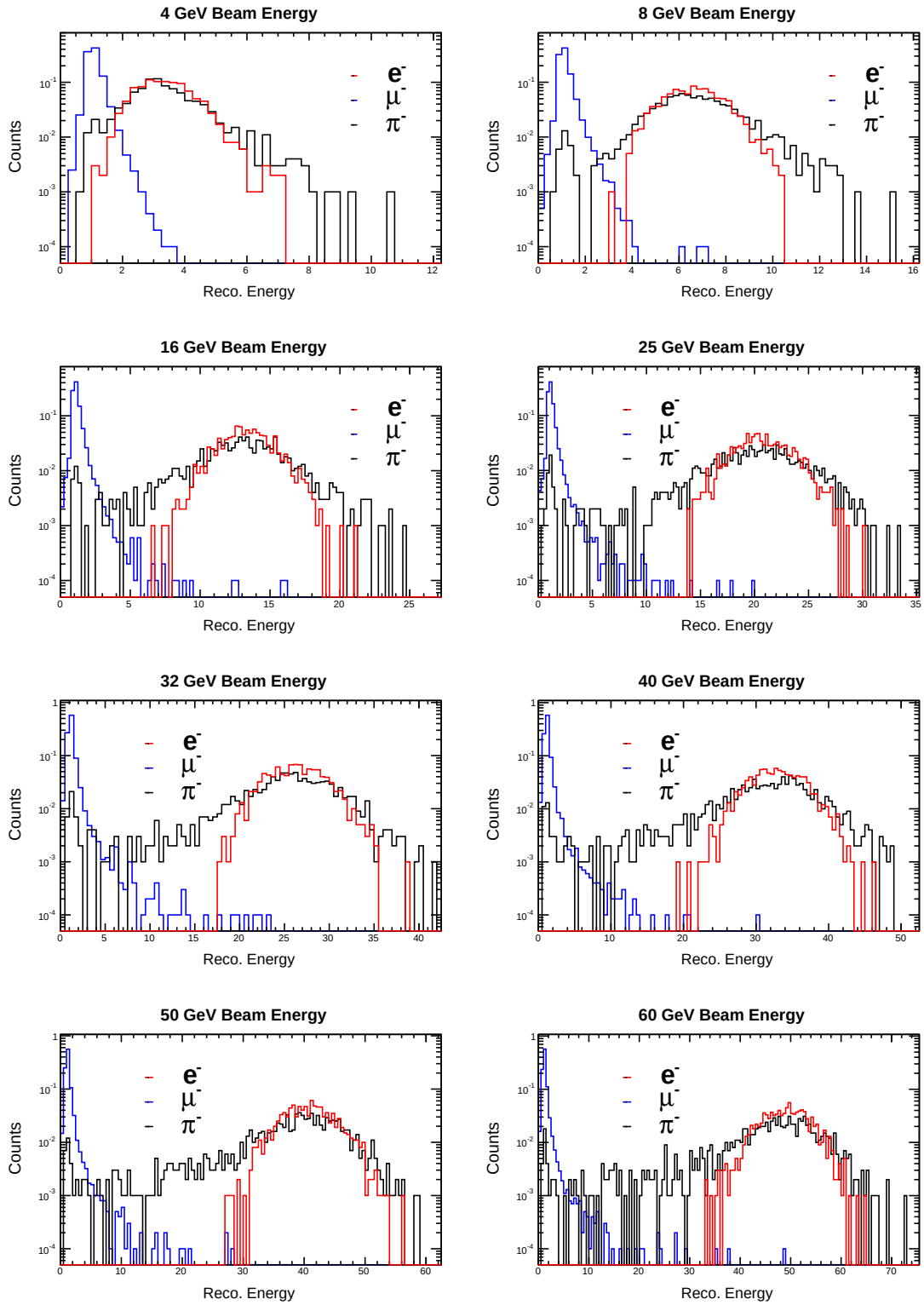

Figure 24: Reconstructed energy distributions for electrons (red), and pions (black) for beam energy from 4 to 60 GeV.

3.4.5 Energy Resolution and Linearity

Using the reconstructed energy distributions we are able to extract the fundamental properties of a calorimeter, i.e., its energy resolution and linearity, from the simulation. The particle identification cuts in Table 4 is also applied to simulation to make a meaningful comparison with the measured results from the test beam data as discussed in Section 5.7.

Since the energy resolution for detecting the original particle is highly dependent on the fluctuations occurring in the shower development especially if the sampling fraction is larger than 1% as described in [6], we make a cut on the tower energy threshold and then determine the energy resolution at each threshold value. The results are shown in Fig. 25 with standard calorimeter resolution fits. A few observations are given as follows:

- The energy resolution gets worse for higher tower energy threshold cuts. This is understandable because of larger fluctuations at higher tower thresholds. The constant term of the fit seems decreasing as the increasing of the energy.
- It is clear to see that the energy resolution for electrons is better for pions. This is also consistent with the expectation since at the same energy the electromagnetic showers have no equivalent fluctuations at the nuclear level as for hadronic showers [6].
- The constant term for electrons stays the same at about 7%.

The calorimeter energy linearity is given in Fig. 26. For electrons, there is a near perfect linearity. However, one starts to see slight deviations at higher tower energy thresholds as one would expect.

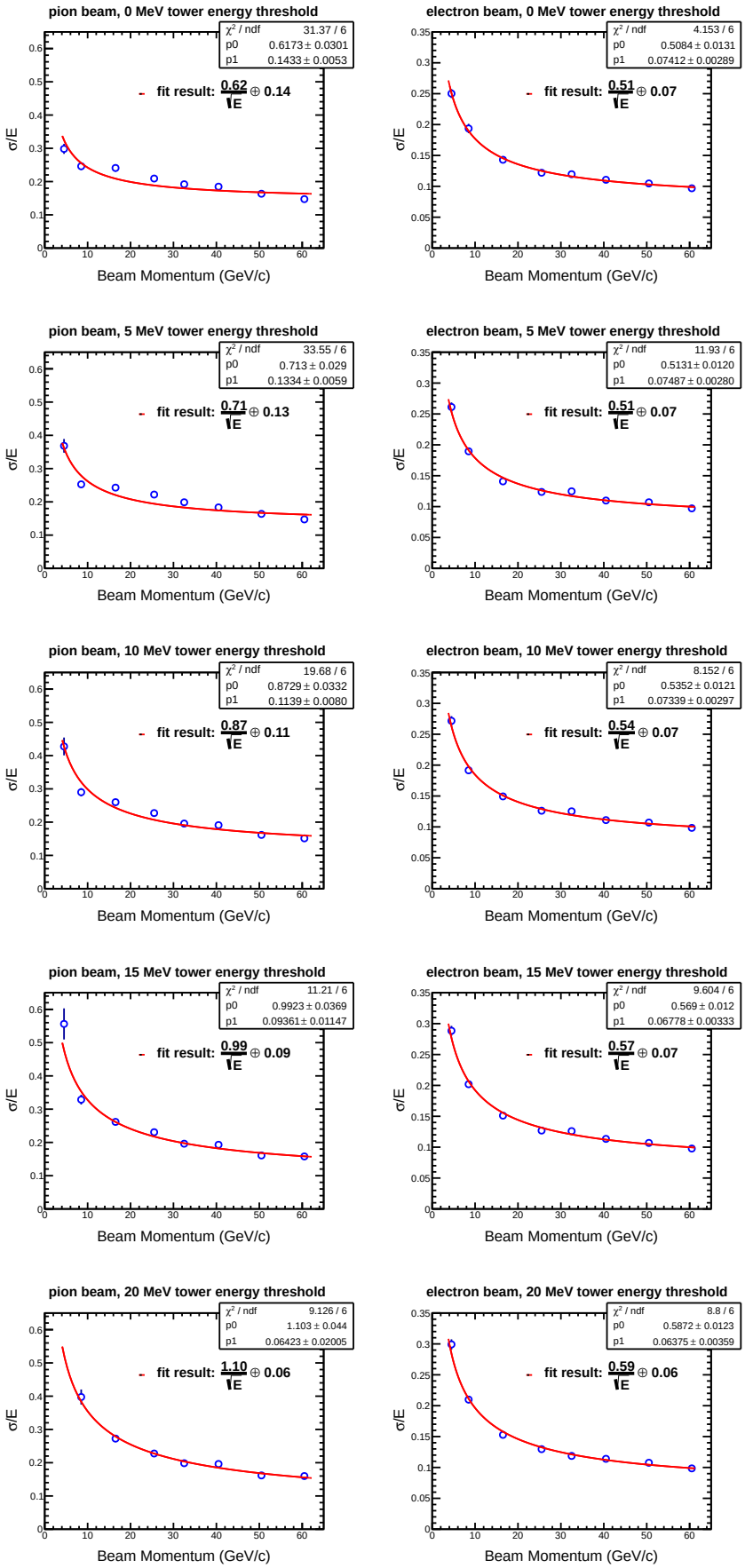

Figure 25: Energy resolution obtained from simulation for pions and electrons with different tower energy threshold cuts.

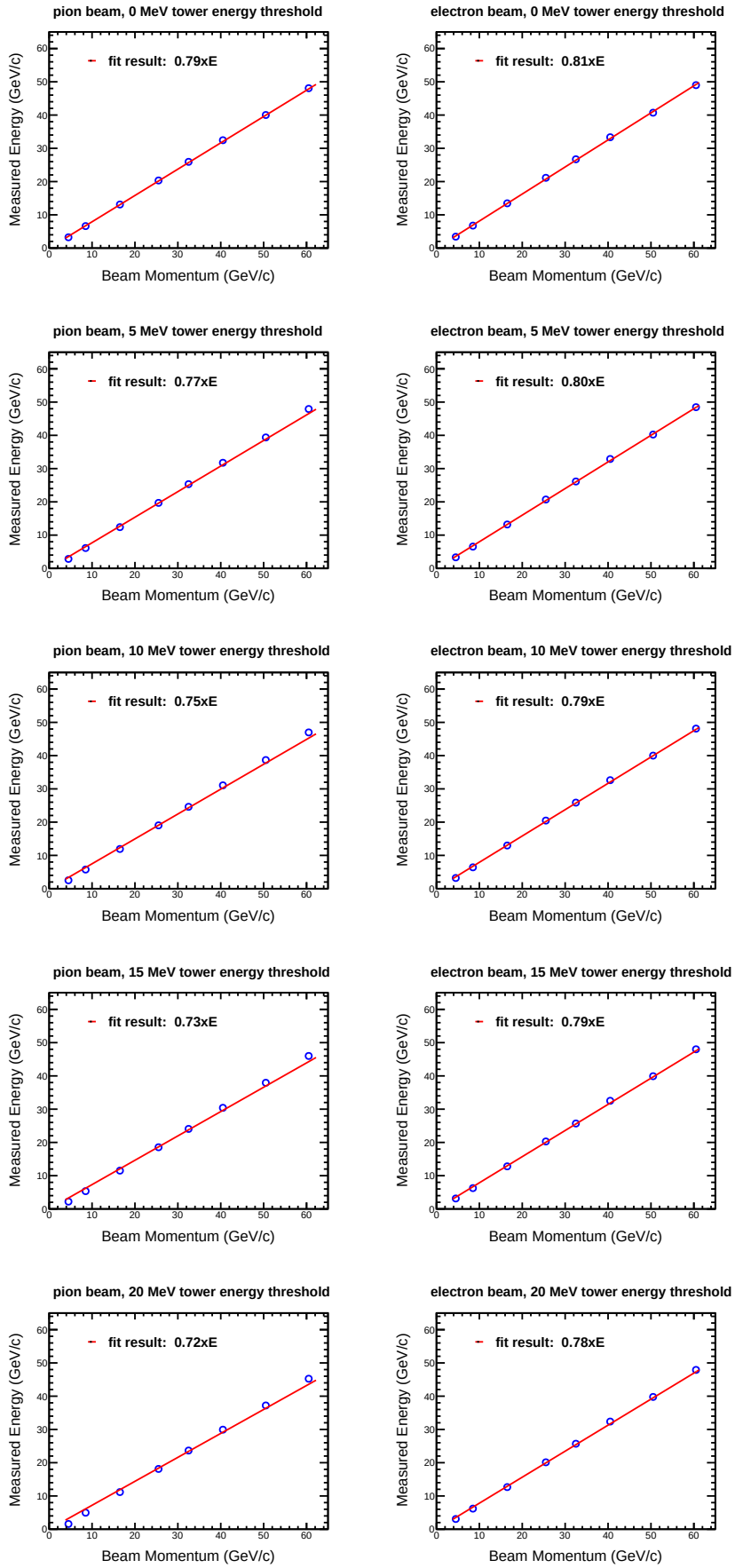

Figure 26: Energy linearity obtained from simulation for pions and electrons with different tower energy threshold cuts.

3.4.6 Energy Leakage

To quantify the longitudinal and lateral energy leakage of the HCal prototype, the HCal prototype detector is shielded at the back, left, right, top and bottom as shown in Fig. 27 using the sPHENIX default "black hole" material (close to vacuum). All tracks reaching to the inside of the shielding material are stopped and their kinetic energies are recorded as the deposited energy. The deposited energy recorded inside each of the side-block and their sum (called the total external energy leakage) are shown in Fig 28. The peak value of the total external energy leakage as shown in black square in Fig 28 (in upper left panel) are determined by Landau fits as shown in Fig 29. The results is very consistent with the energy leakage documented in the MIE proposal.

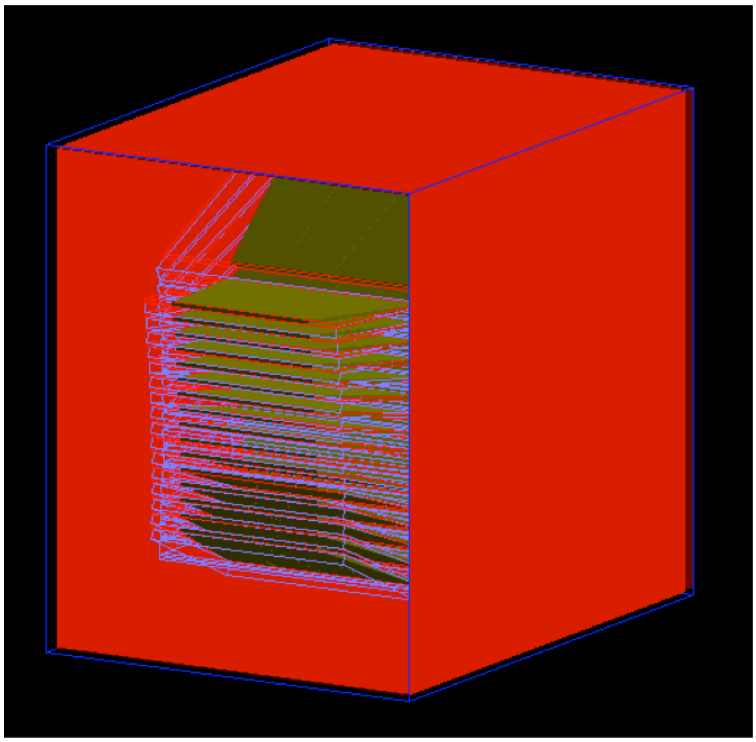

Figure 27: HCal prototype detector shielded by five blocks of material at the back, left, right, top and bottom.

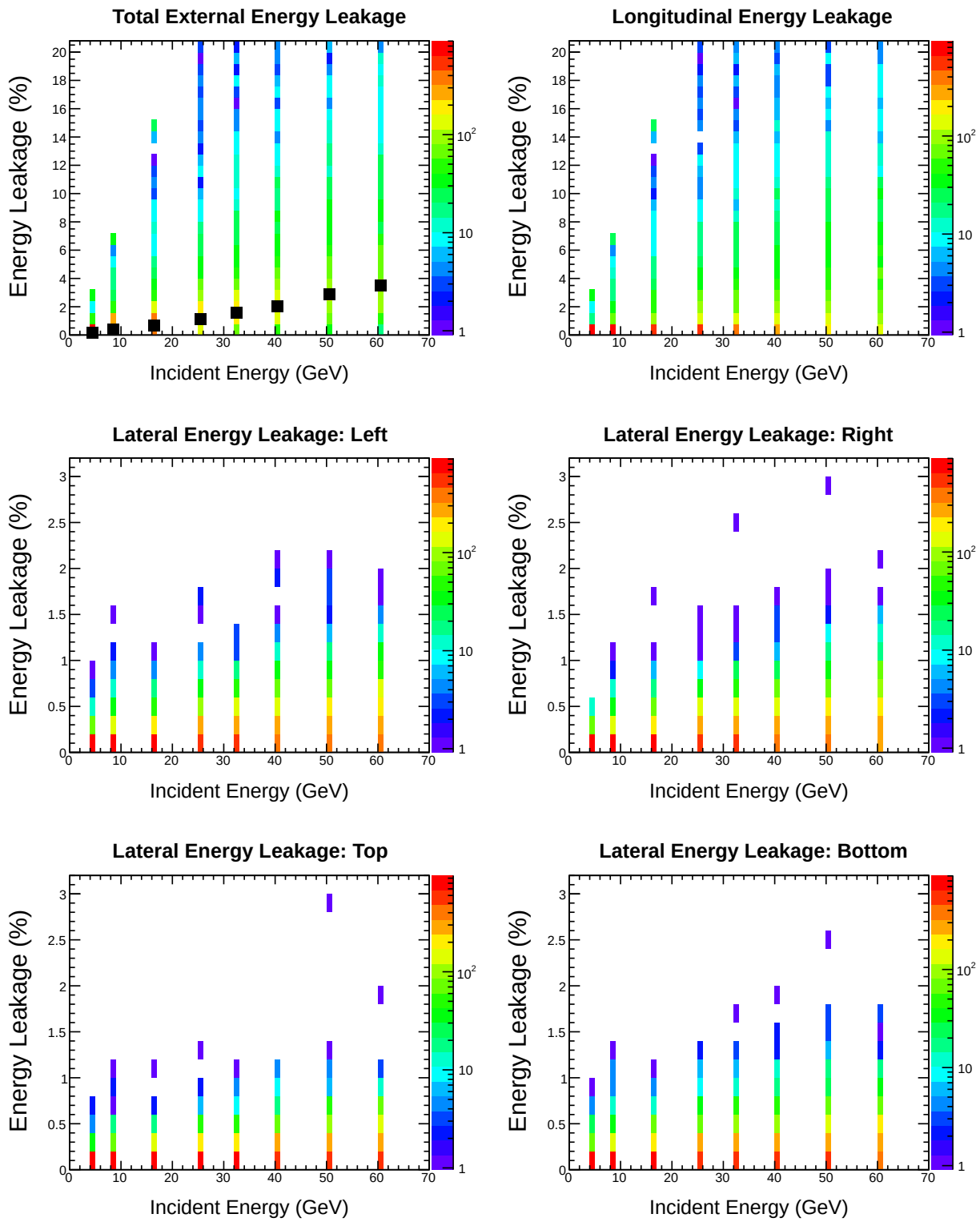

Figure 28: The total energy leakage (to the outside of the HCal) and the energy leakage contributed from each of the side-block at the back (i.e., longitudinal), left, right, top and bottom of the HCal calculated from the simulation.

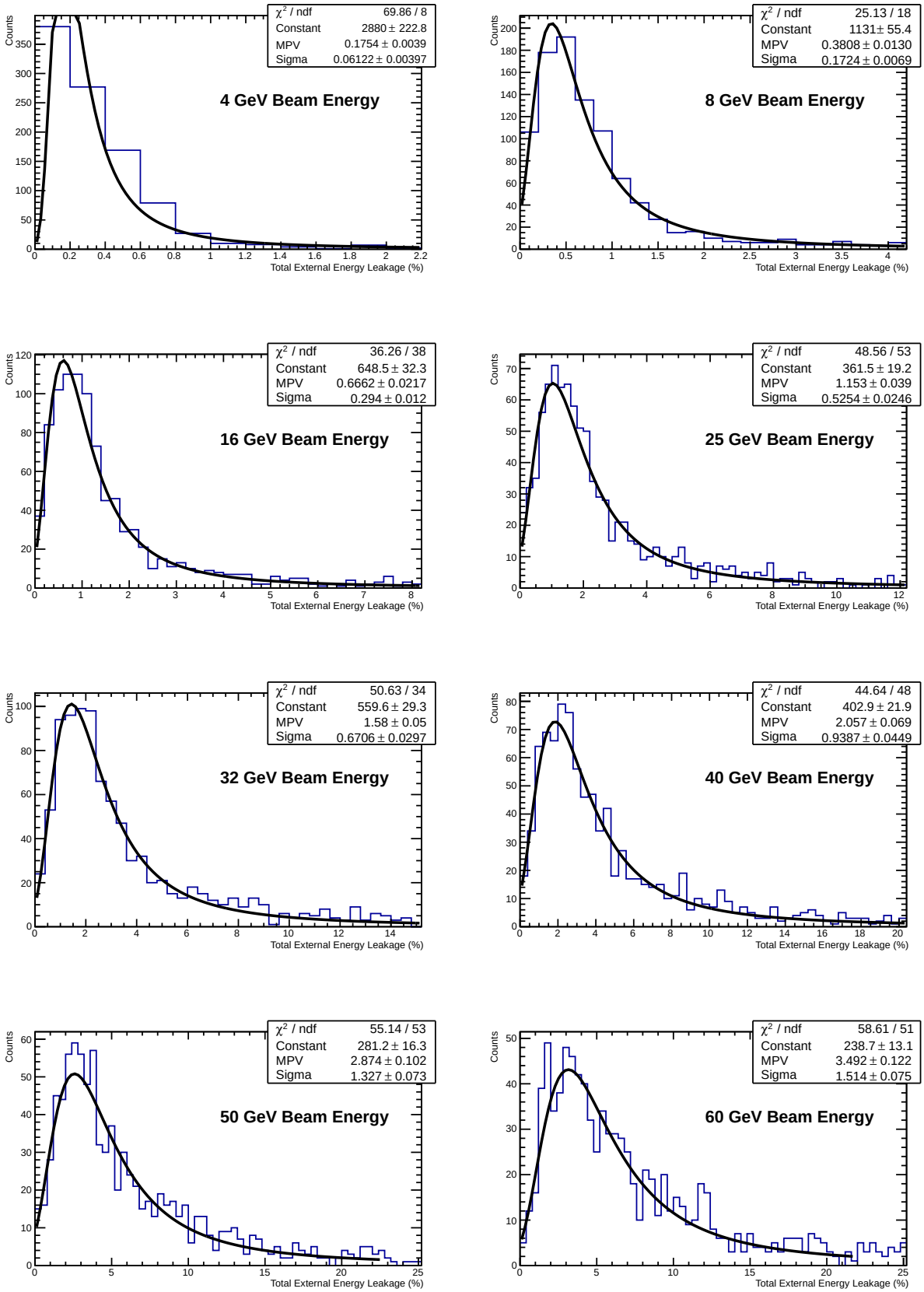

Figure 29: Total external energy leakage fitted by Landau distributions.

3.4.7 e/π Ratio

The e/π ratio of the HCal prototype is evaluated via formula:

$$e/\pi = \frac{\langle E_e \rangle}{\langle E_\pi \rangle} \ , \tag{1}$$

where $\langle E_e \rangle$, and $\langle E_\pi \rangle$ are the mean total reconstructed energy for electron and pions as shown in Fig 26. The results in shown in Fig 30.

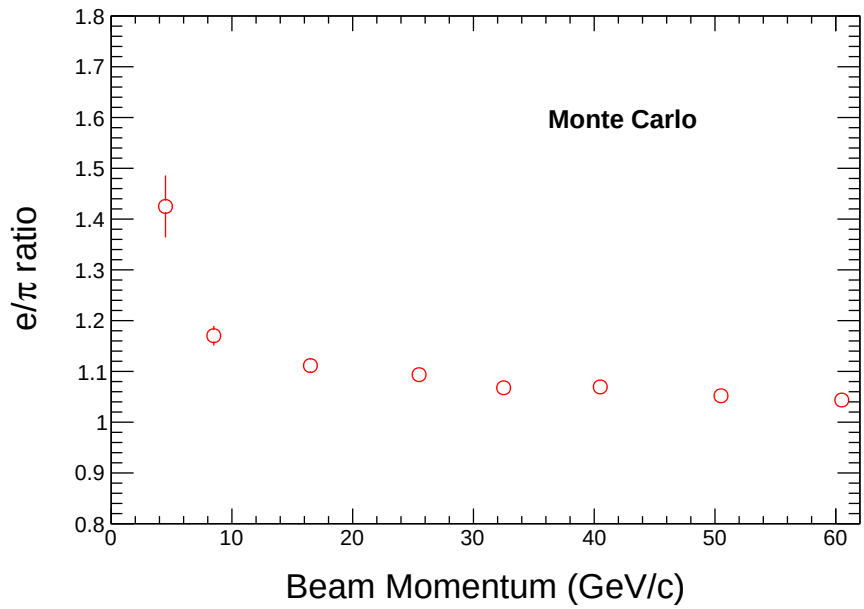

Figure 30: e/π ratio evaluated with single electrons and single pion from simulation with tower energy cut of 15 MeV.

3.4.8 Cosmic Muon Simulation

We used comic rays for the energy calibration and simulated the cosmic muons entering to the top of the detector at an average energy of 4 GeV. An event display is shown in Fig. 31 as an example. Figures 32 and 33 show the histograms of the deposited energy in each tower both in H1 and H2 segments from 250k muons launched vertically downward to the top of the calorimeter at 4 GeV energy. We also simulated for muons at 2 and 6 GeV and the tower energy distributions are pretty much the same. The mean energy loss in each tower is about 5.5 MeV which will be used for calibrating the energy measured in the calorimeter in the test beam.

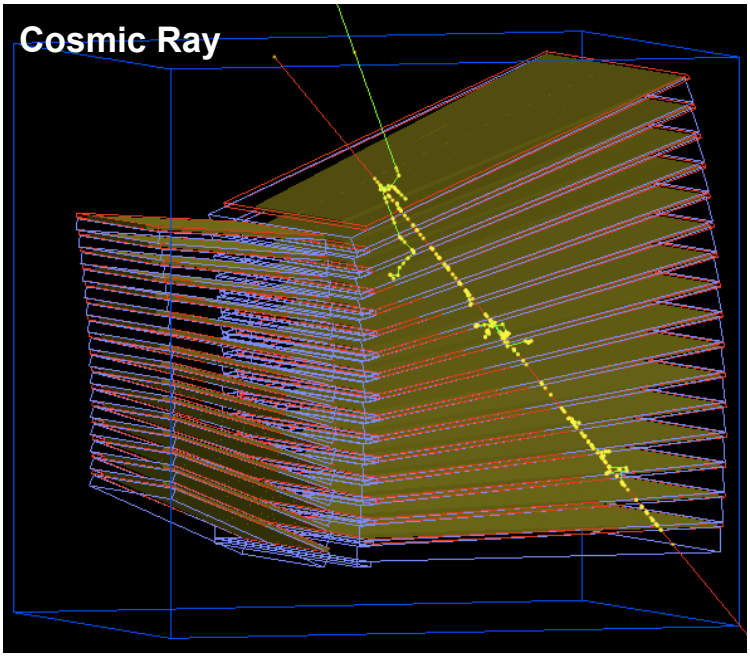

Figure 31: Event display for a cosmic ray event in the HCal prototype.

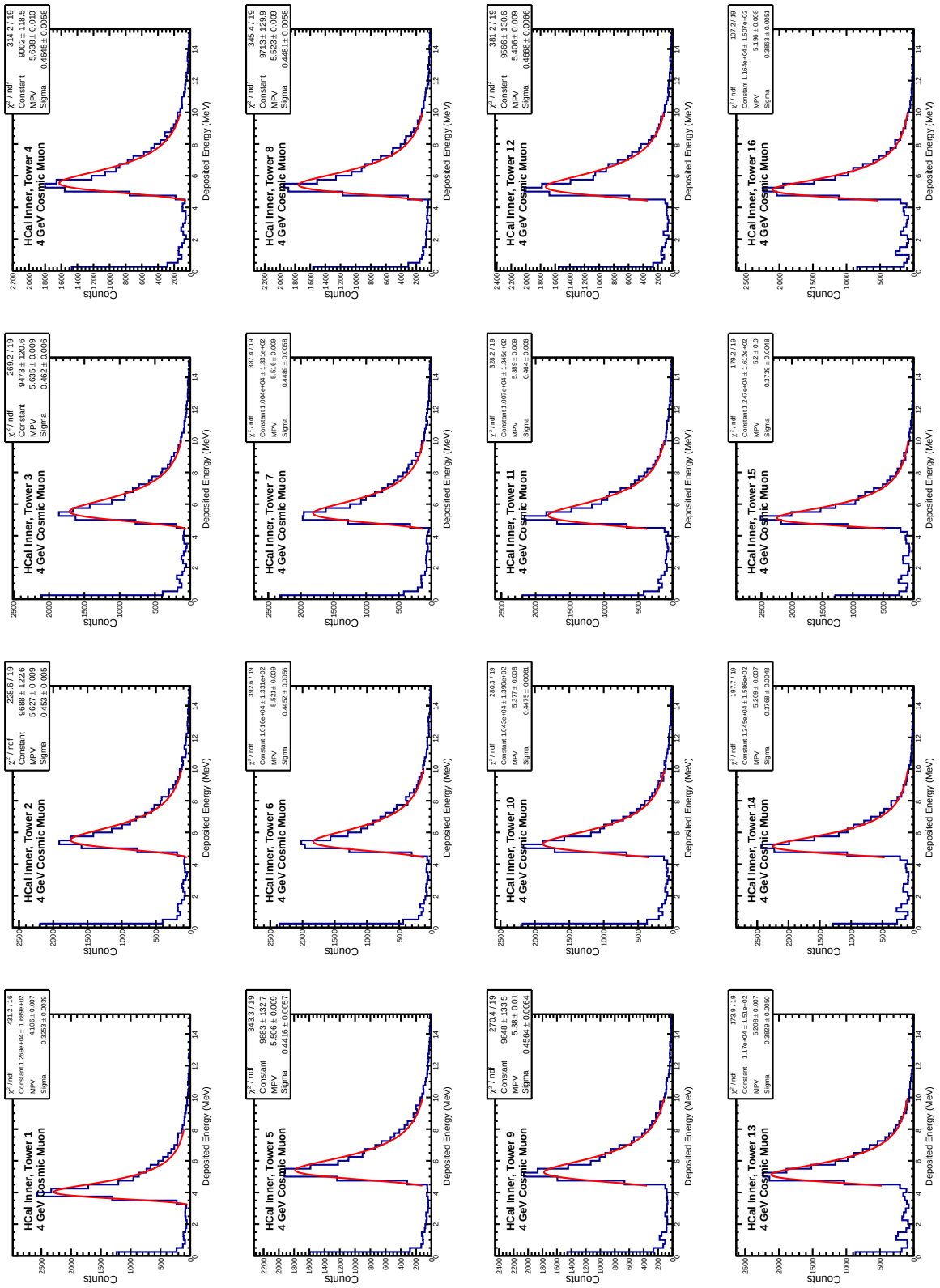

Figure 32: Cosmic ray signal (deposited energy) in each towers of the inner HCal prototype (H1).

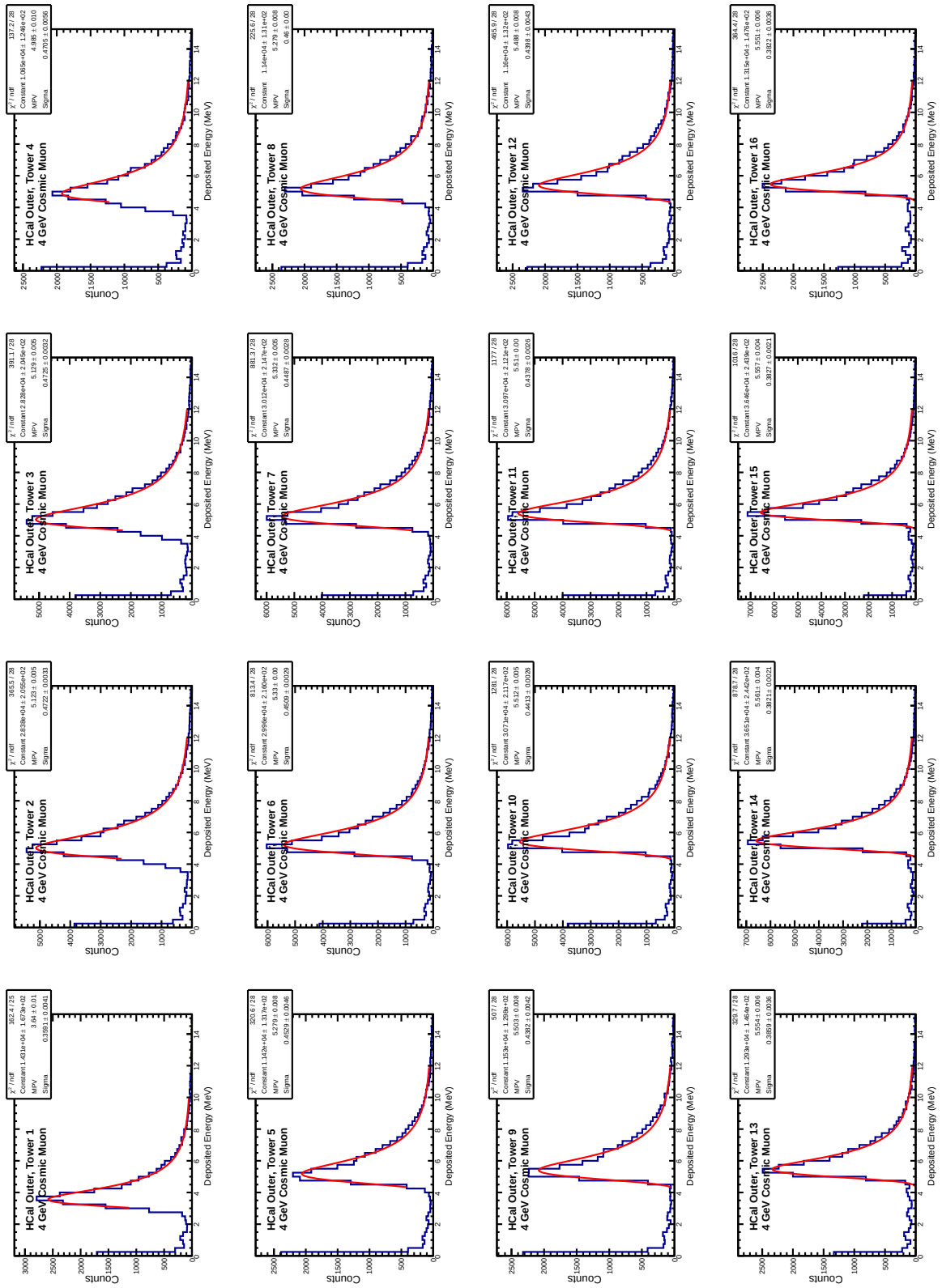

Figure 33: Cosmic ray signal (deposited energy) in each tower of the outer HCal prototype (H2).

4 Test Beam Data Analysis

4.1 Analysis Code

The HCal prototype test beam data production and analysis code have also been committed into the PHENIX CVS repository:

- Data analysis code
  `offline/analysis/sphnx_hcalprotoTB/`
- Macros for making the plots of this technique note
  `offline/analysis/sphnx_hcalprotoTB/technote/`

4.2 ADC Readout

The HCal readout utilizes a custom designed preamp and readout circuit that incorporate a programmable bias adjustment for each SiPM along with temperature sensors and feedback circuit. The temperature feedback could automatically correct for the gain variation with a temperature change. The analog signals from the preamps are sent along ∼15 m cables to a system of fast digitizing ADCs. These ADCs were previously used for the Hadron Blind Detector in the PHENIX experiment and digitized at a sampling rate of 60 MHz. An LED pulse system is also used for testing and calibration of all readout channels (one channel = one tower) for both H1 and H2 [5].

The ADC signal pulse is digitized into 24 samples with a timing step of 16 ns as shown in Fig. 34 for H1 segment and in Fig. 35 for H2. The first two samples constitute the "pedestal window" and the pedestal is the average sample in this window. The subsequent sample timing range defines the "signal window" and is used to determine the ADC peak value, i.e.

$$\text{Max of } (adc_i - ped)\ , \qquad 2 \leq i \leq 24.$$

The ADC peak sample and the other two samples adjoin it are used to compute the most probable peak ADC value and the timing position for the ADC waveform by solving the parabola equation. [Need to be checked and add more details by Edward K and Liang.]

4.3 Optimizing Signal ADC Ingration

An optimized algorithm has been developed to compute the pedestal, and the integrated ADC for each readout channel event by event. To determine the timing position of all ADC samples, we first sum the pulses from all of the 32 channels within the signal timing window

$$S_i = \Sigma_{j=1}^{32}(adc[j][i] - ped[j]), \tag{2}$$

where $2 \leq i \leq 13$ is the ADC sample index within the signal timing window, $ped[j]$ is the pedestal for channel j that was evaluated using method described in the previous section. An amplitude weighted timing position was calculated based on the summed samples via,

$$t_w = \frac{\Sigma_{i=m-3}^{m+4} i \times S_i}{\Sigma_{i=m-3}^{m+4} S_i}, \tag{3}$$

where m is the index for the maximum ADC sample, S_i is the summed pulse samples. The first $t_w - 3$ samples constitute the new pedestal window and a new pedestal is recalculated by averaging the ADC samples in the window channel by channel. The samples between $t_w - 3$ and $t_w + 5$ defined as the new signal window. And the integrated ADC signal, $I(ch)$, is calculated by summing all of the ADCs samples within the new signal window

$$I(ch) = \Sigma_{i=t_w-3}^{t_w+5} adc[ch][i] - ped[ch], \tag{4}$$

which is then used to determine the deposited energy.

4.4 Energy Calibration and Correction with Cosmic Ray Muons

The HCal energy calibration is done with cosmic ray events. A set of cosmic ray data were taken at Fermilab during the beam test period. The cosmic ray events were triggered with scintillator paddles installed at the top and the bottom of the HCAL as shown in Fig. 5. There are total 12 cosmic runs. The run numbers are 212, 215, 216, 218, 223, 337, 338, 339, 405, 406, 229, and 240.

Figure 36 and 37 show the integrated ADC spectra of all towers in the H1 and H2 segment, respectively. We fit the ADC spectra using a "Landau + Gaussian" function. The Landau distribution represents the pedestal. The signals follow a Gaussian-like distribution with a tail. Table 5 and 6 list the ADC values at the Gaussian peaks for every tower in H1 and H2.

Table 5: ADC values of the Gaussian peak in each tower of H1.

tower 13 / 59.1	tower 14 / 45.2	tower 15 / 33.6	tower 16 / 64.0
tower 9 / 47.8	tower 10 / 65.0	tower 11 / 45.0	tower 12 / 63.3
tower 5 / 51.1	tower 6 / 46.0	tower 7 / 21.4	tower 8 / 86.3
tower 1 / 82.5	tower 2 / 31.7	tower 3 / 63.3	tower 4 / 45.9

Table 6: ADC values of the Gaussian peak in each tower of H2.

tower 13 / 62.9	tower 14 / 32.1	tower 15 / 31.0	tower 16 / 52.0
tower 9 / 48.8	tower 10 / 37.2	tower 11 / 51.6	tower 12 / 83.1
tower 5 / 40.1	tower 6 / 41.0	tower 7 / 30.5	tower 8 / 36.2
tower 1 / 30.3	tower 2 / 27.4	tower 3 / 22.8	tower 4 / 37.3

As it is discussed in Section 3.4.8, we ran simulations by launching cosmic muons at 4 GeV (mean muon energy at sea level) at the top of the HCal prototype vertically downward. Figure 38 shows the deposited energy for cosmic ray muons in inner HCal tower 6 as an example. The distribution is fitted with a Landau function, and the mean energy loss of cosmic muons in each tower is 5.5 MeV. We then use this value to convert the ADC signal in each tower to the corresponding energy loss from the test beam.

Once the integrated ADC signal is determined properly, it is relatively easy to evaluate the deposited energy as follows

$$E(ch) = I(ch) \times \frac{E_{dep}^{cosmic}(ch)}{ADC_{dep}^{cosmic}(ch) \times SF(muon)}, \tag{5}$$

where $E_{dep}^{cosmic}(ch)$ is the total deposited energy extracted from the Geant4 simulation, $ADC_{dep}^{cosmic}(ch)$ is the integrated ADC measured from the cosmic data, SF(muon) is the muon sampling fraction factor calculated by using the Geant4 simulation. In order to remove detector noise, minimum threshold value cut (= 15 MeV) is applied to $E(ch)$ in calculating the total deposited energy.

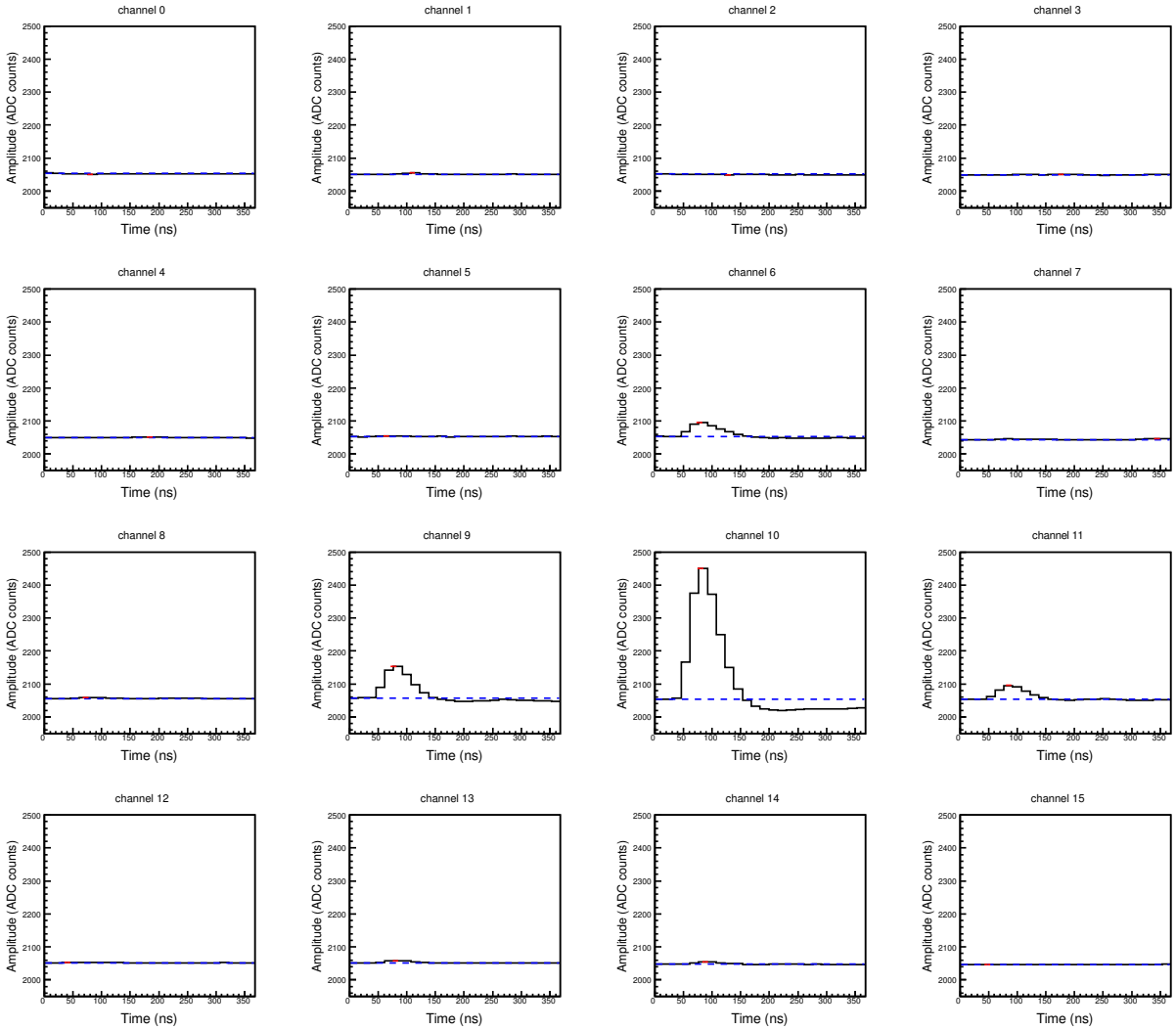

Figure 34: An example of a digitized ADC signal wave form from all 16 towers (channels) of H1 from a single event. The dashed blue lines correspond to the pedestals, and red lines presents the signal peak timing position.

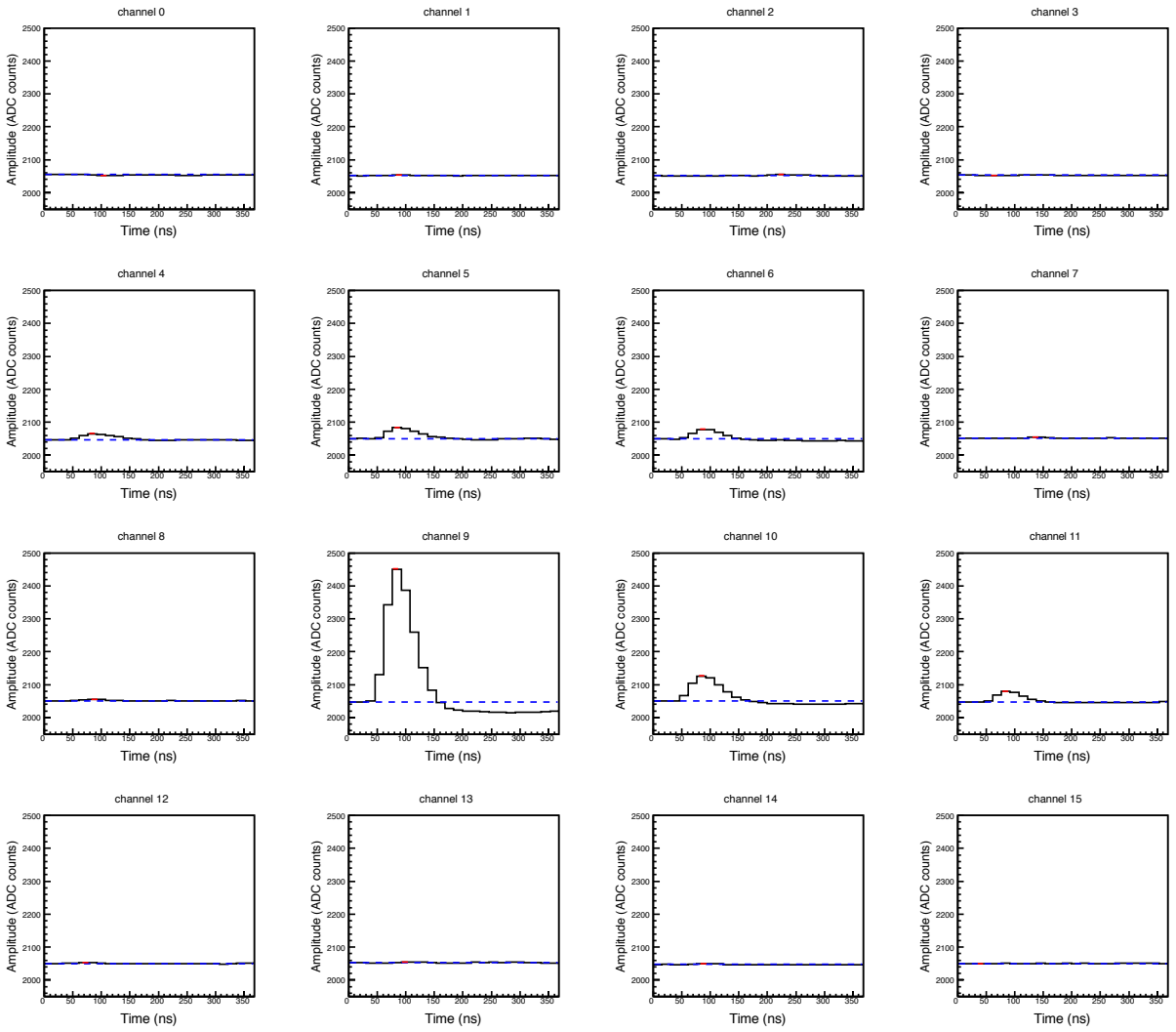

Figure 35: An example of a digitized ADC signal wave form from all 16 towers (channels) of H2 from a single event. The dashed blue lines correspond to the pedestals, and red lines presents the signal peak timing position.

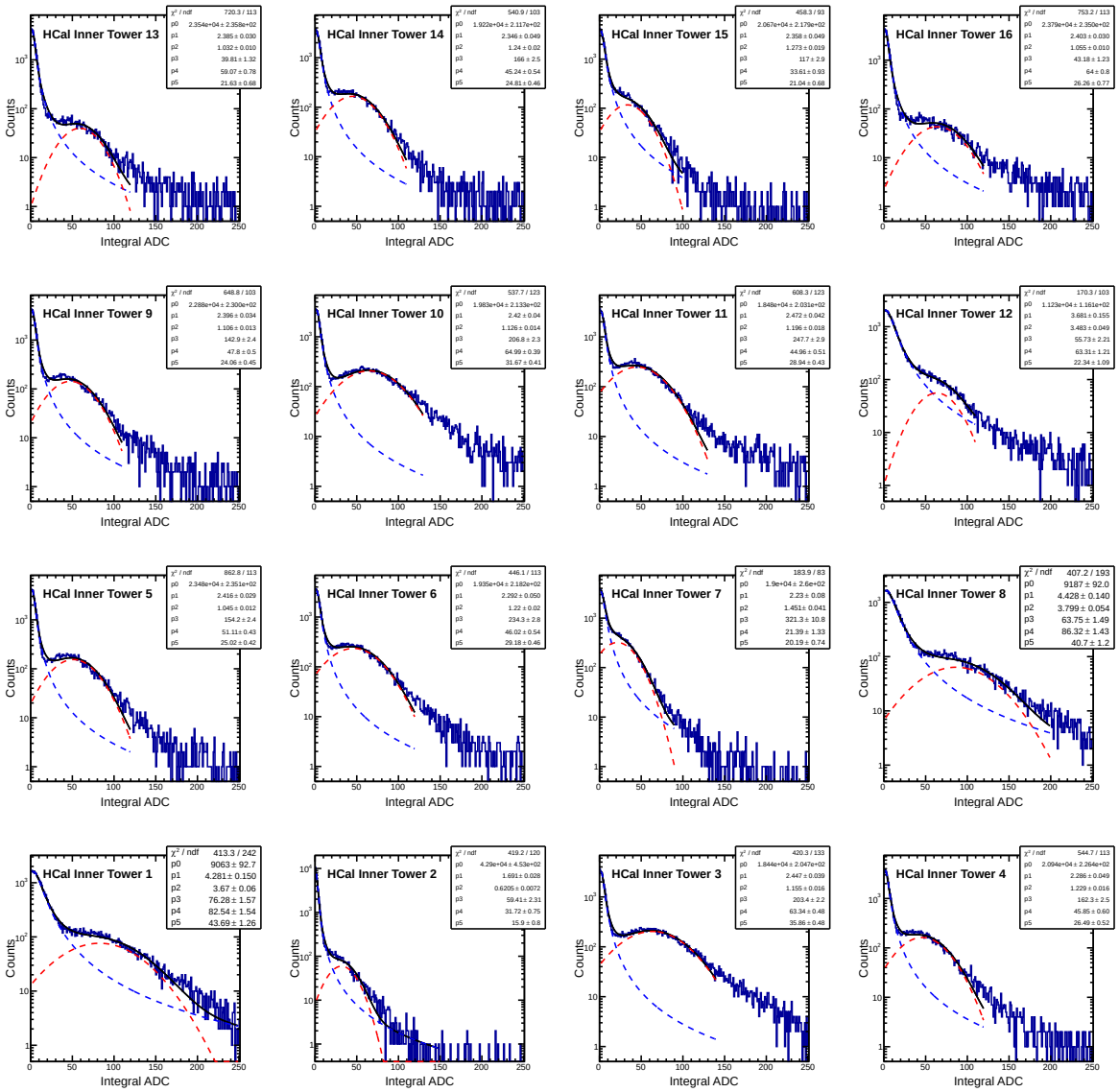

Figure 36: Integrated ADC spectra from cosmic ray events in all towers of H1. The blue dashed line is a fit with a Landau function. The red dashed line is a fit with Gaussian function.

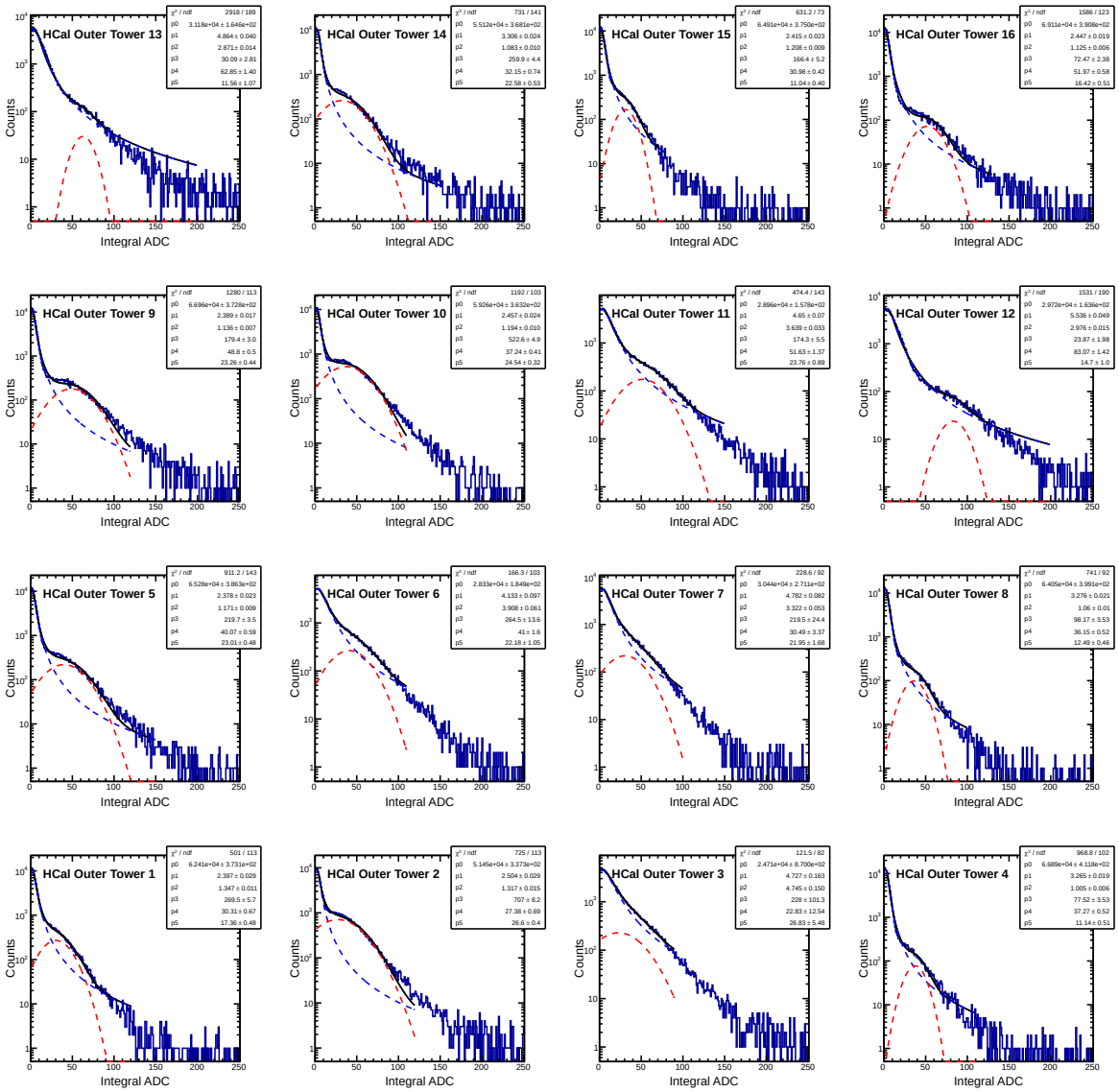

Figure 37: Integrated ADC spectra from cosmic ray events in all towers of H2. The blue dashed line is a fit with a Landau function. The red dashed line is a fit with Gaussian function.

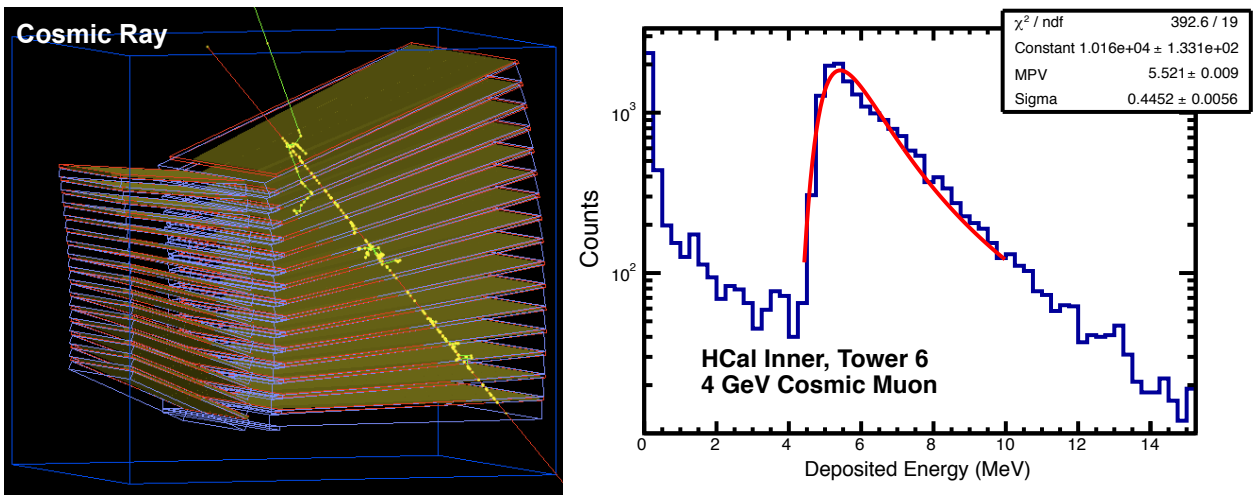

Figure 38: Event displays of cosmic ray simulation (left panel), and signal in H1 tower 6.

5 Beam Test Results

5.1 Beam Spot Distribution

The beam spot distribution is calculated by using the tower energy weighted center of gravity both for H1 and H2. The results are shown in Figs. 39 and 40. These distributions are consistent with these obtained from our simulation (see Figs. 10 and 11).

5.2 Beam Particle Identification

The test beams produced at the Fermilab MT6 Test Beam Facility, contain in general a mixture of electrons, muons, and pions. The component percentage depends on the beam energy. Therefore, it is necessary to identify the type of the particle impinging on the HCal prototype. The impinging particle can be identified by either an external detector like the Cherenkov counter, or by the calorimeter itself. For this analysis, we picked the later for the beam particle identification.

Electromagnetic showers mostly start earlier in the calorimeter, thus deposited most of its energy in the front segment. The hadronic showers in general develop longitudinally deeper than the electromagnetic showers. It is, therefore, a natural approach to use the energy asymmetry from the two calorimeter segments to characterize the longitudinal shower profile and to identify particles impinging on the front of the HCal. The energy asymmetry, E_{asy}, is given as follows

$$E_{asy} = \frac{E1 - E2}{E1 + E2}, \tag{6}$$

where $E1$ and $E2$ are the reconstructed energy in the front (H1) and the back (H2) segment.

Figure 41 shows the total reconstructed energy as a function of the energy asymmetry for test beam from 4 to 60 GeV. Based on our simulation results (see Section 3), one should be able to identify beam particle spieces by using the reconstructed total energy and the energy asymmetry values. A set of incident energy dependent energy asymmetry cut and total energy cut has been obtained from simulation and is listed in Table 4.

As it has been shown in Fig. 22 from our simulation, it is impossible to make a clean separation of the incident particle types using the E_{asy} alone. We therefore made conservative cuts in E_{asy} for cleaning up the mixture of different particle types in our event samples for quantify the calorimeter performance. These cuts are varied for different beam energies and are represented by the dashed-line box regions in Fig. 41.

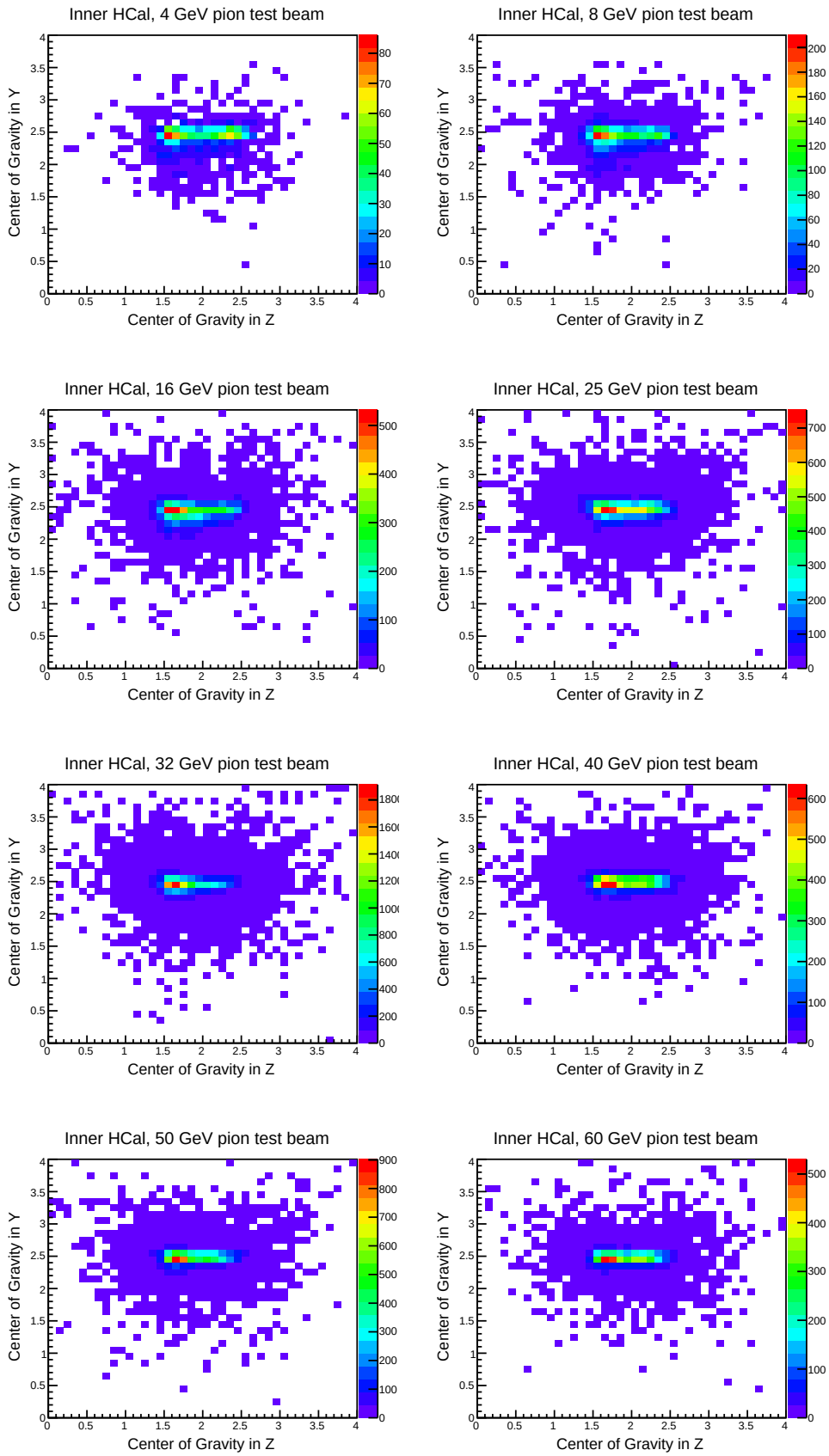

Figure 39: Beam spot distributions at each beam energies at the front face of H1 calculated with the tower energy weighted center of gravity.

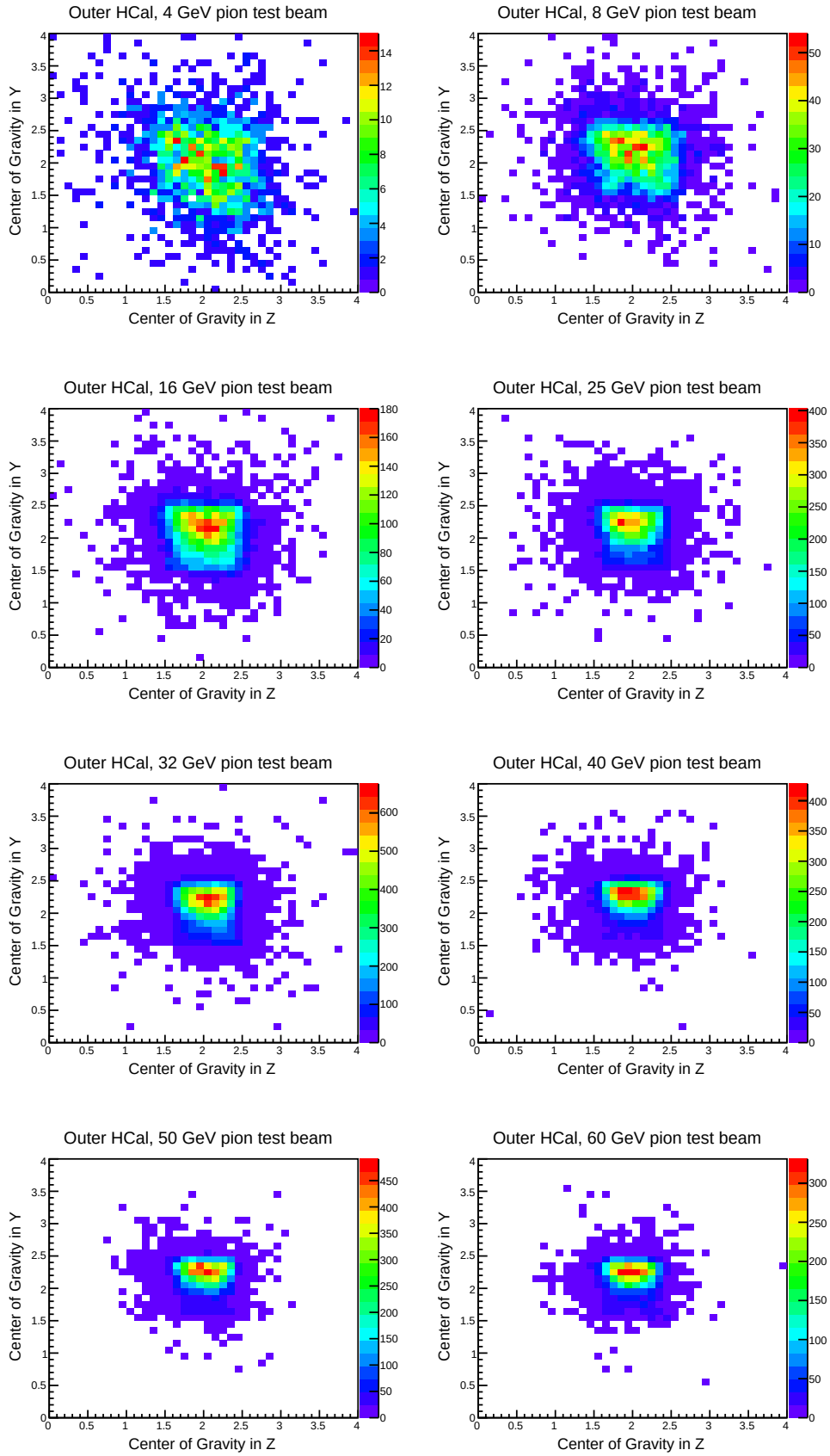

Figure 40: Beam spot distributions at each beam energies at the front face of H2 calculated with the tower energy weighted center of gravity.

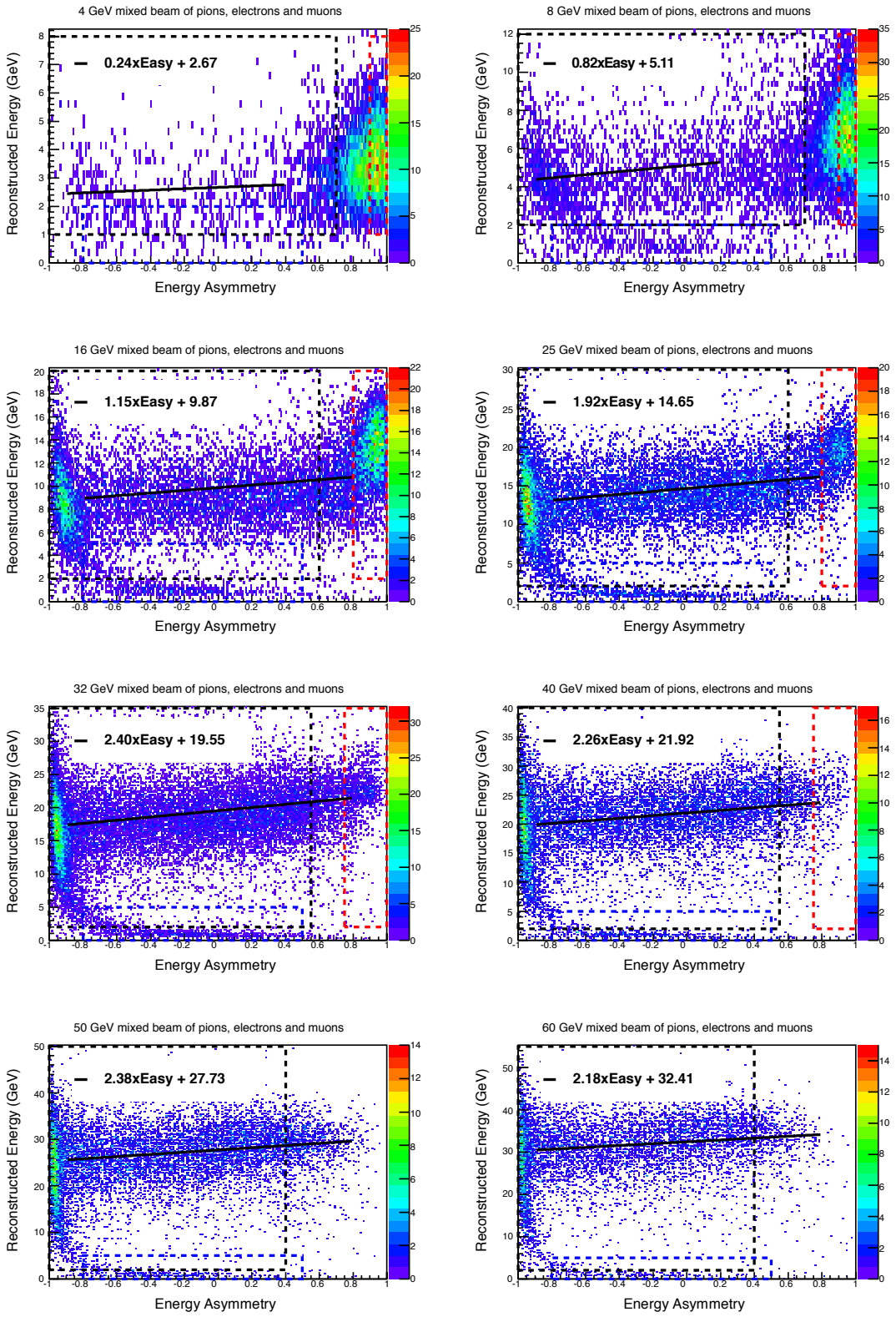

Figure 41: Beam particle identification using the reconstructed total energy and the energy asymmetry for test beam energies ranging from 4 GeV to 60 GeV. See text for details. Black dashed box: pions, Red dashed box: electrons and Blue dashed box: muons. Black lines represents a linear fit for the pion data sample.

5.3 Energy Leveling and Scaling

A linearly rising trend of the reconstructed energy as a function of the energy asymmetry is seen in Fig. 41 for hadronic (i.e. from pions) showers. This rising trend is not observed in our GEANT4 simulation (see Fig. 22). This dependence could be due to the fact that we have used cosmic muons for the energy calibration and a uniform sampling fraction factor obtained from GEANT4 simulation for energy scaling. In the PHENIX TechNote.469 , it has been shown that the sampling fraction factors are indeed CG dependent (see Figs. 33 and 34 in the note).

A quick approach for removing this linearly rising dependence is to level the total reconstructed energy with respect to the energy at the zero energy asymmetry. We call this the leveling. The results of this leveling is given in Fig. 42.

Given the fact that the electromagnetic showers from 4 GeV electrons are completely contained within the calorimeter, we therefore introduced an energy scale factor of 0.825 (extracted from the 4 GeV electron events) and applied to all other energies to correct the effects of the expected leakage. Figure 43 shows the total reconstructed energy after this scaling is applied.

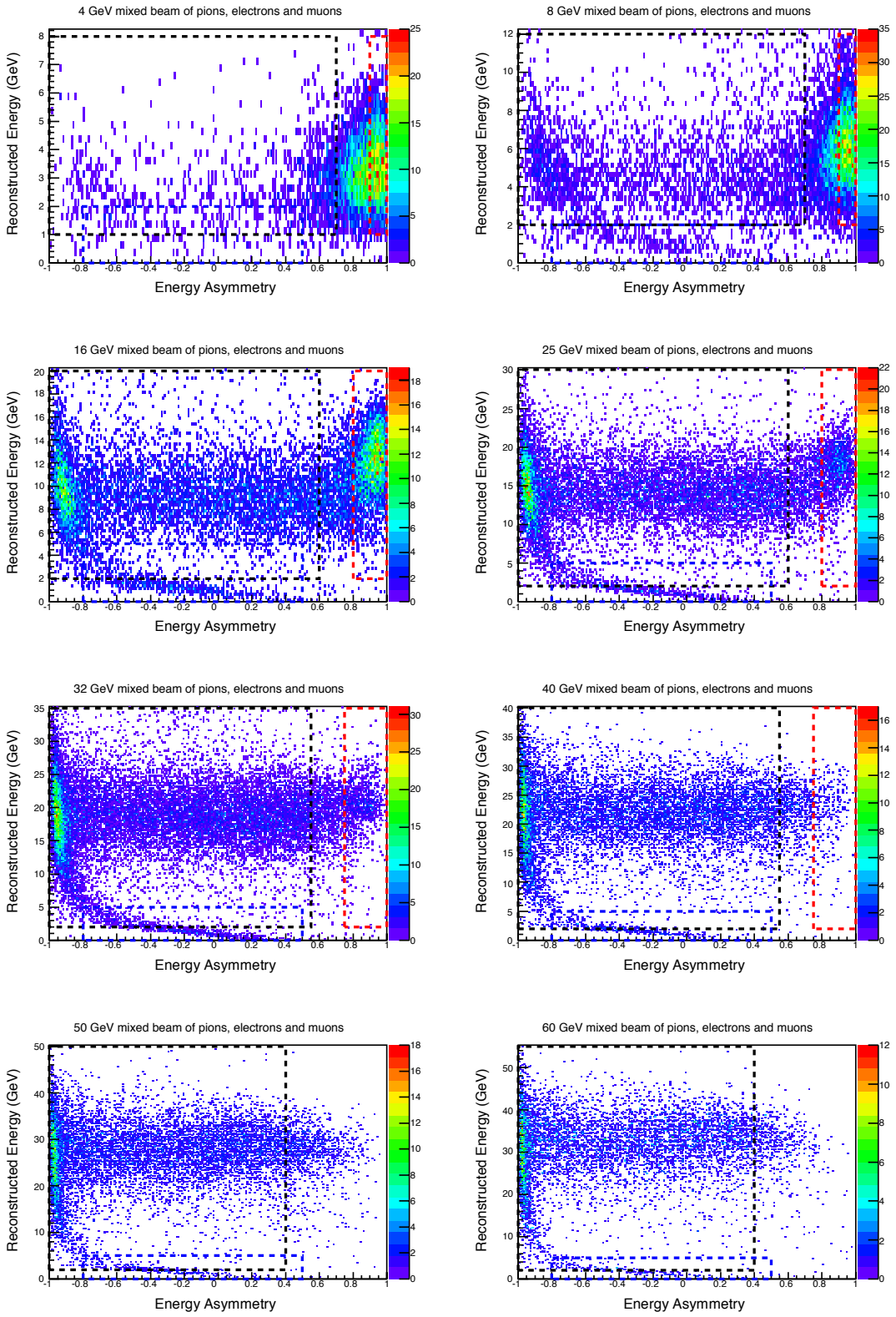

Figure 42: Reconstructed total energy as a function of the energy asymmetry after leveling correction. Black dashed box: pions, Red dashed box: electrons and Blue dashed box: muons.

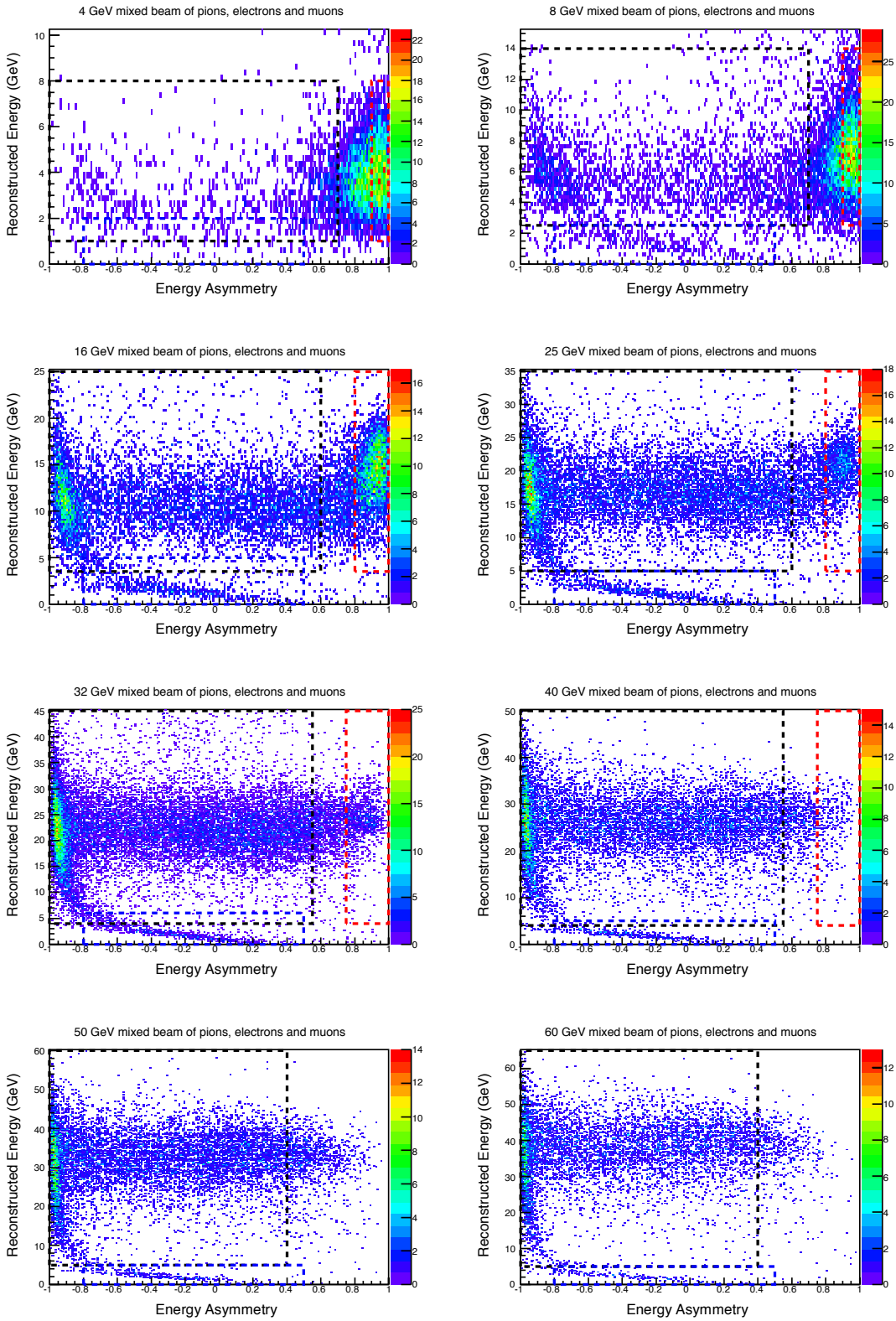

Figure 43: Reconstructed total energy (after the leveling correction is applied) scaled with a factor extract from 4 GeV electrons. Black dashed box: pions, Red dashed box: electrons and Blue dashed box: muons.

5.4 Reconstructed Energy Spectra

Figure 44 shows the reconstructed total energy for pions at beam energies of 4, 8, 16, 25, 32, 40, 50 and 60 GeV after the leveling and scaling corrections are applied. The reconstructed energy spectra are fitted with a gaussian distribution. The extracted fitting parameters are given in Table 7. It should be noticed that the reconstructed total energy is about 30% lower than the beam energy. This number should be compared with the same quantity obtained from our simulation, which is about 25%. Since the energy reconstruction procedure is the same both for the simulation and for the beam data and the same sampling fraction number is used (which is obtained from simulation with muons), this 5% discrepancy should be dominated by the inaccuracy of the cosmic ray calibration since we did have much muons in beam for doing the calibration.

Table 7: The mean and sigma values of gaussian fit to the total energy spectra from pion beam after leveling and scaling corrections.

Beam Energy (GeV)	Mean Value (GeV)	Sigma (GeV)	E_{Mean}/E_{Beam} (%)	E_M/E_B in Simu (%) at 15 MeV cut
4	2.69	1.71	67	55
8	5.53	1.98	69	67
16	11.02	2.77	69	72
25	17.33	3.93	69	74
32	22.74	4.66	70	75
40	26.98	5.13	68	76
50	33.56	6.15	67	76
60	39.74	6.74	66	77

We also reconstructed the total energy spectra for electrons using the same cuts criterions as list in Table 4. Figure 45 shows the electron energy spectra for 4, 8, 16, 25, 32 and 40 GeV. There is little electron statistics both at 50 and 60 GeV energies. The extracted gaussian fit parameters are listed in Table 8.

Based on the extracted fitting parameter values, we use the following normalization factor to scale the reconstructed energy spectra in order to match the mean of the energy distribution to the beam energy:

$$\text{normalization factor} = \frac{\text{beam energy}}{\text{mean of the raw spectra}} \ . \tag{7}$$

The normalized spectra are given in Figs. 46 and 47 for pion beam and electron beam, respectively.

Table 8: The mean and sigma values of Gaussian fits to the total energy spectra from electrons.

Beam Energy (GeV)	Mean Value (GeV)	Sigma (GeV)
4	3.95	1.52
8	7.40	1.95
16	14.95	3.0
25	21.43	2.99
32	24.73	2.24
40	29.07	3.93

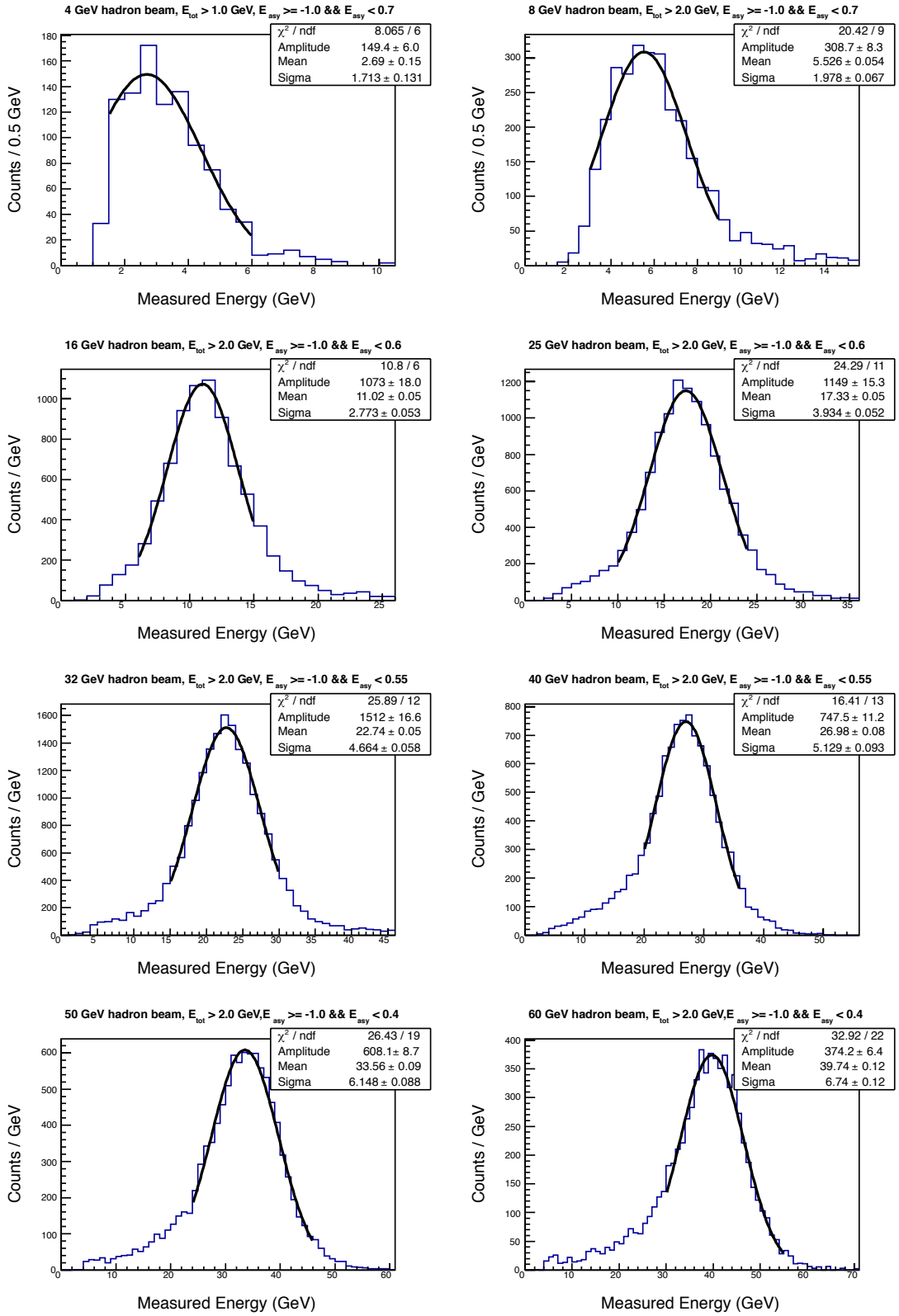

Figure 44: Reconstructed total energy in HCal for pion beams after leveling and scaling.

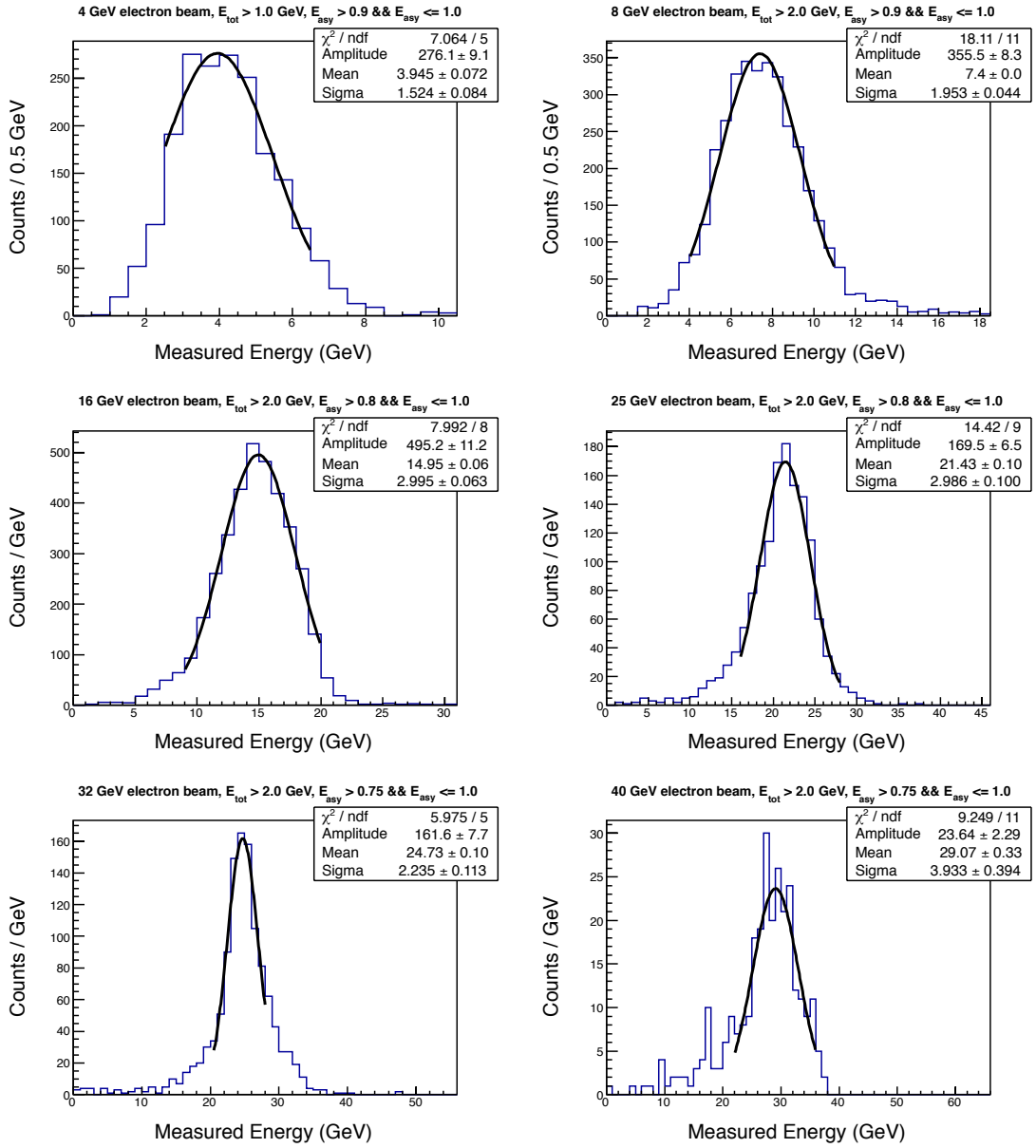

Figure 45: Reconstructed total energy in HCal for electron beams.

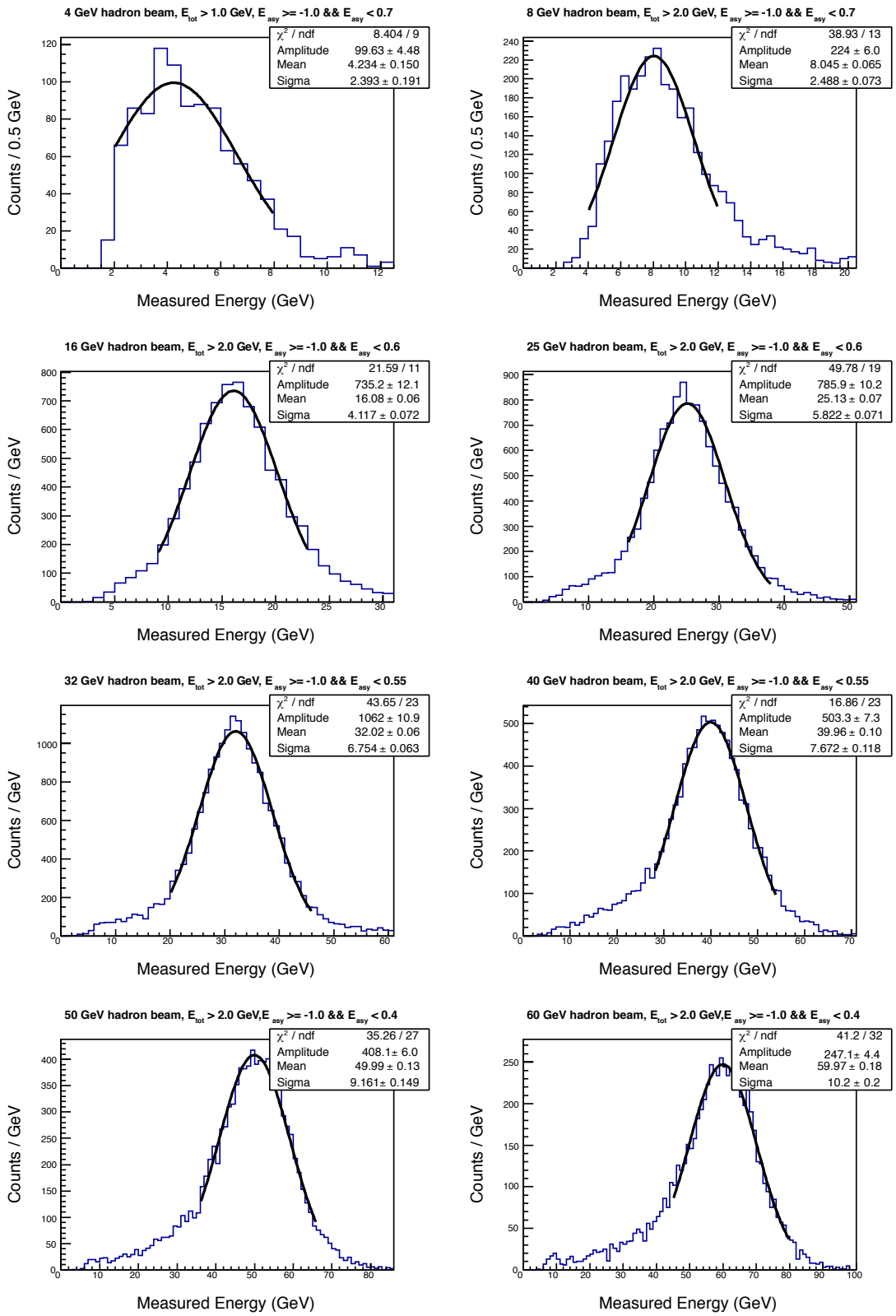

Figure 46: Reconstructed total energy in HCal for pion beams after beam energy normalization. See text for details about the normalization procedure.

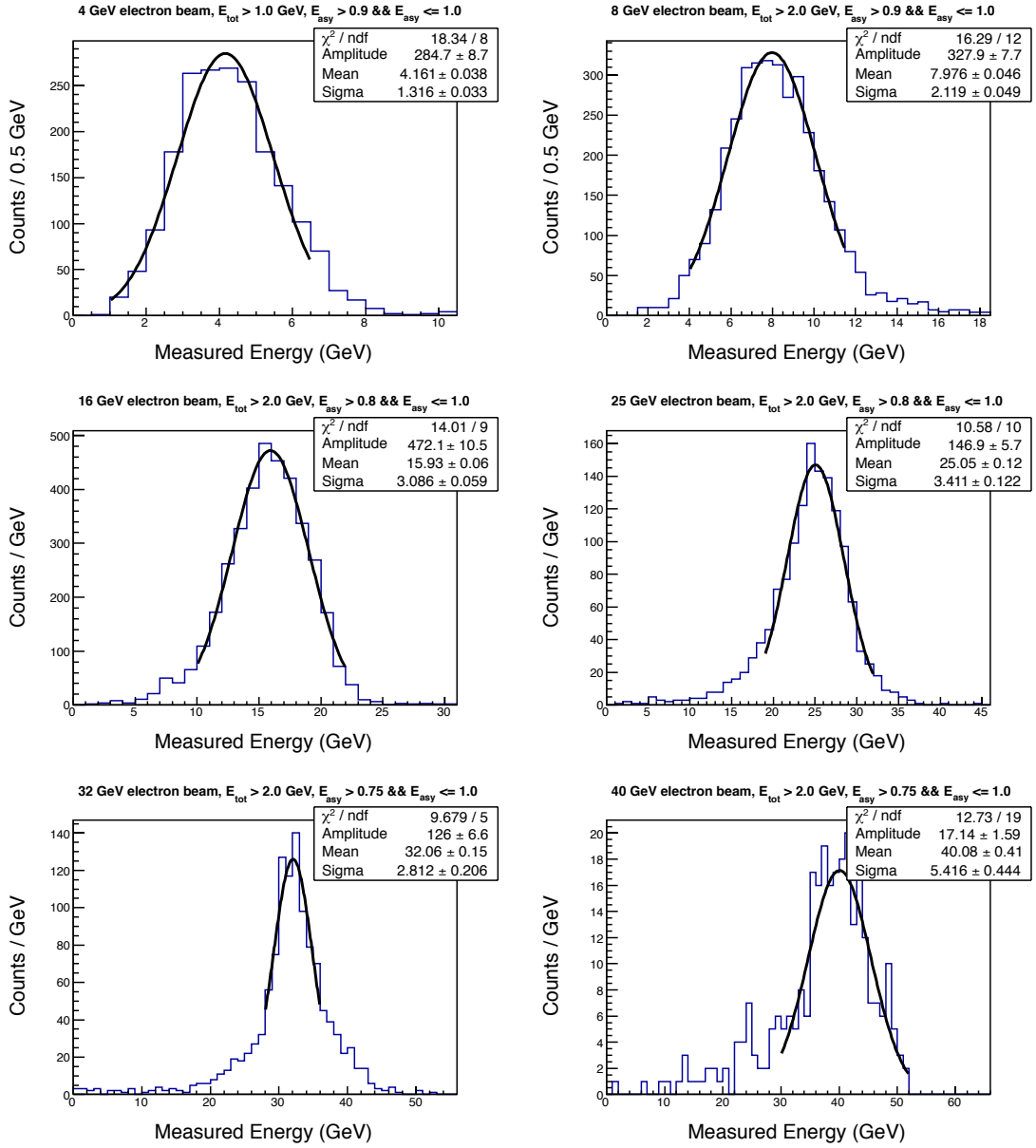

Figure 47: Reconstructed total energy in HCal for electron beams after beam energy normalization. See text for details about the normalization procedure.

5.5 Calorimeter Energy Resolution and Linearity

Using the reconstructed energy spectra, we are able to determine the calorimeter energy resolution and its linearity. The results are shown in Fig. 48 and 49, respectively. The fractional energy resolution is fitted with the "standard" functional form (i.e., a stochastic term plus a constant term)

$$\frac{\sigma}{E} = \frac{a}{\sqrt{E}} \oplus b \ , \tag{8}$$

where a and b are the stochastic and constant contributions to the resolution, respectively.

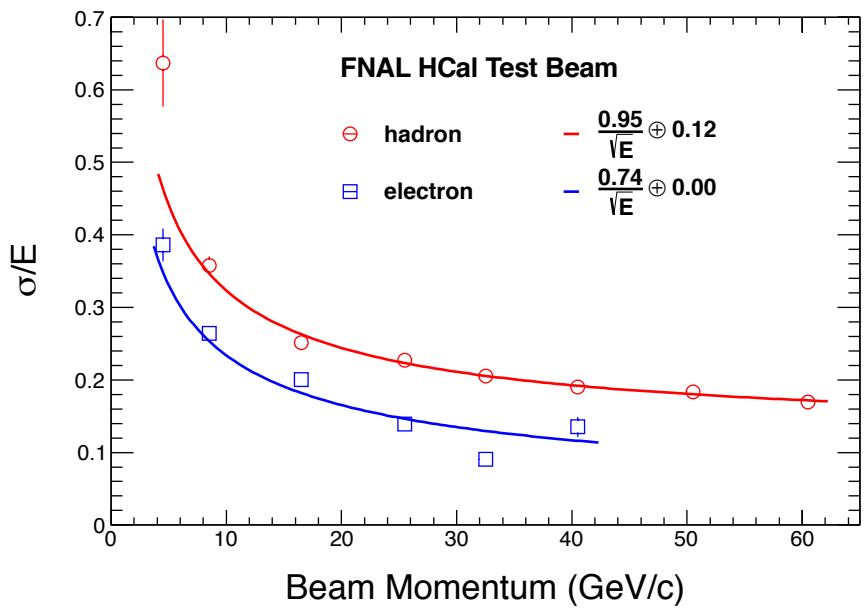

Figure 48: sPHENIX HCAL prototype energy resolution for pions and electrons obtained from the FNAL test beam data.

5.6 Reconstructed e/π Ratio

From the reconstructed energy spectra, the e/π ratio is calculated as follows

$$e/\pi = \frac{\langle E_e \rangle}{\langle E_\pi \rangle} \ , \tag{9}$$

where $\langle E_e \rangle$, and $\langle E_\pi \rangle$ are the reconstructed mean energy for electron and pions, respectively. And the e/h ratio is then determined by fitting e/π distribution with formular:

$$e/\pi = \frac{e/h}{(e/h) f_{\pi^0} + (1 - f_{\pi^0})} \ , \tag{10}$$

where $f_{\pi^0} = k \ln(E)$ is the average fraction of electromagnetic energy in the hadronic shower, and k = 0.11 [6].

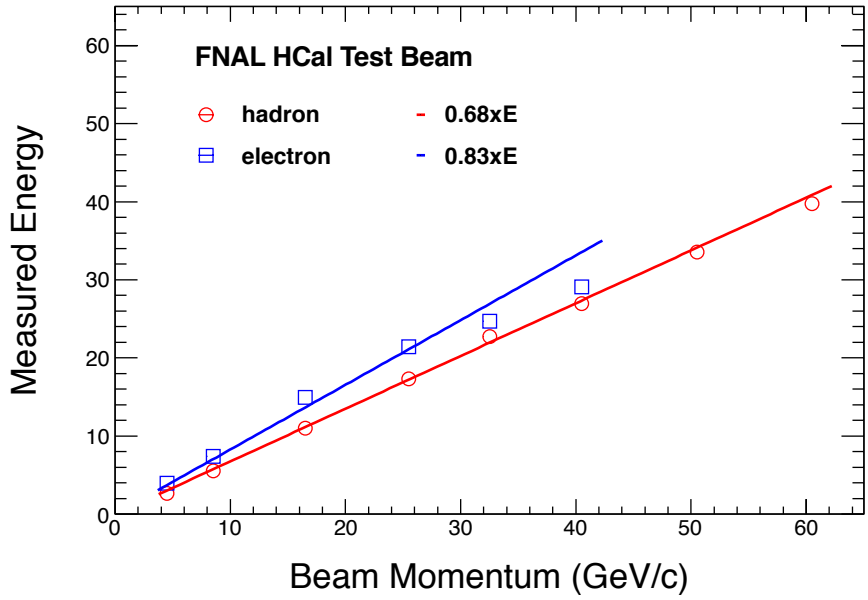

Figure 49: sPHENIX HCAL prototype energy linearity for pions and electrons obtained from the FNAL test beam data.

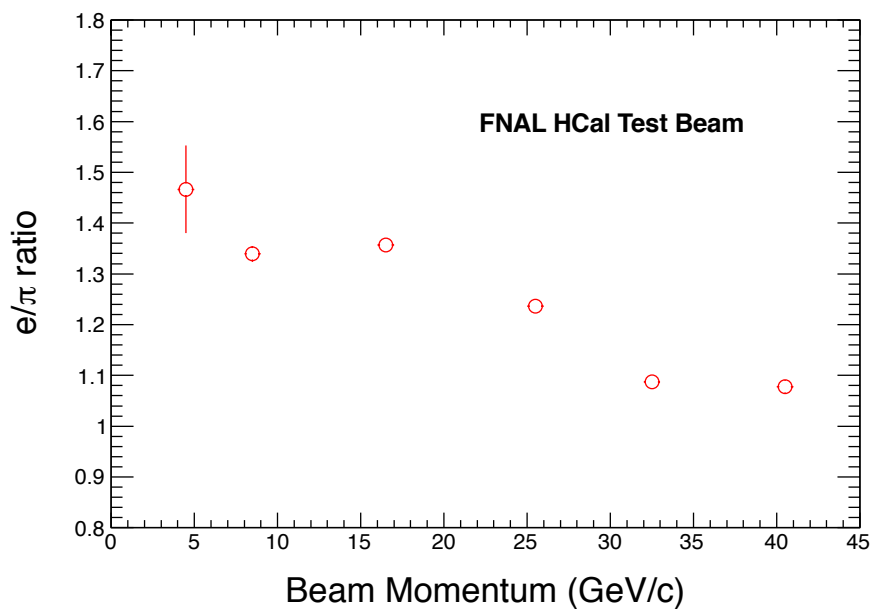

Figure 50: e/π ratio of the HCal prototype.

5.7 Comparison with Geant4 Simulation

We have compared the test beam results with the results from the Geant4 simulations. Figures 51 and 52 show the energy spectra comparison between the test beam results and the spectra from the Geant4 simulation for electrons and pions from 4 to 60 GeV. Figure 54 show the energy resolution comparison between data and the Geant4 simulation.

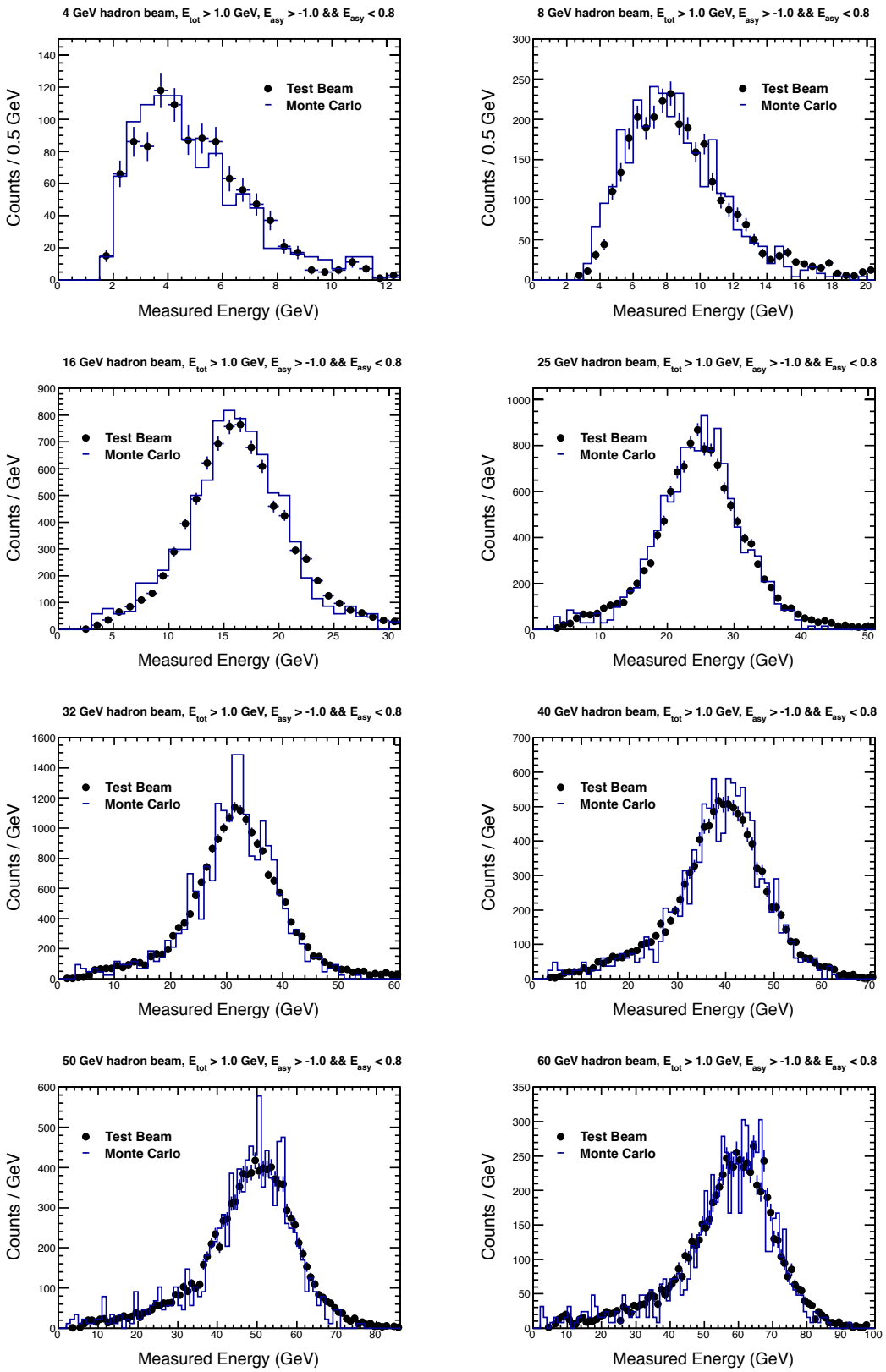

Figure 51: Comparison of the hadronic energy spectrum between test beam data and the Geant4 simulation.

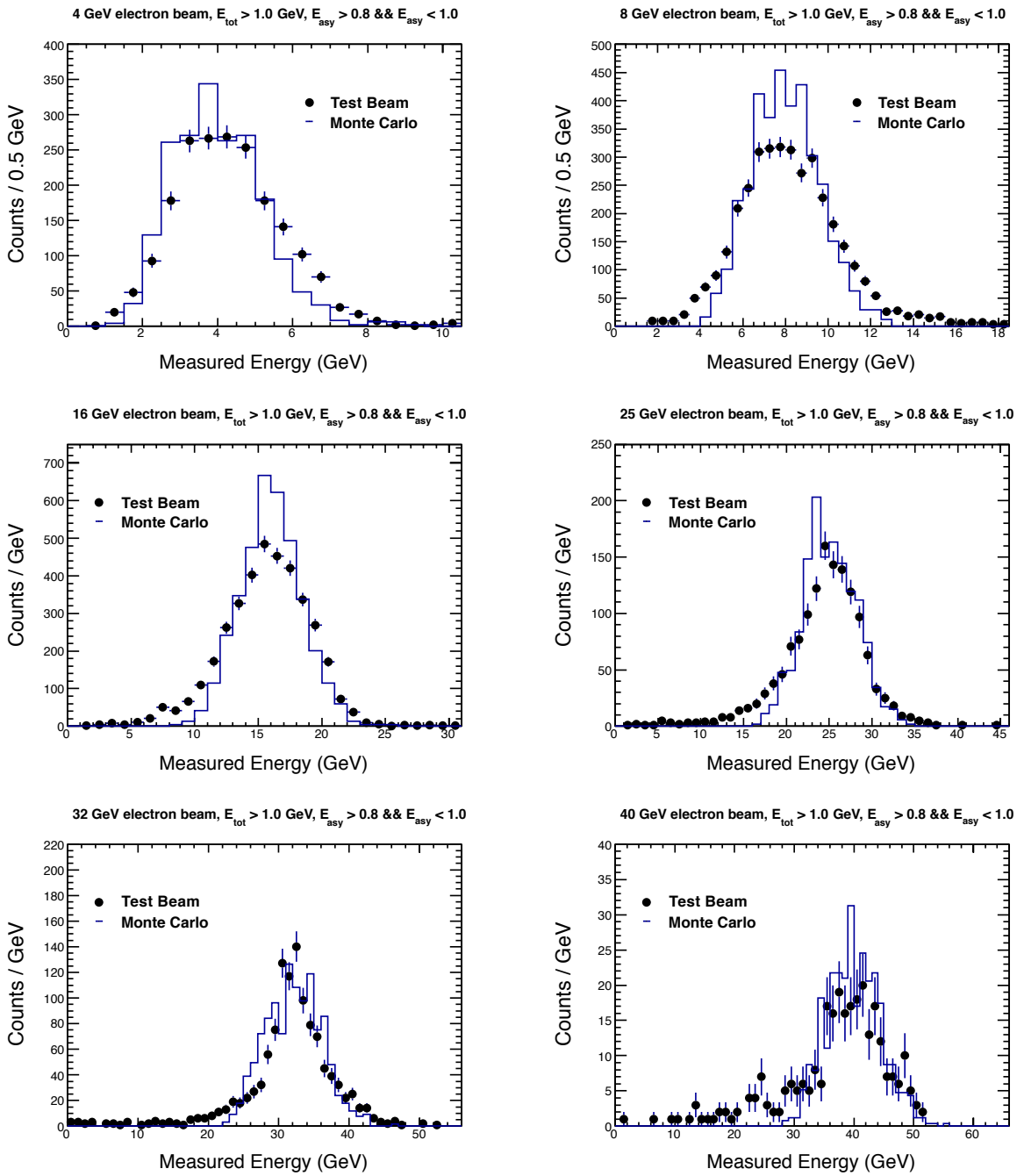

Figure 52: Comparison of the electron energy spectrum between test beam data and the Geant4 simulation.

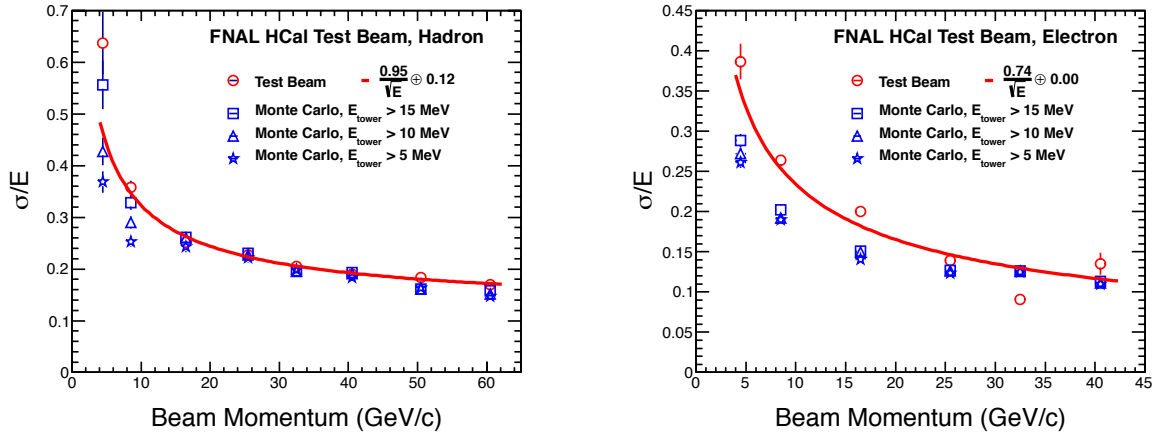

Figure 53: Comparison of the energy resolution of pions (left panel) and electrons (right panel) between test beam data and the Geant4 simulation.

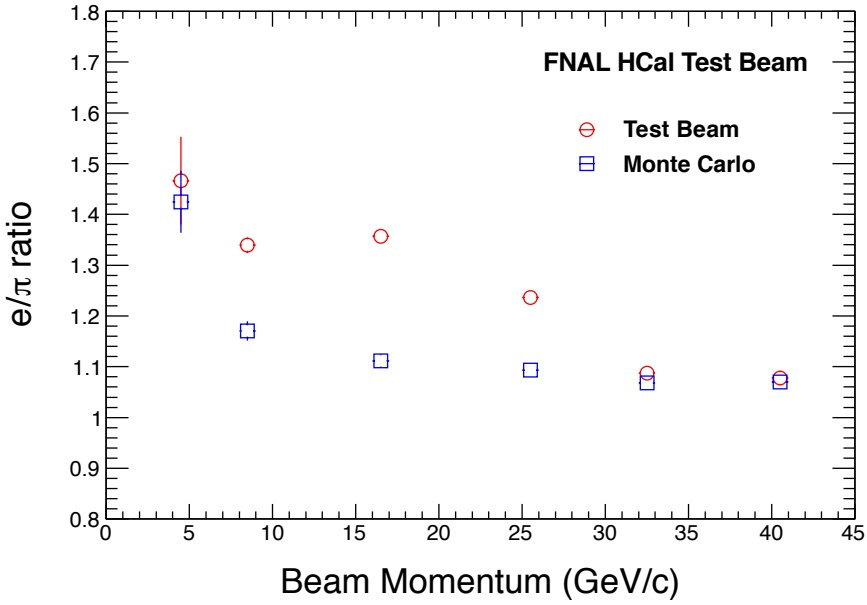

Figure 54: Comparison of the e/pi ratios evaluated from test beam data and the GEANT4 simulation.

6 Summary

The first sPHENIX HCal prototype beam test is very successful. The fundamental properties (energy resolution, signal linearity and e/π ratio) of this hadronic calorimeter have been extracted from the test beam data.

The results for the energy resolution and signal linearity are very consistent with the results obtained from the Geant4 simulation. It is very encouraging to see the shape of the reconstructed energy spectra well matched with the simulated results.

One should note that the results obtained from this beam test is for the measurement at the central rapidity without magnetic field. Also, given the limited test beam time, there is no reliable data for making the combined EMCal and HCal measurement study. Another beam test is under preparation for studying the HCal performance at large rapidities and using efficient light collection schemes.

One should also note that we have used cosmic rays for determining the energy scale (i.e., calibration). These cosmic ray tracks are perpendicular to the direction of the beam particles impinging at the front of the calorimeter. This could be one of the sources for the 5% discrepancy in the ratio of the reconstructed mean energy to the beam energy between the data and simulation. See Section 5.4 for details. It is important to address this issue in the next beam test.

The results show that the accordion-like hadronic calorimeter design will perform at the level which is required by the sPHENIX jet measurements.

References

[1] A. Adare et al., (PHENIX collaboration) arXiv: 1207.6378v2 [nucl-ex] (2012).

[2] http://Geant4.cern.cn

[3] P. Adragna, et al., Nuclear Instruments and Methods in Physics Research A 615 (2010) 158-181.

[4] http://www.slac.stanford.edu/comp/physics/matprop.html

[5] E. Kistenev, et al., CALOR 2014 proceeding.

[6] R. Wigmans, NIM A265 (1988) 273.

A HCal Design Drawings

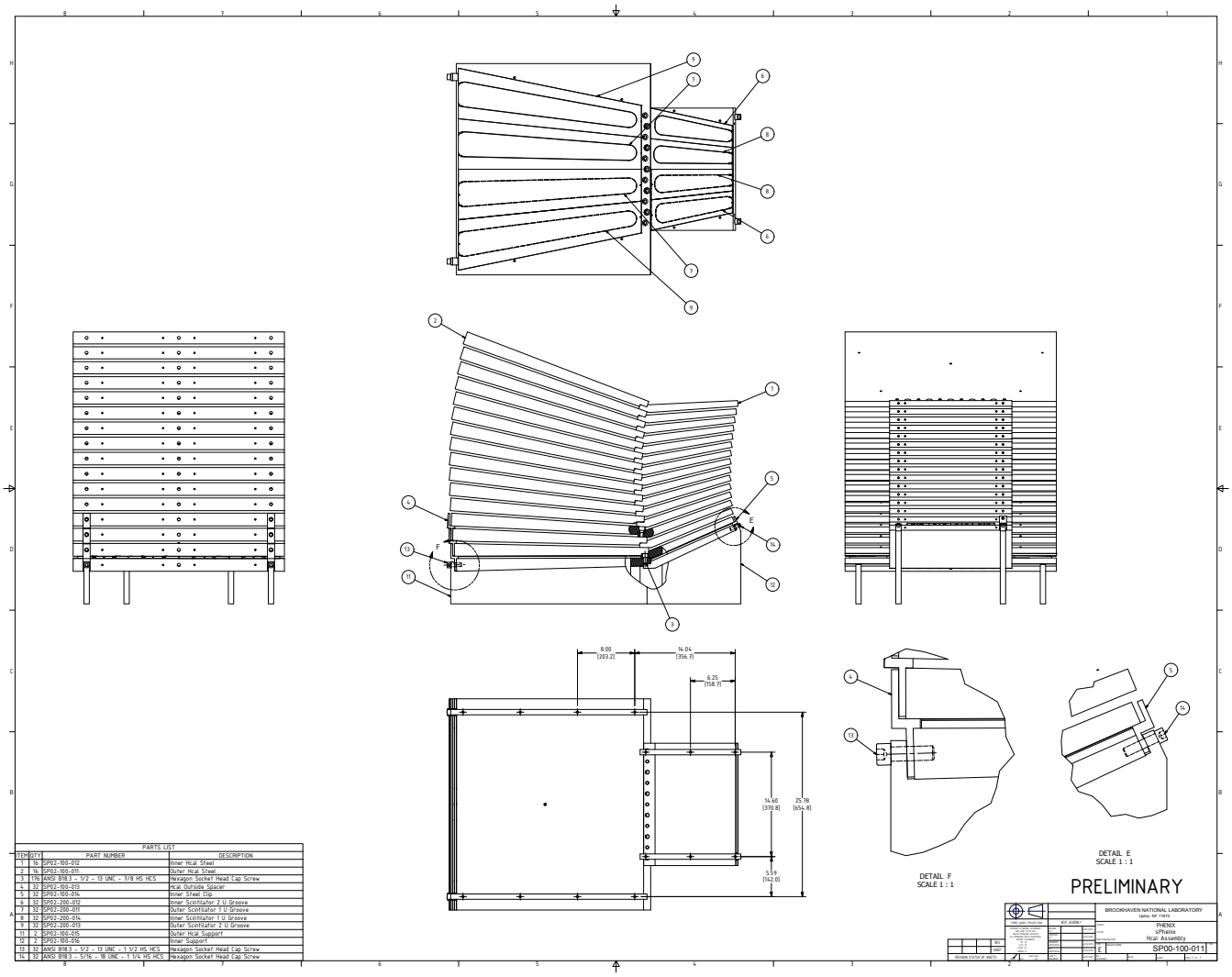

Figure 1: Engineering drawings of the sPHENIX HCal assembly. Provided by Don Lynch.

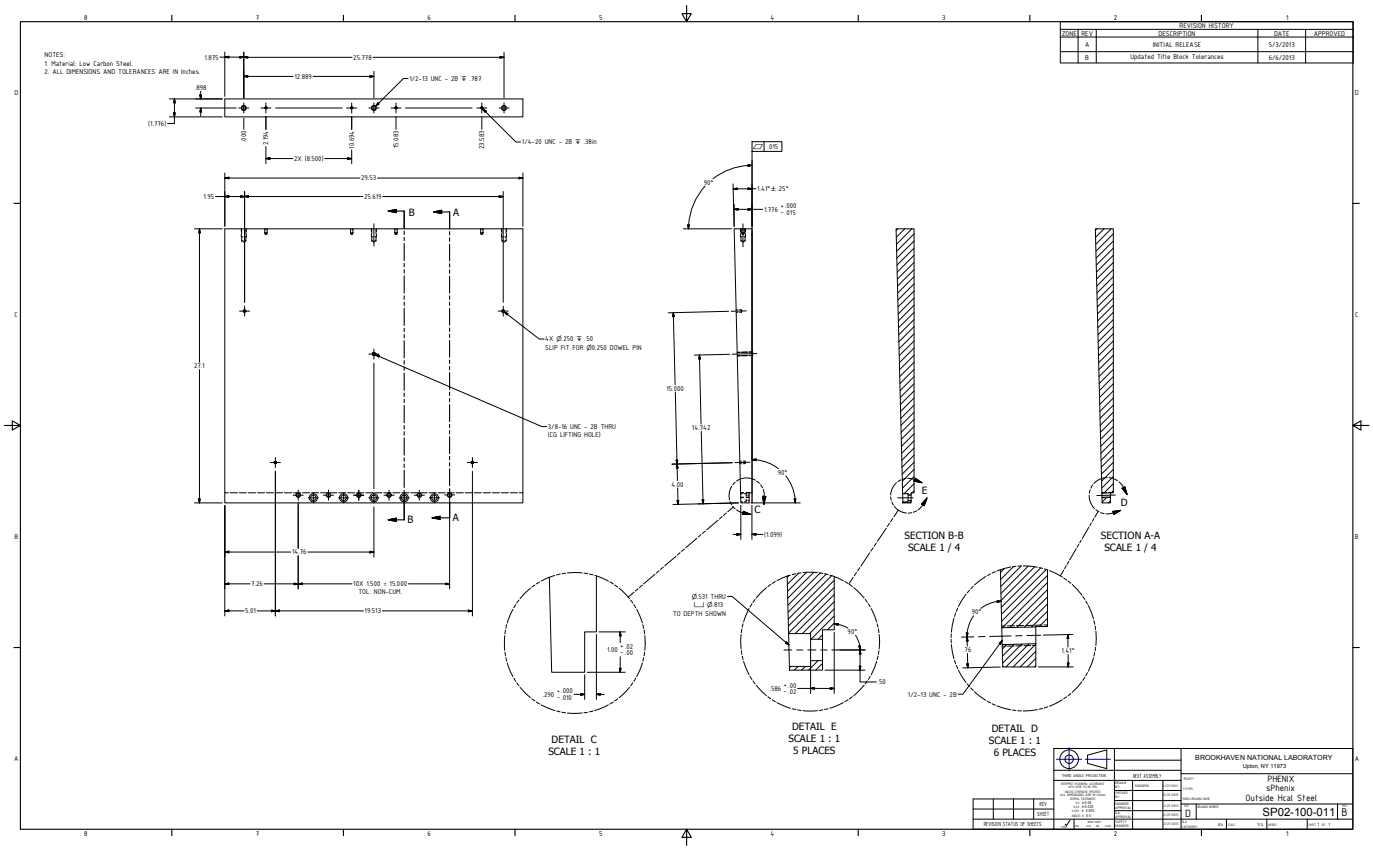

Figure 2: Engineering drawings of the outer HCal steel plate. Provided by Don Lynch.

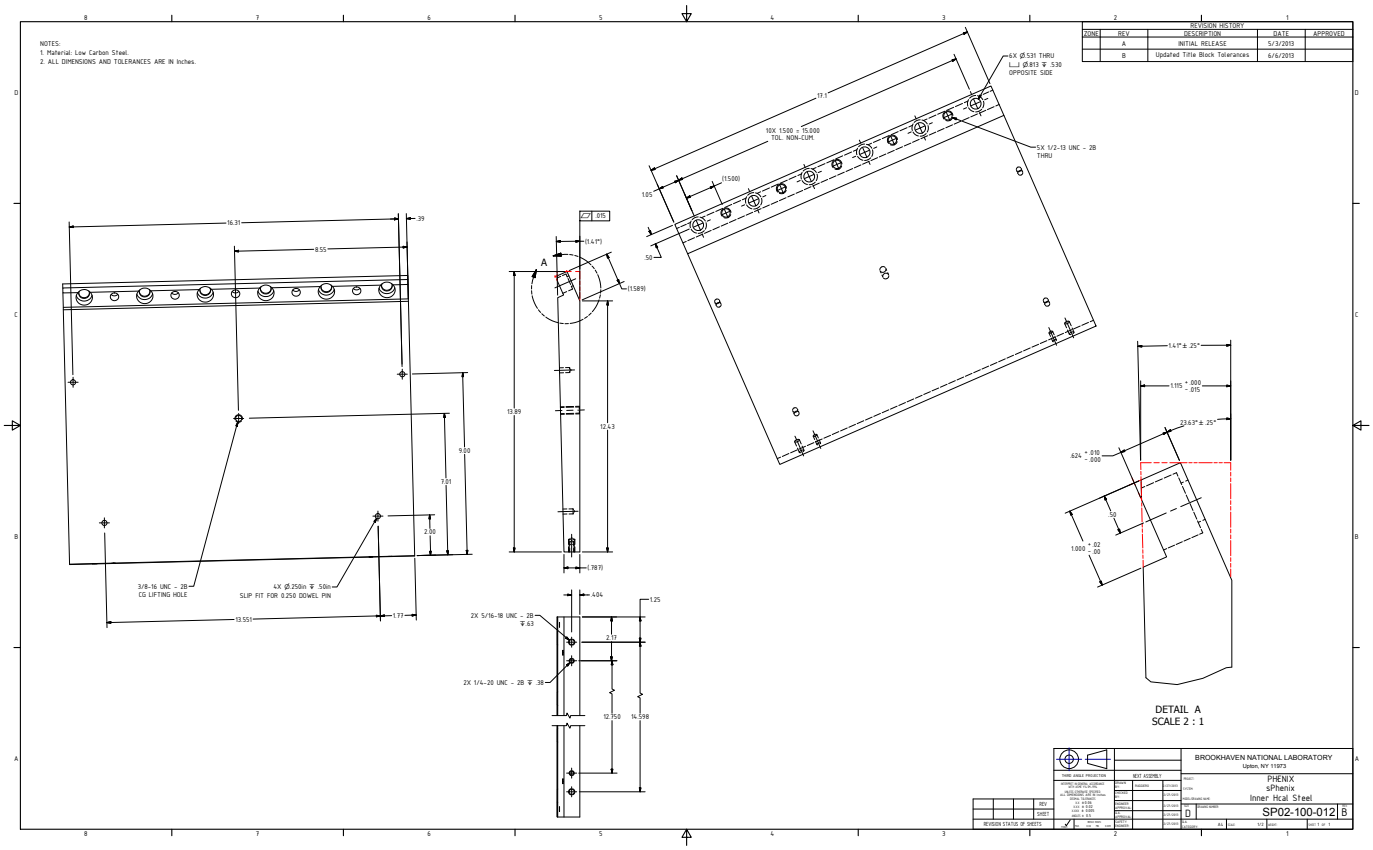

Figure 3: Engineering drawings of the inner HCal steel plate. Provided by Don Lynch.

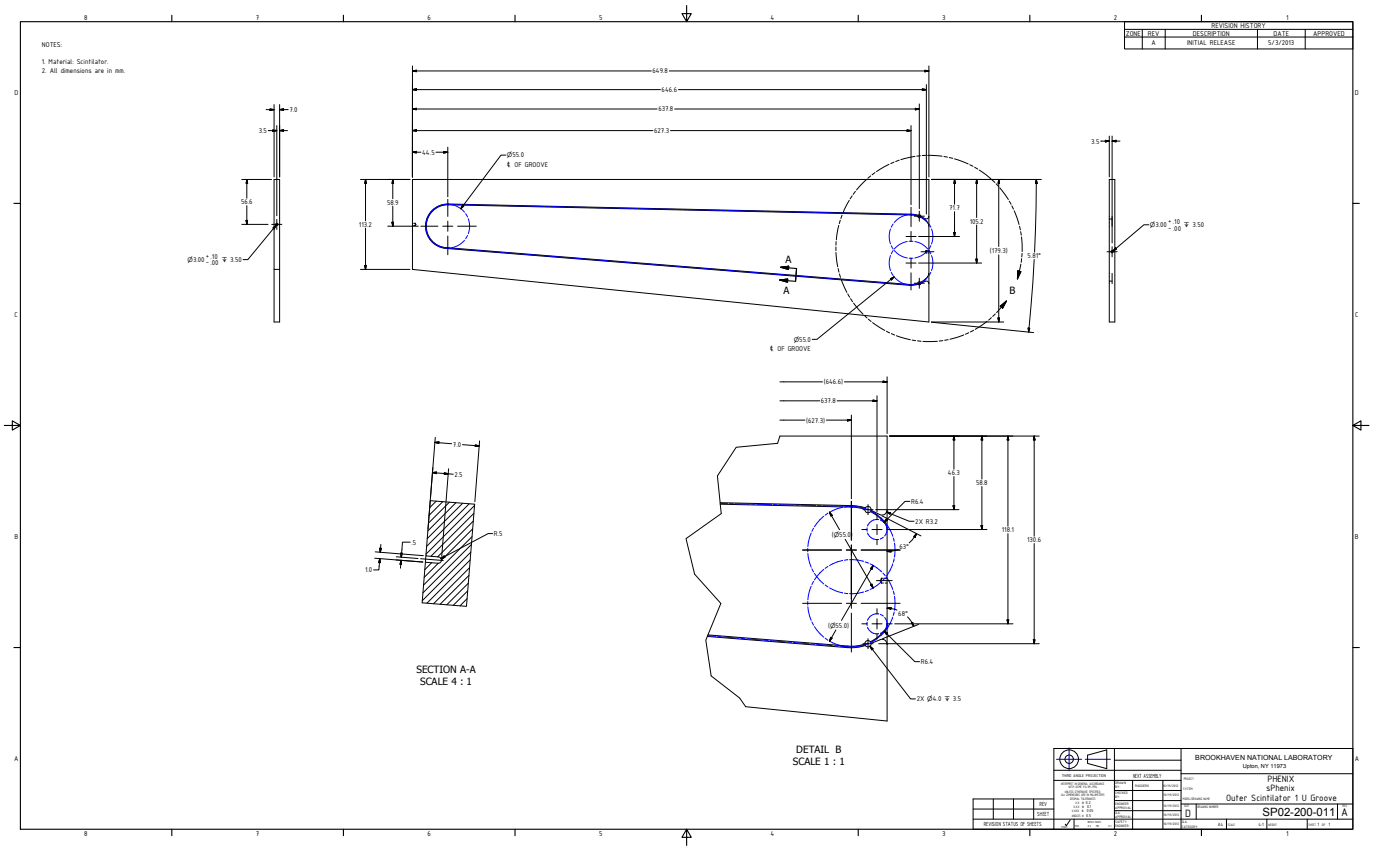

Figure 4: Engineering drawings of the outer scintillator 1U sheet. Provided by Don Lynch.

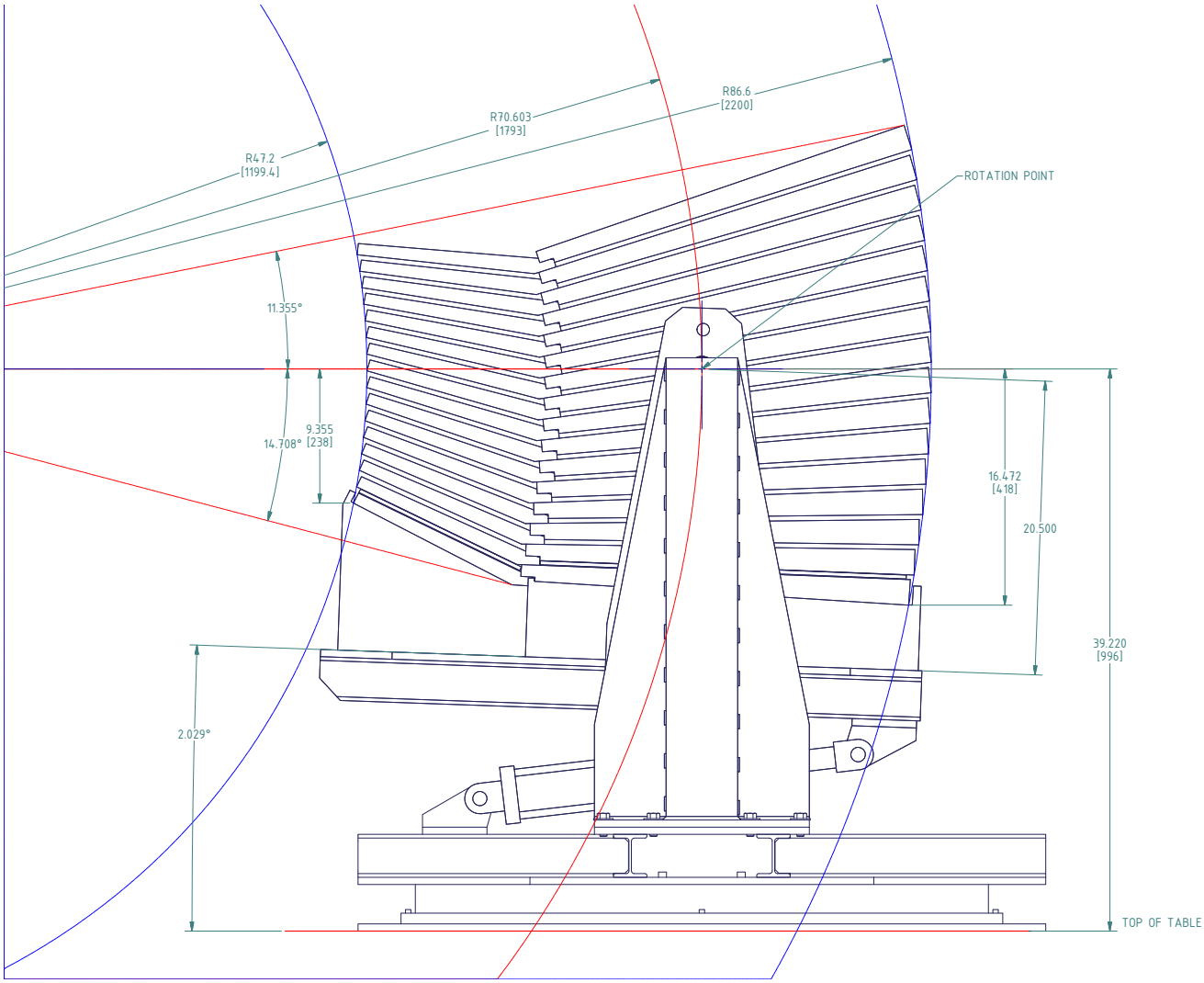

Figure 5: Engineering drawings of the HCal rotation design. Provided by Don Lynch.